Title

Cerebellar Dysfunction in Schizophrenia- and Autism-Associated Copy Number Variants

ISBN

9798190924695

Author

Fung, Hoki

Publication Date

2026-09-08

Peer reviewed|Thesis/dissertation

UNIVERSITY OF CALIFORNIA

Los Angeles

Cerebellar Dysfunction in Schizophrenia- and Autism-Associated Copy Number Variants

A dissertation submitted in partial satisfaction of the requirements

for the degree Doctor of Philosophy in Neuroscience

by

Hoki Fung

2026

ABSTRACT OF THE DISSERTATION

Cerebellar Dysfunction in

Schizophrenia- and Autism-Associated

Copy Number Variants

by

Hoki Fung

Doctor of Philosophy in Neuroscience

University of California, Los Angeles, 2026

Professor Carrie E. Bearden, Chair

Clinically defined neuropsychiatric and neurodevelopmental disorders such as schizophrenia and autism spectrum disorder (ASD) are behaviorally and etiologically heterogeneous, limiting the ability of diagnosis-first approaches to identify their underlying neurobiological mechanisms. Copy number variants (CNVs) at the 22q11.2 locus offer a genetics-first model for identifying convergent and divergent neurobiological pathways contributing to risk. Reciprocal deletions (22qDel) and duplications (22qDup) of the same 22q11.2 genomic segment provide a genetics-first model of gene-dosage effects, with 22qDel conferring markedly elevated schizophrenia risk, while 22qDup is associated with substantially lower risk, potentially protective relative to the general population. Both CNVs, however, converge in conferring elevated risk for ASD and intellectual disability. Although cortical and subcortical systems have

been relatively well studied in 22q11.2 CNVs, the cerebellum, long regarded as a purely motor structure but now understood to also support cognition, social processing, and affect, has remained comparatively unexplored. This dissertation asks whether the cerebellum represents an important and gene-dosage-sensitive substrate of neuropsychiatric and neurodevelopmental risk, and whether cerebellar vulnerability converges across distinct high-risk CNVs. The first manuscript establishes the cerebellar structural phenotype in reciprocal 22q11.2 CNVs, identifying widespread volume reductions in 22qDel but comparatively preserved and regionally selective alterations in 22qDup, with Vermis VII representing a shared site of vulnerability. The second manuscript extends this work to cerebellar white matter microstructure and resting-state functional connectivity, revealing a striking dissociation across imaging modalities. Whereas cerebellar volume abnormalities were most pronounced in 22qDel, white matter microstructural alterations were unexpectedly more widespread in 22qDup, affecting all three cerebellar peduncles; 22qDel showed more selective, opposite-direction effects concentrated in the superior cerebellar peduncle. Functional connectivity alterations were comparatively limited overall, with significant hypoconnectivity detected only in 22qDel. Integrating volume, microstructure, and connectivity into multimodal profiles improved discrimination of CNV groups, with cerebellar volume contributing most strongly to 22qDel-related distinctions and peduncular diffusion measures contributing most strongly to 22qDup-related distinctions. The third manuscript tests whether this cerebellar vulnerability is specific to 22qDel or reflects a more general mechanism of neuropsychiatric risk, using normative modeling to directly compare cerebellar volume deviations in 22qDel and 3q29Del

within a common analytic framework. Both syndromes showed substantial reductions in total cerebellar volume relative to a large normative reference sample, with no statistically detectable difference in the magnitude of reduction between CNVs. Regional analyses revealed broad convergence, alongside a smaller subset of regions showing CNV-specific differences. Together, these findings identify the cerebellum as a robust but multidimensional substrate of neurodevelopmental risk. Distinct genomic perturbations converge on substantial cerebellar volume reduction, while reciprocal 22q11.2 dosage produces divergent effects on cerebellar white matter and functional circuitry. This work demonstrates the value of a genetics-first, multimodal approach for identifying neurobiological phenotypes that may be obscured by the etiological heterogeneity of conventional psychiatric diagnoses, and provides a foundation for investigating how distinct genetic risk factors converge on shared brain systems while producing different patterns of circuit-level dysfunction.

The dissertation of Hoki Fung is approved.

Leanna Marie Hernandez

Paul J. Mathews

Jennifer Gladys Mulle

Lucina Qazi Uddin

Carrie E. Bearden, Committee Chair

University of California, Los Angeles

2026

DEDICATION

To my younger self.

CONTENTS

ACKNOWLEDGEMENTS

I would like to express my deepest gratitude to my committee chair, Professor Carrie Bearden, whose mentorship shaped not only this dissertation but my entire scientific development as a graduate student. Her rigor, generosity with her time, and unwavering support through every setback and long night of writing have made this work possible, and I am profoundly grateful for the example she has set as a scientist and mentor. I also thank my committee members, Professors Leanna Hernandez, Paul Mathews, Jennifer Mulle, and Lucina Uddin, for their thoughtful guidance, insightful feedback, and generosity of time throughout this process.

I am deeply grateful to the many mentors and colleagues who supported and encouraged me throughout my research training prior to UCLA, and whose influence continues to shape how I approach academic life and research today. From the Gopnik Lab at UC Berkeley, I thank Professor Alison Gopnik, Dr. Adrienne Wente, and Professor Tony Cheng. From the Institute of Cognitive Neuroscience at University College London, I thank Professor Sam Gilbert. From the Clinical Brain Lab at Nanyang Technological University, I thank Professor Annabel Chen, Professor Shu-Hui Lee, Hsin-Yu Lin, and Su Ren Gan. From the Cognition & Attention Laboratory at Yale-NUS College, I thank Professor Chris Asplund. From the National University of Singapore, I thank Professor John Totman, Dr. Mary Stephenson, Professor Michael Chee, Professor Helen Zhou, Professor Thomas Yeo, Professor Ju Lynn Ong, and Professor June Lo. From the Society for Neuroscience Singapore Chapter, I thank Professor Ajay S. Mathuru and Dr. Sangyu Xu. From the Meditation Research Program at

Massachusetts General Hospital and Harvard Medical School, I thank Professor Matthew Sacchet and Ruby M. Potash.

I am also grateful for the perspective gained through my roles in industry, where I saw research translated into real-world application, an experience that continues to shape how I think about research impact. From Datature, I thank Keechin Goh and Meng Da Lee. From Neuroglee Health, I thank Aniket Singh Rajput and Dr. Michael Patterson. From Vibe Science, I thank Emma Zhang and Jonathan Rechtman. I am also grateful to Dr. Paul Rochon, Biman LIyanage, Dr. Masoud Rahmani, and Marina Tran-Vu for what I learned from working alongside them.

At UCLA I thank Professor Felix Schweizer and Jenny Lee of the Neuroscience Interdepartmental Program for their support throughout my graduate education. I also thank Professor Sung-Jae Lee and Professor Christopher Colwell for the opportunity to serve as a teaching assistant in their courses, which was a rewarding part of my graduate training.

To my colleagues in the Bearden Lab, thank you for your contributions to this work and the camaraderie that made these four years a blast: Leila Kushan-Wells, Sarah Chang, Charlie Schleifer, Kathleen O'Hora, Rune Bøen, Carolyn Amir, Jee Won Kang, Tyler Dietterich, Haley Wang, Dylan Hughes, Sam Klein, Elizabeth Bondy, Isabelle Lee, Margaret Chu, Monica Espana, Jamie Zinberg, Rui Ma, and Zhen-Qi Liu. I also thank the mentees I have been fortunate enough to work with, who have taught me as much as I hope I taught them.

I thank my collaborators who contributed directly to this work: Dr. Priyanka Sigar, Dr. Jason Nomi, Professor Sarah Shultz, Dr. Kuaikuai Duan, and Dr. Milin Kim.

I am sincerely grateful to the many research participants and their families who made this work possible.

I am also fortunate to have built many great friendships at UCLA, with cohort mates, colleagues in other labs, and friends across campus, who made my time here memorable.

Finally, I thank my family and friends, whose support and encouragement throughout my life have carried me to this point.

Chapter 1, in full, is a version of: Fung, H., O'Hora, K.P., Boen, R., Wang, H.R., Amir, C.M., Schleifer, C.H., Kushan-Wells, L., Miranda, B.A., Bondy, E.K., Mathews, P.J., and Bearden, C.E. (2026). Convergent and divergent cerebellar alterations in 22q11.2 copy number variants. Biological Psychiatry: Global Open Science, 6(4), p.100718. The dissertation author was the primary investigator and author of this paper.

Chapter 2, in part, is a version of material in preparation for publication: Fung, H., Schleifer, C.H., O'Hora, K.P., Boen, R., Dietterich, T.E., Wang, H.R., Kang, J.W., Sigar, P., Nomi, J.S., Liu, Z.Q., Kushan-Wells, L., Mathews, P.J., Hernandez, L.M., Uddin, L.Q., and Bearden, C.E. Multimodal Cerebellar Alterations Reveal Distinct Effects of 22q11.2 Deletion and Duplication. Manuscript in preparation. The dissertation author was the primary investigator and author of this paper.

Chapter 3, in part, is a version of material in preparation for publication: Fung, H., Kushan-Wells, L., Kim, M., Duan, K., Shultz, S., Mulle, J., and Bearden, C.E. Convergent and Divergent Cerebellar Alterations Across High-Risk Neuropsychiatric Copy Number Variants. Manuscript in preparation. The dissertation author was the primary investigator and author of this paper.

This work was supported by the National Institute of Mental Health (Grant Nos. R01/R37MH085953, R01MH129858, U01MH101779, U01MH119736, and R21MH116473, awarded to Carrie E. Bearden, and R01MH118534 awarded to Jennifer Mulle), the Department of Defense (Grant No. W81XWH-12-1-0081, awarded to Carrie E. Bearden), the Simons Foundation Autism Research Initiative Explorer Award (awarded to Carrie E. Bearden), and the Uytengsu-Hamilton 22q11 Neuropsychiatry Research Award (awarded to Carrie E. Bearden).

I also acknowledge the UCLA Graduate Program in Bioscience and the UCLA Neuroscience Interdepartmental Program for their training and support.

VITA

EDUCATION

2015 Bachelor of Arts in Psychology, University of California, Berkeley

2016 Master of Research in Cognitive Neuroscience, University College London

2022 Master of Computing in Artificial Intelligence, National University of Singapore

RESEARCH EXPERIENCE

2022–2026 Graduate Student Researcher, Semel Institute, UCLA

2021–2025 Graduate Research Intern, Meditation Research Program, MGH/HMS

2020–2021 Research Associate, Sleep and Cognition Lab, NUS

2019–2020 Data Scientist, Clinical Imaging Research Centre, NUS

2016–2018 Research Associate, Clinical Brain Lab, Nanyang Technological University

2015–2016 Research Assistant, Institute of Cognitive Neuroscience, UCL

2013–2015 Research Assistant, Gopnik Lab, UC Berkeley

PUBLICATIONS

FIRST-AUTHOR PUBLICATIONS

Fung, H., O'Hora, K.P., Boen, R., Wang, H.R., Amir, C.M., Schleifer, C.H., Kushan-Wells, L., Miranda, B.A., Bondy, E.K., Mathews, P.J., and Bearden, C.E. (2026). Convergent and divergent cerebellar alterations in 22q11.2 copy number variants. *Biological Psychiatry: Global Open Science*.

Fung, H., Potash, R.M., Krystal, A.D., Pizzagalli, D.A., and Sacchet, M.D. (2025). Selective KOR antagonist alters functional patch sizes in individualized brain systems: Results from the Fast-fail Trial in Mood and Anxiety Spectrum Disorders (FAST-MAS). *Neuropsychopharmacology*.

Fung, H., and Hoftman, G.D. (2024). Are you maximizing your multimodal, longitudinal dataset? Toward an integrated framework for advancing psychosis research. *Biological Psychiatry: Cognitive Neuroscience and Neuroimaging*.

Fung, H., Yeo, B.T.T., Chen, C., Lo, J.C., Chee, M.W.L., and Ong, J.L. (2023). Adherence to 24h movement recommendations and health indicators in early adolescence: Cross-sectional and longitudinal associations in the ABCD study. *Journal of Adolescent Health*.

CO-AUTHORED PUBLICATIONS

Boen, R., Villalón-Reina, J.E., Kushan, L., O'Hora, K.P., Fung, H., Parker, N., et al., and Bearden, C.E. (2026). Gene dosage effects of 22q11.2 copy number variants on in-vivo measures of white matter axonal density and dispersion. *Molecular Psychiatry*.

Lin, H.Y., Fung, H., Wang, Y., Ho, R.C.M., and Chen, S.H.A. (2025). A functional magnetic resonance imaging investigation of hot and cool executive functions in reward and competition. *Sensors*.

Schleifer, C.H., Chang, S.E., Amir, C.M., O'Hora, K.P., Fung, H., Kang, J.W.D., et al., and Bearden, C.E. (2025). Unique functional neuroimaging signatures of genetic versus clinical high risk for psychosis. *Biological Psychiatry*.

Schleifer, C.H., O'Hora, K.P., Fung, H., Xu, J., Robinson, T.A., Wu, A.S., et al., and Bearden, C.E. (2024). Effects of gene dosage and development on subcortical nuclei volumes in individuals with 22q11.2 copy number variations. *Neuropsychopharmacology*.

Gilbert, S.J., and Fung, H. (2018). Decoding intentions of self and others from fMRI. *NeuroImage*.

Gopnik, A., O'Grady, S., Lucas, C., Griffiths, T., Wente, A., Bridger, S., Aboody, R., Fung, H., and Dahl, R. (2017). Changes in cognitive flexibility and hypothesis search from childhood to adolescence to adulthood. *Proceedings of the National Academy of Sciences*.

INTRODUCTION

This dissertation is motivated by the goal of identifying the neurobiological mechanisms underlying psychiatric and neurodevelopmental disorders. Current psychiatric nosology, as codified in diagnostic systems such as the Diagnostic and Statistical Manual of Mental Disorders (DSM; (1)), relies on operationalized, symptom-based diagnostic criteria. These criteria have demonstrated clinical utility and diagnostic reliability (2), but they were derived independently of neurobiology and do not necessarily correspond to distinct, biologically validated systems (3). Individuals who meet criteria for the same diagnosis can differ considerably in underlying etiology and biological pathophysiology despite sharing a common clinical presentation (4). Conversely, distinct diagnostic categories frequently overlap in their clinical and biological features. Schizophrenia, a psychosis-spectrum disorder typically diagnosed in adolescence or adulthood, is characterized by positive symptoms such as delusions and hallucinations. Autism spectrum disorder (ASD), a neurodevelopmental condition typically diagnosed in early childhood, is characterized by persistent difficulties in social communication and interaction, together with restricted or repetitive behaviors, interests, or activities (1). Despite being formally distinct diagnoses, the two conditions share social communication deficits, negative-symptoms such as diminished emotional expression, and impairments in social cognition, executive function, and language ability, as well as overlapping biological causes, including shared genetic risk factors (5).

From Diagnosis-First to Genetics-First Approaches

The heterogeneity inherent to recruiting individuals by diagnosis has practical consequences for psychiatric research. Case-control samples defined by diagnosis alone are likely to combine individuals whose symptoms arise through distinct underlying biological pathways, which can obscure or dilute neurobiological signals that are present in only a subset of the sample. An alternative strategy, often termed a genetics-first approach, begins instead with a well-defined genetic variant of known effect and characterizes its neurobiological and behavioral consequences directly, irrespective of clinical diagnosis. Because the genetic starting point is held constant across carriers, this approach reduces etiological heterogeneity relative to diagnosis-first designs and enables prospective study of clinical outcomes. It also allows direct characterization of penetrance, the proportion of carriers who develop a given phenotype, and pleiotropy, the tendency of a single genetic variant to give rise to multiple distinct phenotypic outcomes across carriers (6).

Rare Copy Number Variants as a Genetics-First Entry Point

Copy number variants (CNVs), deletions or duplications of segments of chromosomal DNA, offer a particularly tractable entry point for a genetics-first approach. CNVs are an important source of genetic diversity in humans, and most are benign or have modest phenotypic consequences (7). A subset of rare, recurrent CNVs, however, confer substantially elevated risk for neuropsychiatric and neurodevelopmental disorders. Certain regions of the genome are structurally prone to recurrent deletion or duplication, causing the same CNV to arise independently in unrelated individuals across the population. This recurrence allows researchers to identify multiple unrelated

carriers of the same high-risk variant, making it possible to study these variants in cohorts (8). For instance, deletions at the 22q11.2 and 3q29 loci, and duplications at the 16p11.2 locus, are among the CNVs most strongly and consistently associated with schizophrenia (9). Notably, these CNVs also confer elevated risk for ASD (10). This dissertation focuses on two of these loci, 22q11.2 and 3q29.

Reciprocal 22q11.2 Copy Number Variants

The 22q11.2 locus, on the long arm of chromosome 22, is flanked by low-copy repeat sequences that predispose it to non-allelic homologous recombination. When this recombination occurs, it most commonly results in either a missing or an extra copy of the intervening genomic segment, giving rise to a reciprocal CNV: a hemizygous deletion (22qDel) or a duplication (22qDup) of the same region (11).

22qDel, also known as 22q11.2 deletion syndrome or velocardiofacial/DiGeorge syndrome, is the most common contiguous gene deletion syndrome, with prevalence most commonly cited as approximately 1 in 4,000 live births, though estimates range from 1 in 2,000 to 1 in 6,000 depending on ascertainment method (e.g., (12–14)). It is a multisystem condition, with common manifestations including congenital heart defects, palatal abnormalities, immune deficiency, and endocrine dysfunction (14). 22qDel is also one of the strongest known single-locus genetic risk factors for schizophrenia identified to date, conferring an approximately 20- to 25-fold increase in risk (15), and is associated with substantially elevated rates of ASD and intellectual disability (ID) (12).

22qDup is the reciprocal of 22qDel, arising at the same locus and of comparable size, though it is a more recently characterized and less commonly ascertained CNV (16), with an estimated prevalence of approximately 1 in 1,600 live births (12). It affects many of the same organ systems as 22qDel, including developmental delay, craniofacial abnormalities, and cardiovascular defects (17), though manifestations are generally milder and more heterogeneous, and many carriers are clinically unaffected (16). It is associated with reduced risk for schizophrenia relative to the general population (18), while independently conferring elevated risk for ASD and ID (12).

This pattern, in which the same reciprocal CNV gives rise to shared risk for some disorders (e.g., ASD and ID) and diverging risk for another (schizophrenia) depending on copy number, makes 22q11.2 a particularly informative model for studying neurodevelopmental and psychiatric risk within a single genetic framework, and for dissociating shared neurodevelopmental vulnerability from copy-number-dependent risk pathways.

3q29 Deletion Syndrome

Another CNV relevant to this dissertation is a recurrent microdeletion at the 3q29 locus, spanning approximately 1.6 megabases and affecting 21 protein-coding genes (19), with an estimated prevalence of approximately 1 in 30,000 live births (20). Like 22qDel, 3q29 deletion syndrome (3q29Del) is a rare, highly penetrant CNV associated with a range of physical and neurodevelopmental manifestations, including congenital anomalies, gastrointestinal and feeding difficulties, and mild-to-moderate intellectual disability (21). 3q29Del confers more than a 40-fold increase in schizophrenia risk

relative to the general population, among the largest known genetic risk effects for the disorder (22). It is also associated with elevated rates of ASD and ID (21).

Together, 22qDel and 3q29Del illustrate that highly penetrant risk for schizophrenia and ASD can arise from genomically distinct regions, providing an opportunity to test whether these two loci share convergent downstream neurobiological mechanisms, or instead confer risk through distinct, locus-specific pathways.

Neuroimaging Correlates of 22q11.2 and 3q29 CNVs

Cortical and subcortical brain structure and function have been relatively well characterized in 22qDel, with more limited investigation of 22qDup. Structurally, 22qDel carriers consistently show widespread morphological differences relative to typically developing (TD) controls, including smaller intracranial, gray matter, and white matter volume, reduced cortical surface area, increased cortical thickness, smaller hippocampal volume, and larger corpus callosum volume (23–29). Effects in 22qDup are generally subtler and more heterogeneous, with many measures resembling controls and a subset of measures showing effects in the opposite direction from 22qDel (27,29). For white matter microstructure, diffusion imaging studies have reported opposing effects of 22qDel and 22qDup on measures such as fractional anisotropy and neurite density (30,31). Resting-state functional connectivity studies have identified widespread dysconnectivity in 22qDel involving cortical, thalamic, and hippocampal circuits (32–34), with more limited evidence in 22qDup suggesting a partially opposing pattern in select circuits (35).

Neuroimaging in 3q29Del remains considerably more limited, reflecting both the rarity of the deletion and the recency of dedicated 3q29Del neuroimaging cohorts (36). Existing findings on cortical and subcortical structure are sparse, drawn mostly from case reports and radiological observations. By contrast, the cerebellum and posterior fossa have received more targeted attention, motivated by radiological findings of posterior fossa abnormalities in 3q29Del carriers (37), with the first case-control quantitative neuroimaging study in this syndrome, published in 2024, focusing specifically on this region (38).

The Cerebellum: From Motor Structure to Neuropsychiatric Relevance

One brain structure whose role in this broader neurobiological account of psychiatric illness has undergone a particularly striking reconceptualization is the cerebellum. Long conceptualized as a primarily motor structure, the cerebellum has undergone a substantial paradigm shift over the past several decades, with anatomical, lesion, and neuroimaging evidence establishing its contribution to nonmotor function, including cognitive, linguistic, and affective processing (39).

Anatomically, the cerebellum is located at the posterior base of the brain, beneath the occipital and temporal lobes and behind the brainstem. Although it accounts for only approximately 10% of total brain volume, it contains a majority of the brain's neurons, at approximately 80% of the total (40). The cerebellar cortex is organized into ten lobules (I–X), grouped into anterior (lobules I–V), posterior (lobules VI–IX), and flocculonodular (lobule X) lobes, with a midline vermis flanked by two lateral hemispheres (41). Structurally, the cerebellum's connections with the rest of the brain

are relayed through the deep cerebellar nuclei and three pairs of cerebellar peduncles, the primary white matter pathways carrying input to and output from the cerebellum. Cortical input reaches the cerebellum indirectly via the pons, while cerebellar output projects back to the cerebral cortex via the thalamus, together forming closed-loop cortico-cerebellar circuits that link the cerebellum not only to primary motor and sensory cortex but also to prefrontal, parietal, and temporal association cortices (39).

Consistent with this anatomical connectivity, large-scale connectivity studies have shown that cerebellar territories are functionally coupled with cortical networks supporting cognition, language, social processing, and affect, as well as motor and sensory function (42). Anterior and medial cerebellar regions are more consistently linked to motor and sensorimotor processing, and posterior regions to higher-order cognitive and social-affective processing (43), though the boundaries between these functional territories are graded rather than sharply defined (44). Notably, functional parcellations derived directly from task-based activation do not align closely with traditional anatomical lobule boundaries, indicating that functional and anatomical organization of the cerebellum are only partially concordant (45).

This non-motor functional organization has clinical relevance for neuropsychiatric illness. Damage to the posterior cerebellum can lead to executive dysfunction, impaired spatial cognition, personality change, and language deficits, together termed the cerebellar cognitive affective syndrome (CCAS) by Schmahmann and Sherman (46). Associated behavioral changes have since been shown to span autism-spectrum-like and psychosis-spectrum-like symptom domains as well (47). Consistent with this,

cerebellar alterations have been reported in schizophrenia spectrum disorders, including posterior volume reductions in left Crus II and right lobules VI and VIII (48). Cerebello-thalamo-cortical dysconnectivity has also been reported, with reduced connectivity to prefrontal and thalamic regions and increased connectivity to motor, somatosensory, and orbitofrontal regions (49). In ASD, structural cerebellar alterations have similarly been reported in the posterior cerebellum, including volume reductions in right Crus I, left lobule VIIIB and vermis IX (50), alongside cortico-cerebellar dysconnectivity, with hyperconnectivity in sensorimotor regions and hypoconnectivity in cognitive/social regions (51).

The Cerebellum: Understudied in Schizophrenia- and Autism-Associated CNVs

Despite this broader evidence for cerebellar involvement in neuropsychiatric illness, the cerebellum has received comparatively little attention in this population. Prior whole-brain studies of 22qDel occasionally included the cerebellum, and had consistently reported reduced global volume across studies spanning childhood, adolescence, and adulthood (52–57). A recent paper focused on regional cerebellar volume in 22qDel found widespread reductions at the lobule level (58); however, no such characterization existed for 22qDup. Beyond structural volume, cerebellar white matter microstructure and functional connectivity remain largely uncharacterized in either CNV.

In 3q29Del, one recent study has reported reduced total cerebellar gray matter volume in 3q29Del relative to controls, along with reductions in several cerebellar subregions (38). However, this structural finding had not yet been compared to

cerebellar phenotypes in other high-risk CNVs. It therefore remains unknown whether cerebellar vulnerability in 3q29Del reflects a signature shared with 22qDel, or a CNV-specific pattern.

Research Questions and Dissertation Overview

This dissertation addresses three overarching questions: (1) How do 22q11.2 deletion and duplication affect cerebellar organization? (2) Do these alterations relate to cognitive, social, and psychosis-related phenotypes? and (3) Does cerebellar vulnerability extend beyond 22q11.2 to an independent, genetically distinct CNV associated with neuropsychiatric risk? These questions are addressed across three manuscripts that progressively examine cerebellar morphology, multimodal organization, and cross-CNV convergence.

The first manuscript, "Convergent and Divergent Cerebellar Alterations in 22q11.2 Copy Number Variants" (published; *Biological Psychiatry: Global Open Science*), establishes the cerebellar morphological phenotype of reciprocal 22q11.2 CNVs. Using fine-grained regional parcellation, it tests whether 22qDel and 22qDup show convergent or divergent patterns of cerebellar volume alteration relative to typically developing (TD) controls. It further examines whether distributed patterns of cerebellar morphology relate to cognitive ability, social functioning, and psychosis-risk symptoms.

The second manuscript, "Multimodal Cerebellar Alterations Reveal Distinct Effects of 22q11.2 Deletion and Duplication," asks whether the morphological

phenotype identified in the first study extends to other levels of cerebellar organization. It characterizes cerebellar white matter microstructure and resting-state functional connectivity in 22qDel, 22qDup, and TD controls, then integrates these measures with regional volume to determine whether macrostructure, white matter microstructure, and functional coupling show convergent or dissociable effects of 22q11.2 copy number. Multimodal analyses further test whether these complementary features distinguish CNV groups and capture variation in cognitive, social, and psychosis-risk phenotypes. Together, the first two manuscripts move from regional morphology to a broader, multimodal characterization of how reciprocal 22q11.2 dosage affects cerebellar organization and its relationship to neurobehavioral variation.

The third and final manuscript, "Convergent and Divergent Cerebellar Alterations Across High-Risk Neuropsychiatric Copy Number Variants," asks whether the cerebellar vulnerability observed in 22qDel is specific to the 22q11.2 locus or converges with that produced by an independent genetic risk factor. It directly compares cerebellar volume in 22qDel and 3q29 deletion syndrome (3q29Del), two genomically distinct CNVs associated with high risk for both schizophrenia and ASD. Because these two CNVs were recruited and scanned independently at two different sites, the study uses normative modeling to place individual cerebellar volumes on a common standardized deviation scale relative to a large independent reference population, enabling comparison of the magnitude and regional distribution of cerebellar alterations across CNVs. Together, these three manuscripts trace a progression from identifying cerebellar alterations within a reciprocal gene-dosage model, to determining whether those effects converge or dissociate across structural, microstructural, and functional levels, to testing

whether cerebellar vulnerability converges across distinct genomic loci. In doing so, this dissertation uses a genetics-first framework to distinguish neurobiological features that are sensitive to 22q11.2 gene dosage from those that may represent broader points of convergence across genetically distinct forms of neuropsychiatric risk.

References

1. American Psychiatric Association (2022): *Diagnostic and Statistical Manual of Mental Disorders, Fifth Edition, Text Revision (DSM-5-TR®): Test Questions for the Diagnostic Criteria* ((P. R. Muskin, A. L. Dickerman, A. Drysdale, & C. C. Holderness, editors)). Arlington, TX: American Psychiatric Association Publishing.
2. Kendell R, Jablensky A (2003): Distinguishing between the validity and utility of psychiatric diagnoses. *Am J Psychiatry* 160: 4–12.
3. Insel T, Cuthbert B, Garvey M, Heinssen R, Pine DS, Quinn K, *et al.* (2010): Research domain criteria (RDoC): toward a new classification framework for research on mental disorders. *Am J Psychiatry* 167: 748–751.
4. Cuthbert BN, Insel TR (2013): Toward the future of psychiatric diagnosis: the seven pillars of RDoC. *BMC Med* 11: 126.
5. Jutla A, Foss-Feig J, Veenstra-VanderWeele J (2022): Autism spectrum disorder and schizophrenia: An updated conceptual review. *Autism Res* 15: 384–412.
6. Fiksinski AM, Hoftman GD, Vorstman JAS, Bearden CE (2023): A genetics-first approach to understanding autism and schizophrenia spectrum disorders: the 22q11.2 deletion syndrome. *Mol Psychiatry* 28: 341–353.
7. Zhang F, Gu W, Hurles ME, Lupski JR (2009): Copy number variation in human health, disease, and evolution. *Annu Rev Genomics Hum Genet* 10: 451–481.
8. Malhotra D, Sebat J (2012): CNVs: harbingers of a rare variant revolution in psychiatric genetics. *Cell* 148: 1223–1241.

9. Owen MJ, Legge SE, Rees E, Walters JTR, O'Donovan MC (2023): Genomic findings in schizophrenia and their implications. *Mol Psychiatry* 28: 3638–3647.

10. Willsey HR, Willsey AJ, Wang B, State MW (2022): Genomics, convergent neuroscience and progress in understanding autism spectrum disorder. *Nat Rev Neurosci* 23: 323–341.

11. Edelmann L, Pandita RK, Spiteri E, Funke B, Goldberg R, Palanisamy N, *et al.* (1999): A common molecular basis for rearrangement disorders on chromosome 22q11. *Hum Mol Genet* 8: 1157–1167.

12. Olsen L, Sparsø T, Weinsheimer SM, Dos Santos MBQ, Mazin W, Rosengren A, *et al.* (2018): Prevalence of rearrangements in the 22q11.2 region and population-based risk of neuropsychiatric and developmental disorders in a Danish population: a case-cohort study. *Lancet Psychiatry* 5: 573–580.

13. Blagojevic C, Heung T, Theriault M, Tomita-Mitchell A, Chakraborty P, Kernohan K, *et al.* (2021): Estimate of the contemporary live-birth prevalence of recurrent 22q11.2 deletions: a cross-sectional analysis from population-based newborn screening. *CMAJ Open* 9: E802–E809.

14. McDonald-McGinn DM, Sullivan KE, Marino B, Philip N, Swillen A, Vorstman JAS, *et al.* (2015): 22q11.2 deletion syndrome. *Nat Rev Dis Primers* 1: 15072.

15. Brzustowicz LM, Bassett AS (2012): miRNA-mediated risk for schizophrenia in 22q11.2 deletion syndrome. *Front Genet* 3: 291.

16. Portnoï M-F (2009): Microduplication 22q11.2: a new chromosomal syndrome. *Eur J Med Genet* 52: 88–93.

17. Yu A, Turbiville D, Xu F, Ray JW, Britt AD, Lupo PJ, *et al.* (2019): Genotypic and phenotypic variability of 22q11.2 microduplications: An institutional experience. *Am J Med Genet A* 179: 2178–2189.

18. Rees E, Kirov G, Sanders A, Walters JTR, Chambert KD, Shi J, *et al.* (2014): Evidence that duplications of 22q11.2 protect against schizophrenia. *Mol Psychiatry* 19: 37–40.

19. Yilmaz F, Gurusamy U, Mosley TJ, Hallast P, Kim K, Mostovoy Y, *et al.* (2023): High level of complexity and global diversity of the 3q29 locus revealed by optical mapping and long-read sequencing. *Genome Med* 15: 35.

20. Glassford MR, Rosenfeld JA, Freedman AA, Zwick ME, Mulle JG, Unique Rare Chromosome Disorder Support Group (2016): Novel features of 3q29 deletion syndrome: Results from the 3q29 registry: Novel Features of 3q29 Deletion Syndrome. *Am J Med Genet A* 170A: 999–1006.

21. Mulle JG, Dodd AF, McGrath JA, Wolyniec PS, Mitchell AA, Shetty AC, *et al.* (2010): Microdeletions of 3q29 confer high risk for schizophrenia. *Am J Hum Genet* 87: 229–236.

22. Mulle JG (2015): The 3q29 deletion confers >40-fold increase in risk for schizophrenia. *Mol Psychiatry* 20: 1028–1029.

23. Modenato C, Kumar K, Moreau C, Martin-Brevet S, Huguet G, Schramm C, *et al.* (2021): Effects of eight neuropsychiatric copy number variants on human brain structure. *Transl Psychiatry* 11: 399.

24. Sun D, Ching CRK, Lin A, Forsyth JK, Kushan L, Vajdi A, *et al.* (2020): Large-scale mapping of cortical alterations in 22q11.2 deletion syndrome: Convergence with idiopathic psychosis and effects of deletion size. *Mol Psychiatry* 25: 1822–1834.

25. Ching CRK, Gutman BA, Sun D, Villalon Reina J, Ragothaman A, Isaev D, *et al.* (2020): Mapping subcortical brain alterations in 22q11.2 deletion syndrome: Effects of deletion size and convergence with idiopathic neuropsychiatric illness. *Am J Psychiatry* 177: 589–600.

26. Kumar K, Modenato C, Moreau C, Ching CRK, Harvey A, Martin-Brevet S, *et al.* (2023): Subcortical brain alterations in carriers of genomic copy number variants. *Am J Psychiatry* 180: 685–698.

27. Schleifer CH, O'Hora KP, Fung H, Xu J, Robinson T-A, Wu AS, *et al.* (2024): Effects of gene dosage and development on subcortical nuclei volumes in individuals with 22q11.2 copy number variations. *Neuropsychopharmacology* 49: 1024–1032.

28. Jalbrzikowski M, Lin A, Vajdi A, Grigoryan V, Kushan L, Ching CRK, *et al.* (2022): Longitudinal trajectories of cortical development in 22q11.2 copy number variants and typically developing controls. *Mol Psychiatry* 27: 4181–4190.

29. Lin A, Ching CRK, Vajdi A, Sun D, Jonas RK, Jalbrzikowski M, *et al.* (2017): Mapping 22q11.2 gene dosage effects on brain morphometry. *J Neurosci* 37: 6183–6199.

30. Seitz-Holland J, Lyons M, Kushan L, Lin A, Villalon-Reina JE, Cho KIK, *et al.* (2021): Opposing white matter microstructure abnormalities in 22q11.2 deletion and duplication carriers. *Transl Psychiatry* 11: 580.

31. Boen R, Villalón-Reina JE, Kushan L, O'Hora KP, Fung H, Parker N, *et al.* (2026): Gene dosage effects of 22q11.2 copy number variants on in-vivo measures of white matter axonal density and dispersion. *Mol Psychiatry* 31: 3687–3698.

32. Debbané M, Lazouret M, Lagioia A, Schneider M, Van De Ville D, Eliez S (2012): Resting-state networks in adolescents with 22q11.2 deletion syndrome: associations with prodromal symptoms and executive functions. *Schizophr Res* 139: 33–39.

33. Mattiaccio LM, Coman IL, Schreiner MJ, Antshel KM, Fremont WP, Bearden CE, Kates WR (2016): Atypical functional connectivity in resting-state networks of individuals with 22q11.2 deletion syndrome: associations with neurocognitive and psychiatric functioning. *J Neurodev Disord* 8: 2.

34. Schleifer C, Lin A, Kushan L, Ji JL, Yang G, Bearden CE, Anticevic A (2019): Dissociable disruptions in thalamic and hippocampal resting-state functional connectivity in youth with 22q11.2 deletions. *J Neurosci* 39: 1301–1319.

35. Moreau CA, Urchs SGW, Kuldeep K, Orban P, Schramm C, Dumas G, *et al.* (2020): Mutations associated with neuropsychiatric conditions delineate functional brain connectivity dimensions contributing to autism and schizophrenia. *Nat Commun* 11: 5272.

36. Murphy MM, Lindsey Burrell T, Cubells JF, España RA, Gambello MJ, Goines KCB, *et al.* (2018): Study protocol for The Emory 3q29 Project: evaluation of neurodevelopmental, psychiatric, and medical symptoms in 3q29 deletion syndrome. *BMC Psychiatry* 18: 183.

37. Sanchez Russo R, Gambello MJ, Murphy MM, Aberizk K, Black E, Burrell TL, *et al.* (2021): Deep phenotyping in 3q29 deletion syndrome: recommendations for clinical care. *Genet Med* 23: 872–880.

38. Sefik E, Duan K, Li Y, Sholar B, Evans L, Pincus J, *et al.* (2024): Structural deviations of the posterior fossa and the cerebellum and their cognitive links in a neurodevelopmental deletion syndrome. *Mol Psychiatry* 29: 3395–3411.

39. Schmahmann JD, Guell X, Stoodley CJ, Halko MA (2019): The theory and neuroscience of cerebellar cognition. *Annu Rev Neurosci* 42: 337–364.

40. Azevedo FAC, Carvalho LRB, Grinberg LT, Farfel JM, Ferretti REL, Leite REP, *et al.* (2009): Equal numbers of neuronal and nonneuronal cells make the human brain an isometrically scaled-up primate brain. *J Comp Neurol* 513: 532–541.

41. Schmahmann JD, Doyon J, McDonald D, Holmes C, Lavoie K, Hurwitz AS, *et al.* (1999): Three-dimensional MRI atlas of the human cerebellum in proportional stereotaxic space. *Neuroimage* 10: 233–260.

42. Buckner RL, Krienen FM, Castellanos A, Diaz JC, Yeo BTT (2011): The organization of the human cerebellum estimated by intrinsic functional connectivity. *J Neurophysiol* 106: 2322–2345.

43. Stoodley CJ, Schmahmann JD (2009): Functional topography in the human cerebellum: a meta-analysis of neuroimaging studies. *Neuroimage* 44: 489–501.

44. Guell X, Schmahmann JD, Gabrieli JDE, Ghosh SS (2018): Functional gradients of the cerebellum. *Elife* 7: e36652.

45. King M, Hernandez-Castillo CR, Poldrack RA, Ivry RB, Diedrichsen J (2019): Functional boundaries in the human cerebellum revealed by a multi-domain task battery. *Nat Neurosci* 22: 1371–1378.

46. Schmahmann JD, Sherman JC (1998): The cerebellar cognitive affective syndrome. *Brain* 121 (Pt 4): 561–579.

47. Schmahmann JD, Weilburg JB, Sherman JC (2007): The neuropsychiatry of the cerebellum - insights from the clinic. *Cerebellum* 6: 254–267.

48. Li X, Liu N, Yang C, Zhang W, Lui S (2022): Cerebellar gray matter volume changes in patients with schizophrenia: A voxel-based meta-analysis. *Front Psychiatry* 13: 1083480.

49. Lányi O, Zahemszky D, Wenning AS, Engh MA, Molnár Z, Horváth AA, *et al.* (2026): Cerebello-thalamo-cortical dysconnectivity in schizophrenia spectrum disorders: A resting-state functional magnetic resonance imaging meta-analysis. *Biol Psychiatry Cogn Neurosci Neuroimaging* 11: 329–346.

50. Stoodley CJ (2014): Distinct regions of the cerebellum show gray matter decreases in autism, ADHD, and developmental dyslexia. *Front Syst Neurosci* 8: 92.

51. Khan AJ, Nair A, Keown CL, Datko MC, Lincoln AJ, Müller R-A (2015): Cerebro-cerebellar resting-state functional connectivity in children and adolescents with autism spectrum disorder. *Biol Psychiatry* 78: 625–634.

52. Gothelf D, Penniman L, Gu E, Eliez S, Reiss AL (2007): Developmental trajectories of brain structure in adolescents with 22q11.2 deletion syndrome: a longitudinal study. *Schizophr Res* 96: 72–81.

53. van Amelsvoort T, Daly E, Robertson D, Suckling J, Ng V, Critchley H, *et al.* (2001): Structural brain abnormalities associated with deletion at chromosome 22q11: quantitative neuroimaging study of adults with velo-cardio-facial syndrome. *Br J Psychiatry* 178: 412–419.

54. van Amelsvoort T, Daly E, Henry J, Robertson D, Ng V, Owen M, *et al.* (2004): Brain anatomy in adults with velocardiofacial syndrome with and without schizophrenia: preliminary results of a structural magnetic resonance imaging study: Preliminary results of a structural magnetic resonance imaging study. *Arch Gen Psychiatry* 61: 1085–1096.

55. Campbell LE, Daly E, Toal F, Stevens A, Azuma R, Catani M, *et al.* (2006): Brain and behaviour in children with 22q11.2 deletion syndrome: a volumetric and voxel-based morphometry MRI study. *Brain* 129: 1218–1228.

56. Bish JP, Pendyal A, Ding L, Ferrante H, Nguyen V, McDonald-McGinn D, *et al.* (2006): Specific cerebellar reductions in children with chromosome 22q11.2 deletion syndrome. *Neurosci Lett* 399: 245–248.

57. Shashi V, Kwapil TR, Kaczorowski J, Berry MN, Santos CS, Howard TD, *et al.* (2010): Evidence of gray matter reduction and dysfunction in chromosome 22q11.2 deletion syndrome. *Psychiatry Res* 181: 1–8.

58. Schmitt JE, DeBevits JJ, Roalf DR, Ruparel K, Gallagher RS, Gur RC, *et al.* (2023): A comprehensive analysis of cerebellar volumes in the 22q11.2 deletion syndrome. *Biol Psychiatry Cogn Neurosci Neuroimaging* 8: 79–90.

CHAPTER 1: CONVERGENT AND DIVERGENT CEREBELLAR ALTERATIONS IN 22q11.2 COPY NUMBER VARIANTS

Hoki Fung[1,2], Kathleen P. O'Hora[1,2], Rune Boen[1], Haley R. Wang[1,3], Carolyn M. Amir[1,2], Charles H. Schleifer[1,2], Leila Kushan-Wells[1], Blake A. Miranda[2,3], Elizabeth K. Bondy[1], Paul J. Mathews[4,5], Carrie E. Bearden[1,3]

1. Department of Psychiatry and Biobehavioral Sciences, Semel Institute for Neuroscience and Human Behavior, University of California, Los Angeles, CA, USA.
2. Neuroscience Interdepartmental Program, University of California Los Angeles, Los Angeles, CA, USA
3. Department of Psychology, University of California, Los Angeles, CA, USA.
4. Department of Neurology, University of California, Los Angeles School of Medicine, Los Angeles, Los Angeles, CA, USA.
5. The Lundquist Institute at Harbor-UCLA, Torrance, CA, USA

A version of this chapter has been published in Biological Psychiatry: Global Open Science (2026).

ABSTRACT

Background

Copy number variants (CNVs) at 22q11.2 confer substantial risk for neurodevelopmental and psychiatric disorders. Both the 22q11.2 deletion (22qDel) and duplication (22qDup) are associated with increased risk for autism spectrum disorder and intellectual disability. In contrast, while 22qDel markedly increases risk for schizophrenia, 22qDup may be protective. Prior neuroimaging work has focused primarily on the cerebrum, leaving cerebellar contributions understudied despite growing evidence for their relevance to cognition and psychopathology. Here, we characterize regional cerebellar structure and examine multivariate cerebellar–behavior associations in individuals with reciprocal 22q11.2 CNVs.

Methods

We analyzed 514 structural MRI scans from 315 participants (mean age = 16.4 ± 8.8 years; 52% female), comprising 22qDel carriers (n=111), 22qDup carriers (n=37), and typically developing (TD) controls (n=167). The cerebellum was parcellated into 28 subregions using ACAPULCO. Group differences in total and regional cerebellar volumes were examined using linear mixed-effects models with FDR correction. Multivariate brain–behavior associations were assessed using partial least squares correlation (PLSC).

Results

Relative to TD controls, 22qDel carriers showed widespread cerebellar volume reductions, whereas alterations in 22qDup were milder and regionally selective. Vermis VII was reduced in both 22q11.2 CNVs, indicating a shared site of anatomical vulnerability. PLSC identified domain-specific cerebellar patterns, with posterior regions—most prominently bilateral Lobule VIIIA—associated with cognitive and social functioning, and bilateral Crus II and medial regions associated with psychosis-risk symptoms.

Conclusions

Reciprocal 22q11.2 CNVs show shared and divergent cerebellar alterations, with distinct subregions contributing to different behavioral domains, underscoring the cerebellum's multifaceted role in neurodevelopment and psychiatric disease risk.

INTRODUCTION

Copy number variants (CNVs; i.e., deletions or duplications) at the 22q11.2 locus have a profound impact on neurodevelopment and clinical outcomes, encompassing a wide range of cognitive, psychiatric, and socio-affective symptoms (1–3). 22q11.2 deletion (22qDel), a hemizygous deletion of ~1.5–2.6 Megabases on the long arm of chromosome 22, is the most common contiguous gene deletion syndrome, occurring in ~1 in 3,700 live births (4). Along with craniofacial abnormalities, congenital heart defects, and other medical conditions, 22qDel confers greatly increased likelihood of developmental neuropsychiatric disorders including autism spectrum disorder (ASD), intellectual disability (ID), attention deficit hyperactivity disorder (ADHD), and anxiety disorders (1). Notably, 22qDel is one of the strongest known genetic risk factor for schizophrenia, with ~1 in 10 carriers meeting diagnostic criteria (5) and approximately one-third exhibiting clinically significant sub-threshold psychosis symptoms (6,7).

The 22q11.2 duplication (22qDup) is the reciprocal of the 22qDel, occurring at the same locus and typically of comparable size (8). It affects many of the same bodily systems and may also be associated with developmental delays, craniofacial abnormalities, cardiovascular defects, and other congenital abnormalities (9). Common neurobehavioral features include learning difficulties, motor impairment, attention deficits, and social and behavioral problems (10). Clinical and behavioral manifestations are generally milder and more heterogeneous than in 22qDel, and many individuals appear clinically unaffected (4). Consistent with this, the 22qDup is often under-ascertained clinically and may be more common in the general population than 22qDel, with an estimated prevalence of ~1 in 1,600 live births (4). Despite its overall milder

presentation, the 22qDup is associated with elevated risk for several neurodevelopmental and psychiatric conditions, including ASD, ID, ADHD, and anxiety disorders, at levels comparable to 22qDel (4,11,12). In contrast, 22qDup does not confer the same elevated risk for schizophrenia and may even be associated with reduced risk relative to the general population (4,13,14). Together, this combination of shared neurodevelopmental features and divergent psychosis risk positions reciprocal 22q11.2 CNVs as a powerful genetics-first model for dissecting neurobiological mechanisms underlying shared and divergent cognitive, socio-affective, and psychiatric vulnerabilities.

Despite this compelling premise, neuroimaging data on 22qDup carriers remain scarce; our recent findings nevertheless indicate that copy number variation at the 22q11.2 locus is associated with systematic differences in brain morphology across a number of metrics (7,15–21). Across studies, two general patterns have emerged. First, 22qDel carriers consistently exhibit widespread reductions across multiple brain metrics, including intracranial, gray, and white matter volumes, on average, relative to controls (15–17,22). Second, structural findings in 22qDup carriers are generally subtler and more heterogeneous, with many measures resembling typically developing (TD) controls and only a subset exhibiting opposing effects relative to 22qDel. For instance, 22qDel is associated with reduced cortical surface area, increased cortical thickness, smaller hippocampal volume, larger corpus callosum volume and higher fractional anisotropy assessed via diffusion weighted imaging, whereas 22qDup carriers show the opposite pattern (15,19,20). Together, these findings provide initial evidence that copy-number–dependent effects at the 22q11.2 locus are selective rather than uniformly

symmetric across brain measures, underscoring the need for targeted characterization of neural systems relevant to cognition, autism-related traits, and psychosis risk.

The cerebellum is of particular relevance in this context. The cerebellum contains up to 80% of all neurons in the human brain, despite only representing 10% of total brain mass (23). While traditionally viewed as a motor structure, the cerebellum has become of increasing interest as a critical hub for cognitive, affective, and social processing, with rapidly growing evidence for altered development in neuropsychiatric and neurodevelopmental disorders, including schizophrenia and ASD (24). Neuroimaging studies have revealed a topographic organization of the cerebellum, with motor functions localized to the anterior lobe and part of lobules IV and VIII, cognitive functions to the posterior lobe—primarily lobule VII—and affective processes to the posterior vermis and adjacent regions (25–27). Reduced cerebellar grey matter volume has been consistently reported in idiopathic schizophrenia, with widespread reductions across multiple cerebellar lobules. These reductions are most pronounced in posterior regions linked to higher-order cognitive networks, while anterior, motor-related regions appear relatively less affected (28). Findings in idiopathic ASD are less consistent, with reports of both increased and decreased total cerebellar volumes, but converging evidence implicates cerebellar regions that support social and cognitive functions (29,30).

Within this framework, genetically defined CNV populations offer a unique opportunity to examine cerebellar contributions to behavioral features and clinical risks in a more etiologically homogeneous manner. In 22qDel, reduced total cerebellar volume has been consistently observed across cross-sectional studies conducted in

childhood, adolescence, and adulthood (31–36), yet regional characterization remains limited, with only one study to date reporting widespread lobular reductions at fine anatomical resolution (37). In contrast, cerebellar structure has not been systematically examined in 22qDup. Consequently, it is unknown whether cerebellar alterations are present in 22qDup, whether they overlap with or diverge from those observed in 22qDel, and how such patterns may relate to shared versus distinct neurobehavioral phenotypes across the two CNVs.

Addressing this gap is particularly important given accumulating evidence that individuals with 22qDup exhibit clinically meaningful impairments in cognition and social functioning (12), despite the absence of elevated psychosis risk. Direct comparison of cerebellar structure between 22qDel and 22qDup therefore provides a critical opportunity to disentangle cerebellar alterations associated with shared neurodevelopmental vulnerabilities from those that may contribute to divergent psychiatric outcomes, including psychosis.

Here, we investigate volumetric differences in the cerebellum and its subregions across individuals with 22q11.2 deletions, duplications, and TD controls, leveraging the largest structural magnetic resonance imaging (MRI) dataset of 22qDup currently available. Guided by prior work, we hypothesize that cerebellar volumes will differ across CNV groups, with both shared and CNV-specific patterns revealed through direct comparison of 22qDel and 22qDup. We address these aims using ACAPULCO, a novel deep-learning–based cerebellar parcellation method (38), applied to the largest MRI sample of reciprocal 22q11.2 CNVs available to date. To assess functional relevance, we further employ a data-driven multivariate approach using partial least squares

correlation (PLSC) to examine patterns of covariation between cerebellar volumes and behavioral and clinical measures. We hypothesize that cerebellar regions associated with cognitive functioning and autism-related traits will be distinct from those associated with psychosis-risk symptoms.

METHODS AND MATERIALS

Participants and Study Design

In this study, we collected 524 longitudinal structural MRI scans from 317 unique individuals across three groups: 22qDel, 22qDup, and TD controls. Participants with molecularly confirmed 22qDel or 22qDup were recruited as part of an ongoing longitudinal study at the University of California, Los Angeles (UCLA). Recruitment occurred through clinical referrals, community outreach, and research registries. TD controls were recruited from the same communities as CNV carriers. All participants underwent cognitive testing, clinical assessments, and structural MRI scanning across one to six annual visits (mean number of visits per participant = 1.63). Written informed consent (or assent with parental consent for minors) was obtained from all participants. All procedures were approved by the Institutional Review Board at UCLA. Additional recruitment and exclusion details are provided in the Supplementary Methods.

Behavioral and Clinical Measures

Cognitive ability was assessed using the Wechsler Abbreviated Scale of Intelligence (WASI or WASI-II) (39,40). Autism-related traits were measured with the Social Responsiveness Scale, Second Edition (SRS-2) (41). Psychosis-risk symptoms

were evaluated using the Structured Interview for Psychosis-Risk Syndromes (SIPS) (42). Full descriptions of each instrument, scoring procedure, and the number of available observations, are provided in the Supplementary Methods.

MRI Acquisition, Image Processing, and Harmonization

Structural MRI data were acquired at UCLA using three 3T Siemens scanners (Trio and Prisma) with standardized T1-weighted MPRAGE sequences (43). Images were visually inspected for quality, and total intracranial volume (eTIV) was estimated using FreeSurfer (v5.3/v6.0) (44). Cerebellar parcellation was performed using ACAPULCO (v3.0) (38), a state-of-the-art, deep learning-based method that automatically segments the cerebellum from raw T1-weighted images into 28 anatomically defined subregions using two cascaded convolutional networks (see Supplementary Table S2 for the full list of regions). Volumes were harmonized across scanners using Longitudinal ComBat (45). Detailed acquisition parameters, preprocessing steps, and quality-control procedures are provided in the Supplementary Methods.

Statistical Analysis

Group differences in total and regional cerebellar volumes were examined using linear mixed-effects models with fixed effects for group, sex, mean-centered age (linear and quadratic), and eTIV, with a random intercept for subject. False Discovery Rate (FDR) correction was applied across 28 subregions. Sensitivity analyses assessing robustness to current psychotropic medication use and age stratification, along with

model specifications, data transformations, and visualization methods are described in the Supplementary Methods.

To examine multivariate brain–behavior associations, we used partial least squares correlation (PLSC) to identify latent components capturing shared covariance between regional cerebellar volumes and neurobehavioral measures (46,47). Guided by prior evidence of convergent alterations in cognition and social functioning (12) and gene-dosage–dependent differences in psychosis risk in 22q11.2 CNVs (13,14), we specified two separate PLSC models: one examining cognitive ability and reciprocal social functioning, and a second examining psychosis-risk symptoms. PLSC analyses were conducted on harmonized cerebellar volumes and relevant behavioral and clinical measures, with statistical significance assessed using permutation testing. Full methodological details, including the complete list of measures included in each PLSC model, are provided in the Supplementary Methods.

RESULTS

Participant Characteristics

The full sample included 317 unique participants and 524 MRI sessions. Following parcellation quality control, 10 scans were excluded due to poor-quality cerebellar segmentations, resulting in a final analytic sample of 514 sessions from 315 participants: 111 with 22qDel, 37 with 22qDup, and 167 TD controls. Baseline demographic and behavioral characteristics of the study sample, along with group comparison statistics, are summarized in Table 1. Briefly, groups were comparable in sex and age. Both CNV groups showed lower IQ and elevated autism-related traits

versus TD controls. Psychosis symptoms were elevated in 22qDel versus both 22qDup and TD controls. These patterns are consistent with a previous cross-sectional characterization of phenotypic features of 22q11.2 CNVs in a subset of this cohort (12).

Total Cerebellar Volume

A linear mixed-effects model revealed significantly smaller total cerebellar volume in 22qDel compared to TD controls (B = −16,072.03, p < 0.001), while 22qDup displayed no significant difference to TD controls (B = 1,579.76, p = 0.46; see Supplementary Table S1 for full model output). Direct comparison between the two CNV groups indicated that total cerebellar volume was significantly smaller in 22qDel relative to 22qDup.

Regional Cerebellar Volume

To characterize regional cerebellar volume differences across groups, we conducted region-wise analyses across 28 anatomically defined regions. When TD controls were used as the reference group (Figure 1A), individuals with 22qDel showed widespread cerebellar volume reductions, with 25 of 28 regions (except bilateral Lobule IV and left Lobule V) significantly smaller after FDR correction (q < 0.05). Non-thresholded beta estimates are displayed on a cerebellar flatmap in Figure 2A, and full model results are provided in Supplementary Table S2.

In contrast, individuals with 22qDup showed a more heterogeneous pattern of regional volume differences relative to TD controls (Figure 1A). Although beta estimates suggested larger volumes in some regions and smaller volumes in others (Figure 2B),

effect sizes were generally smaller. Only Vermis VII was significantly smaller in 22qDup compared with TD controls after FDR correction ($B = -100.05$; $q < 0.05$). At the nominal threshold ($p < 0.05$), right Lobule VIIIA ($B = -358.09$, $p = 0.047$, $q = 0.36$) was smaller and Vermis IX ($B = 61.02$, $p = 0.041$, $q = 0.36$) was larger in 22qDup relative to TD controls. See Supplementary Table S2 for full model results.

Direct comparisons between the two CNV groups, implemented by reparameterizing the original models with 22qDel as the reference group (Figure 1B), revealed significantly larger regional volumes in 22qDup relative to 22qDel across the majority of cerebellar regions (20 of 28). The largest group differences were observed in Vermis IX (B = 229.48, p < 0.001), left Lobule VIIIB (B = 660.72, p < 0.001), right Crus II (B = 1228.06, p < 0.001) and the corpus medullare (B = 2098.59, p < 0.001). Full model results are provided in Supplementary Table S3.

To distinguish regions showing shared versus CNV-specific patterns of alterations, we integrated TD-referenced and 22qDel-referenced results. At the FDR-corrected level (Figure 2C–2D), Vermis VII was significantly smaller in both 22q11.2 CNV groups relative to TD controls and did not differ significantly between 22qDel and 22qDup (B = 24.93, p = 0.43), indicating a convergent reduction of comparable magnitude across CNVs (22qDel ≈ 22qDup < TD). At the nominal level, right Lobule VIIIA was smaller in both CNV groups relative to TD controls (Figure 2E) but showed significantly larger volume in 22qDup than in 22qDel ($B = 454.53$, $p = 0.02$), consistent with a graded effect (22qDel < 22qDup < TD). In contrast, Vermis IX exhibited a distinct gene-dosage–dependent pattern across groups (22qDel < TD < 22qDup; Figure 2F).

Sensitivity analyses

Adjusting for current medication use (antipsychotics, antidepressants, psychostimulants, and any psychotropic medication) and repeating analyses separately in pediatric (<18 years) and adult (≥18 years) subgroups did not alter the overall pattern or interpretation of total or regional cerebellar volume differences. Detailed results are provided in the Supplementary Results (Section 1; Supplementary Tables S4–S6).

Associations Between Cerebellar Volume and Neurobehavioral Outcomes

PLSC: Cognitive Ability and Autism-Related Traits

PLS correlation analysis identified a single significant latent component (LC; FDR-corrected $q<0.05$) capturing 95.3% of the covariance between cerebellar regional volumes and measures of cognitive ability and reciprocal social behavior. Cerebellar and behavioral composite scores were significantly correlated across all participants ($r = 0.41$, $p < 0.001$; Figure 3A), indicating a robust multivariate association between cerebellar structure and cognitive and social functioning. To characterize the nature of this association, we examined the LC loadings (Figure 3E–F). These loadings indicate that higher LC scores reflect smaller cerebellar volumes across multiple regions, lower cognitive ability, and greater autism-related social difficulties. Cerebellar contributions were strongest in posterior regions (Figure 3B), including left Lobule VIIIA ($r=-0.36$), right Lobule VIIIA ($r=-0.35$), left Lobule VIIB ($r=-0.32$), Vermis IX ($r=-0.30$), and left Lobule VI ($r=-0.29$). Together, these findings suggest that multiregional cerebellar volume reduction—particularly in Lobule VIIIA—is associated with lower cognitive ability and greater social functioning impairments across groups.

Group comparisons of LC composite scores revealed differences across groups: behavioral composite scores (i.e., reflecting lower cognitive ability and greater autism-related social difficulties) were higher in CNV groups relative to TD controls (Figure 3C), whereas cerebellar composite scores (i.e., reflecting smaller multiregional cerebellar volumes) were higher in 22qDel compared with both TD controls and 22qDup (Figure 3D). Detailed results, including within-group correlations and the full set of cerebellar and behavioral measures contributing to the latent component, are provided in the Supplementary Results.

PLSC: Psychosis-Risk Symptoms

PLS correlation analysis identified a single significant latent component (LC; FDR-corrected $q < 0.05$) capturing 94.0% of the covariance between cerebellar regional volumes and psychosis-risk symptoms. Cerebellar and behavioral composite scores were significantly correlated across all participants included in the analysis ($r = 0.28$, $p < 0.001$; Figure 4A), indicating a robust multivariate association between cerebellar structure and psychosis-risk symptom severity. To characterize the nature of this association, we examined the LC loadings (Figure 4E–F). Higher LC scores are characterized by smaller cerebellar volumes across multiple regions, and greater severity of positive psychosis-risk symptoms. Cerebellar contributions were strongest in left Crus II ($r=-0.27$), right Crus II ($r=-0.27$), corpus medullare ($r=-0.26$) and Vermis IX ($r=-0.24$) (Figure 4B). Together, these findings suggest that multiregional cerebellar volume reduction—particularly in Crus II—is associated with greater severity of positive psychosis-risk symptoms across groups.

Group comparisons of LC composite scores revealed differences across groups. Psychosis-risk behavioral composite scores (i.e., reflecting greater psychosis-risk symptom severity) were highest in 22qDel, intermediate in 22qDup, and lowest in TD controls (Figure 4C). Cerebellar composite scores (i.e., reflecting smaller multiregional cerebellar volumes) were higher in 22qDel relative to both 22qDup and TD controls (Figure 4D). Detailed results, including within-group correlations and the full set of cerebellar and psychosis-risk clinical measures contributing to the latent component, are provided in the Supplementary Results.

DISCUSSION

This study examined cerebellar volumetric alterations and their behavioral relevance in individuals with reciprocal 22q11.2 CNVs using high-resolution structural MRI data and lobule-specific parcellation. Extending prior reports of reduced cortical and cerebellar volume in 22q11.2 deletion carriers (15–17,22), we find that cerebellar involvement in 22q11.2 copy number variation is not characterized by simple reciprocal gene-dosage effects. While individuals with 22qDel showed widespread reductions in total and regional cerebellar volume, alterations in 22qDup were comparatively subtle and heterogeneous, with preserved global volume but focal regional deviations. This pattern reveals a previously unrecognized, regionally selective architecture of cerebellar vulnerability, comprising both shared and CNV-specific effects rather than a uniform 22qDel < TD < 22qDup gradient. Notably, Vermis VII—implicated in motor learning and coordination and cognitive-affective functions (48,49)—was significantly reduced in both CNV groups, reflecting a shared locus of cerebellar vulnerability. Multivariate brain–

behavior analyses identified two robust, domain-specific cerebellar covariance patterns, with posterior cerebellar regions, including bilateral Lobule VIIIA, contributing most strongly to cognitive–social functioning and bilateral Crus II to psychosis-risk symptoms. Together, these findings highlight selective and region-specific cerebellar involvement in 22q11.2 CNVs and provide the first lobule-level characterization of cerebellar volume alterations in individuals with 22q11.2 duplication.

Cerebellar Alterations in 22q11.2 Duplication

A central contribution of this study is the comprehensive characterization of cerebellar morphology in individuals with 22q11.2 duplications, enabling direct comparison with 22q11.2 deletion carriers. Unlike the widespread hypoplasia observed in deletion carriers, the 22q11.2 duplication was associated with regionally specific alterations, including a significant reduction in Vermis VII and nominal trends toward reduction of right Lobule VIIIA but enlargement of Vermis IX The absence of a group-level difference in total cerebellar volume may reflect this bidirectional regional pattern, in which local increases and decreases offset one another at the global scale. These findings indicate that 22qDup does not represent simply the inverse of 22qDel but instead exerts subtler, spatially selective effects on cerebellar development. This asymmetry is consistent with prior reports in cortical and subcortical systems, in which deletions—both at 22q11.2 and more broadly—show large, pervasive effects, whereas duplications exhibit lower penetrance and more heterogeneous neuroanatomical consequences (15,19,50). Together, these results underscore the importance of

regionally resolved analyses for detecting duplication-related effects that may be obscured by global measures.

Multivariate Cerebellar–Behavior Relationships: Insights from PLSC

Using partial least squares correlation, we identified robust multivariate associations between cerebellar regional volumes and neurobehavioral outcomes that were specific to behavioral domains. For cognitive ability and autism-related social traits, reduced volumes across a broad set of cerebellar regions—particularly within the posterior cerebellum—were associated with lower cognitive performance and greater social impairment, regardless of genetic diagnosis. These findings align with accumulating evidence for the cerebellum's role in higher-order cognitive and socio-affective processes (25,26,51). Bilateral Lobule VIIIA, along with Lobules VI and VIIB, contributes to cognitive functions (25,52), with Lobule VIIb/VIIIa specifically serving as a node within the dorsal attention network and supporting visual working memory representations (53–55). The cerebellar vermis has been implicated in emotional processing (51,56,57) and shows consistent structural abnormalities in idiopathic ASD (58–60). These transdiagnostic cerebellar-behavior associations support the hypothesis that cerebellar dysfunction contributes to cognitive and social deficits observed in both 22q11.2 CNV carriers and idiopathic ASD.

In contrast, psychosis-risk symptoms were associated with a distinct cerebellar pattern characterized by prominent contributions from bilateral Crus II and Vermis IX, with reduced volumes linked to greater positive symptom severity regardless of genetic diagnosis. Widespread posterior cerebellar reductions, particularly in Crus I/II, are a

consistent structural signature of schizophrenia and psychosis (28,61,62). These structural abnormalities align with the cognitive dysmetria framework, which proposes that impaired cerebello-thalamo-cortical circuitry underlies psychotic symptomatology (63–66). The cerebellar vermis shows consistent structural abnormalities across the psychotic-affective spectrum (67,68) and has been implicated in emotional processing (51,56,57), supporting cerebellar dysfunction as a core feature of emerging psychosis (28,69,70).

Together, these findings indicate that distinct cerebellar subregions contribute differentially to cognitive–social functioning and psychosis-related dimensions, reinforcing the cerebellum's multifunctional role in neurodevelopment and psychiatric risk. Importantly, these multivariate associations reflected shared brain–behavior covariance across participants, with diagnostic groups differing in expression rather than in the underlying latent structure, highlighting the value of multivariate approaches for disentangling domain-specific brain–behavior relationships from diagnostic contrasts.

Focal Anatomical Vulnerability and Distributed Brain–Behavior Associations

Across analyses, Vermis VII emerged as the most consistent site of convergent anatomical reduction across both CNV groups. As part of the posterior "limbic cerebellum," Vermis VII has been implicated in emotional processing (51,56,57) and cognitive functions (25,49,71). Structural reductions in vermal lobules VI-VII have been consistently reported in autism spectrum disorder (29,30,60), and align with the social and cognitive deficits observed in these conditions. Notably, Vermis VII contributed to

both multivariate brain–behavior models examined in this study but was not among the strongest regional contributors to either. This dissociation suggests that while Vermis VII represents a shared site of anatomical vulnerability, cerebellar influences on behavioral outcomes are not driven by a single region in isolation. By contrast, Vermis IX showed nominal copy-number–dependent volumetric differences (22qDel < TD < 22qDup) and emerged as a stronger contributor across both multivariate models, highlighting it as a potential locus through which 22q11.2 copy number variation differentially shapes cerebellar contributions to multiple behavioral domains. More broadly, these findings underscore that cerebellar risk in 22q11.2 CNVs is best understood through distributed, multivariate patterns that integrate both shared and divergent regional effects, rather than single-region abnormalities alone.

Limitations

Several limitations should be noted. Although our sample is the largest to examine cerebellar morphology in 22q11.2 CNVs, statistical power remains limited for duplication carriers. Accordingly, findings involving 22qDup should be interpreted as providing a first, foundational characterization of cerebellar features that motivates future replication and extension. The wide age range of the sample represents both a strength and a limitation: it enables examination of cerebellar structure across a broad developmental window but also introduces heterogeneity. Although age was modeled flexibly and supported by sensitivity analyses, developmental trajectories could not be fully examined within the scope of the current study. Finally, while the multivariate analyses revealed stable, data-driven cerebellar–behavioral associations consistent

with prior literature, interpretation should consider the relatively young sample, characterized by low endorsement of positive psychosis-risk symptoms compared with other clinically ascertained cohorts, as well as the effective sample size being constrained to participants with complete multivariate data. As such, the brain-behavior findings should be viewed as complementary and intended to inform future hypothesis-driven studies.

Implications and Future Directions

Using a genetics-first approach, we find that reciprocal 22q11.2 CNV carriers—both associated with elevated ASD risk—share a focal cerebellar vulnerability, with Vermis VII emerging as the most consistently reduced region. This convergence with findings in idiopathic ASD positions the cerebellum as a common neural substrate across genetic and non-genetic forms of risk. At the same time, nominal effects in right Lobule VIIIA (22qDel < 22qDup < TD) and Vermis IX (22qDel < TD < 22qDup) reveal regional heterogeneity, indicating that beyond shared vulnerabilities, cerebellar alterations diverge in a region-specific and copy-number–dependent manner. Multivariate analyses further show that cognitive–social functioning and psychosis risk are associated with distinct distributed cerebellar profiles rather than isolated focal abnormalities. High-resolution lobular parcellation was key to detecting these effects, emphasizing the need for fine-grained brain–behavior mapping across CNV types. Future studies in larger, longitudinal samples will be critical for increasing power to detect group differences and for examining developmental changes in cerebellar structure across 22q11.2 CNVs. As cerebellum-specific, developmentally resolved

gene-expression resources continue to mature (72,73), future work will be well positioned to more directly integrate regional neuroimaging findings with temporospatial patterns of gene expression relevant to 22q11.2 CNVs and their clinical expression. In addition, complementary approaches incorporating functional parcellation, cerebellar functional connectivity, transcriptomics, and detailed behavioral phenotyping will further clarify cerebellar mechanisms in 22q11.2 CNVs. Finally, direct comparisons with clinically and behaviorally defined high-risk groups and other neuropsychiatric CNVs (e.g., 3q29 and 16p11.2 CNVs) will help delineate shared and unique cerebellar mechanisms across neurodevelopmental disorders.

CHAPTER 1 ACKNOWLEDGMENTS AND DISCLOSURES

Author Contributions

HF: Conceptualization, Methodology, Data curation, Formal analysis, Software, Validation, Visualization, Writing – original draft, Writing – review & editing. **KPO:** Methodology, Data curation, Writing – original draft, Writing – review & editing. **RB:** Methodology, Writing – original draft, Writing – review & editing. **HRW:** Methodology, Software, Writing – review & editing. **CMA**: Methodology, Writing – review & editing. **CHS:** Data curation, Software. **LK-W:** Investigation, Data curation, Project administration. **BAM:** Conceptualization, Software. **EB:** Investigation, Validation. **PJM:** Methodology, Supervision, Writing - review & editing. **CEB:** Conceptualization, Methodology, Writing – review & editing, Supervision, Funding acquisition, Resources.

Funding

This work was supported by the National Institute of Mental Health (Grant Nos. R01/R37MH085953, R01MH129858, U01MH101779, U01MH119736, and R21MH116473, all to CEB), the Department of Defense (Grant No. W81XWH-12-1-0081, to CEB), the Simons Foundation Autism Research Initiative Explorer Award (to CEB), the Uytengsu-Hamilton 22q11 Neuropsychiatry Research Award (to CEB), and the Consortium for Neuropsychiatric Phenomics (NIH Roadmap for Medical Research grant UL1-DE019580).

Acknowledgments

We are deeply grateful to the participants and their families for their time, commitment, and invaluable contributions to this study.

Preprint

An earlier version of this manuscript was posted as a preprint on bioRxiv (DOI: https://doi.org/10.1101/2025.10.07.679846).

Disclosures

All authors reported no biomedical financial interests or potential conflicts of interest.

CHAPTER 1 REFERENCES

1. Schneider M, Debbané M, Bassett AS, Chow EWC, Fung WLA, Van Den Bree MBM, *et al.* (2014): Psychiatric disorders from childhood to adulthood in 22q11.2 deletion syndrome: Results from the international consortium on brain and behavior in 22q11.2 deletion syndrome. *Am J Psychiatry* 171: 627–639.
2. McDonald-McGinn DM, Sullivan KE, Marino B, Philip N, Swillen A, Vorstman JAS, *et al.* (2015): 22q11.2 deletion syndrome. *Nat Rev Dis Primers* 1: 15071.
3. Fiksinski AM, Hoftman GD, Vorstman JAS, Bearden CE (2023): A genetics-first approach to understanding autism and schizophrenia spectrum disorders: the 22q11.2 deletion syndrome. *Mol Psychiatry* 28: 341–353.
4. Olsen L, Sparsø T, Weinsheimer SM, Dos Santos MBQ, Mazin W, Rosengren A, *et al.* (2018): Prevalence of rearrangements in the 22q11.2 region and population-based risk of neuropsychiatric and developmental disorders in a Danish population: a case-cohort study. *The Lancet Psychiatry* 5: 573–580.
5. Provenzani U, Damiani S, Bersano I, Singh S, Moschillo A, Accinni T, *et al.* (2022): Prevalence and incidence of psychotic disorders in 22q11.2 deletion syndrome: a meta-analysis. *Int Rev Psychiatry* 34: 676–688.
6. Weisman O, Guri Y, Gur RE, McDonald-McGinn DM, Calkins ME, Tang SX, *et al.* (2017): Subthreshold psychosis in 22q11.2 deletion syndrome: Multisite naturalistic study. *Schizophr Bull* 43: 1079–1089.
7. Jalbrzikowski M, Lin A, Vajdi A, Grigoryan V, Kushan L, Ching CRK, *et al.* (2022): Longitudinal trajectories of cortical development in 22q11.2 copy number variants and typically developing controls. *Mol Psychiatry* 27: 4181–4190.

8. Ou Z, Berg JS, Yonath H, Enciso VB, Miller DT, Picker J, *et al.* (2008): Microduplications of 22q11.2 are frequently inherited and are associated with variable phenotypes. *Genet Med* 10: 267–277.

9. Yu A, Turbiville D, Xu F, Ray JW, Britt AD, Lupo PJ, *et al.* (2019): Genotypic and phenotypic variability of 22q11.2 microduplications: An institutional experience. *Am J Med Genet A* 179: 2178–2189.

10. Van Campenhout S, Devriendt K, Breckpot J, Frijns J-P, Peeters H, Van Buggenhout G, *et al.* (2012): Microduplication 22q11.2: a description of the clinical, developmental and behavioral characteristics during childhood. *Genet Couns* 23: 135–148.

11. Hoeffding LK, Trabjerg BB, Olsen L, Mazin W, Sparsø T, Vangkilde A, *et al.* (2017): Risk of psychiatric disorders among individuals with the 22q11.2 deletion or duplication: A Danish nationwide, register-based study: A danish nationwide, register-based study. *JAMA Psychiatry* 74: 282–290.

12. Lin A, Vajdi A, Kushan-Wells L, Helleman G, Hansen LP, Jonas RK, *et al.* (2020): Reciprocal Copy Number Variations at 22q11.2 Produce Distinct and Convergent Neurobehavioral Impairments Relevant for Schizophrenia and Autism Spectrum Disorder. *Biol Psychiatry* 88: 260–272.

13. Rees E, Walters JTR, Georgieva L, Isles AR, Chambert KD, Richards AL, *et al.* (2014): Analysis of copy number variations at 15 schizophrenia-associated loci. *British Journal of Psychiatry* 204: 108–114.

14. Marshall CR, Howrigan DP, Merico D, Thiruvahindrapuram B, Wu W, Greer DS, *et al.* (2017): Contribution of copy number variants to schizophrenia from a genome-wide study of 41,321 subjects. *Nat Genet* 49: 27–35.

15. Lin A, Ching CRK, Vajdi A, Sun D, Jonas RK, Jalbrzikowski M, *et al.* (2017): Mapping 22q11.2 gene dosage effects on brain morphometry. *Journal of Neuroscience* 37: 6183–6199.

16. Sun D, Ching CRK, Lin A, Forsyth JK, Kushan L, Vajdi A, *et al.* (2020): Large-scale mapping of cortical alterations in 22q11.2 deletion syndrome: Convergence with idiopathic psychosis and effects of deletion size. *Mol Psychiatry* 25: 1822–1834.

17. Ching CRK, Gutman BA, Sun D, Reina JV, Ragothaman A, Isaev D, *et al.* (2020): Mapping subcortical brain alterations in 22q11.2 deletion syndrome: Effects of deletion size and convergence with idiopathic neuropsychiatric illness. *Am J Psychiatry* 177: 589–600.

18. Kumar K, Modenato C, Moreau C, Ching CRK, Harvey A, Martin-Brevet S, *et al.* (2023): Subcortical Brain Alterations in Carriers of Genomic Copy Number Variants. *Am J Psychiatry* 180: 685–698.

19. Schleifer CH, O'Hora KP, Fung H, Xu J, Robinson T-A, Wu AS, et al. (2024): Effects of gene dosage and development on subcortical nuclei volumes in individuals with 22q11.2 copy number variations. Neuropsychopharmacology 49: 1024–1032.

20. Seitz-Holland J, Lyons M, Kushan L, Lin A, Villalon-Reina JE, Cho KIK, *et al.* (2021): Opposing white matter microstructure abnormalities in 22q11.2 deletion and duplication carriers. *Transl Psychiatry* 11: 580.

21. Modenato C, Kumar K, Moreau C, Martin-Brevet S, Huguet G, Schramm C, *et al.* (2021): Effects of eight neuropsychiatric copy number variants on human brain structure. *Transl Psychiatry* 11: 399.

22. Rogdaki M, Gudbrandsen M, McCutcheon RA, Blackmore CE, Brugger S, Ecker C, *et al.* (2020): Magnitude and heterogeneity of brain structural abnormalities in 22q11.2 deletion syndrome: a meta-analysis. *Mol Psychiatry* 25: 1704–1717.

23. Azevedo FAC, Carvalho LRB, Grinberg LT, Farfel JM, Ferretti REL, Leite REP, *et al.* (2009): Equal numbers of neuronal and nonneuronal cells make the human brain an isometrically scaled-up primate brain. *J Comp Neurol* 513: 532–541.

24. Buckner RL (2013): The cerebellum and cognitive function: 25 years of insight from anatomy and neuroimaging. *Neuron* 80: 807–815.

25. Stoodley CJ, Schmahmann JD (2009): Functional topography in the human cerebellum: a meta-analysis of neuroimaging studies. *Neuroimage* 44: 489–501.

26. Buckner RL, Krienen FM, Castellanos A, Diaz JC, Yeo BTT (2011): The organization of the human cerebellum estimated by intrinsic functional connectivity. *J Neurophysiol* 106: 2322–2345.

27. King M, Hernandez-Castillo CR, Poldrack RA, Ivry RB, Diedrichsen J (2019): Functional boundaries in the human cerebellum revealed by a multi-domain task battery. *Nat Neurosci* 22: 1371–1378.

28. Moberget T, Doan NT, Alnæs D, Kaufmann T, Córdova-Palomera A, Lagerberg TV, *et al.* (2018): Cerebellar volume and cerebellocerebral structural covariance in schizophrenia: a multisite mega-analysis of 983 patients and 1349 healthy controls. *Mol Psychiatry* 23: 1512–1520.

29. Rodrigues BA, Silva J do N, Kawamoto EM (2025): Cerebellar alterations in autism spectrum disorder: A mini-review. *Cerebellum* 24: 52.

30. Mapelli L, Soda T, D'Angelo E, Prestori F (2022): The cerebellar involvement in autism spectrum disorders: From the social brain to mouse models. *Int J Mol Sci* 23: 3894.

31. Gothelf D, Penniman L, Gu E, Eliez S, Reiss AL (2007): Developmental trajectories of brain structure in adolescents with 22q11.2 deletion syndrome: a longitudinal study. *Schizophr Res* 96: 72–81.

32. van Amelsvoort T, Daly E, Robertson D, Suckling J, Ng V, Critchley H, *et al.* (2001): Structural brain abnormalities associated with deletion at chromosome 22q11: quantitative neuroimaging study of adults with velo-cardio-facial syndrome. *Br J Psychiatry* 178: 412–419.

33. van Amelsvoort T, Daly E, Henry J, Robertson D, Ng V, Owen M, *et al.* (2004): Brain anatomy in adults with velocardiofacial syndrome with and without schizophrenia: preliminary results of a structural magnetic resonance imaging study: Preliminary results of a structural magnetic resonance imaging study. *Arch Gen Psychiatry* 61: 1085–1096.

34. Campbell LE, Daly E, Toal F, Stevens A, Azuma R, Catani M, *et al.* (2006): Brain and behaviour in children with 22q11.2 deletion syndrome: a volumetric and voxel-based morphometry MRI study. *Brain* 129: 1218–1228.

35. Bish JP, Pendyal A, Ding L, Ferrante H, Nguyen V, McDonald-McGinn D, *et al.* (2006): Specific cerebellar reductions in children with chromosome 22q11.2 deletion syndrome. *Neurosci Lett* 399: 245–248.

36. Shashi V, Kwapil TR, Kaczorowski J, Berry MN, Santos CS, Howard TD, *et al.* (2010): Evidence of gray matter reduction and dysfunction in chromosome 22q11.2 deletion syndrome. *Psychiatry Res* 181: 1–8.

37. Schmitt JE, DeBevits JJ, Roalf DR, Ruparel K, Gallagher RS, Gur RC, *et al.* (2023): A comprehensive analysis of cerebellar volumes in the 22q11.2 deletion syndrome. *Biol Psychiatry Cogn Neurosci Neuroimaging* 8: 79–90.

38. Han S, Carass A, He Y, Prince JL (2020): Automatic cerebellum anatomical parcellation using U-Net with locally constrained optimization. *Neuroimage* 218: 116819.

39. Wechsler D (1999): *Manual for the Wechsler Abbreviated Intelligence Scale (WASI)*. San Antonio, TX: The Psychological Corporation.

40. Wechsler D (2011): *Wechsler Abbreviated Scale of Intelligence, Second Edition*. San Antonio, TX: Pearson.

41. Constantino JN, Gruber CP (2005): Social Responsiveness Scale 2nd ed: Western Psychological Services.

42. McGlashan TH, Miller TJ, Woods SW, Hoffman RE, Davidson L (2001): Instrument for the assessment of prodromal symptoms and states. *Early Intervention in Psychotic Disorders*. Dordrecht: Springer Netherlands, pp 135–149.

43. Mugler JP 3rd, Brookeman JR (1990): Three-dimensional magnetization-prepared rapid gradient-echo imaging (3D MP RAGE). *Magn Reson Med* 15: 152–157.

44. Fischl B (2012): FreeSurfer. *Neuroimage* 62: 774–781.

45. Beer JC, Tustison NJ, Cook PA, Davatzikos C, Sheline YI, Shinohara RT, *et al.* (2020): Longitudinal ComBat: A method for harmonizing longitudinal multi-scanner imaging data. *Neuroimage* 220: 117129.

46. Moser DA, Doucet GE, Lee WH, Rasgon A, Krinsky H, Leibu E, *et al.* (2018): Multivariate associations among behavioral, clinical, and multimodal imaging phenotypes in patients with psychosis. *JAMA Psychiatry* 75: 386–395.

47. Wang HR, Liu Z-Q, Nakua H, Hegarty CE, Thies MB, Patel PK, *et al.* (2025): Decoding early psychoses: Unraveling stable microstructural features associated with psychopathology across independent cohorts. *Biol Psychiatry* 97: 167–177.

48. Coffman KA, Dum RP, Strick PL (2011): Cerebellar vermis is a target of projections from the motor areas in the cerebral cortex. *Proc Natl Acad Sci U S A* 108: 16068–16073.

49. Stoodley CJ, Schmahmann JD (2010): Evidence for topographic organization in the cerebellum of motor control versus cognitive and affective processing. *Cortex* 46: 831–844.

50. Männik K, Mägi R, Macé A, Cole B, Guyatt AL, Shihab HA, *et al.* (2015): Copy number variations and cognitive phenotypes in unselected populations. *JAMA* 313: 2044–2054.

51. Schmahmann JD, Oblak AL, Blatt GJ (2021): Cerebellar connections with limbic circuits: Anatomy and functional implications. *Handbook of the Cerebellum and Cerebellar Disorders*. Cham: Springer International Publishing, pp 1–21.

52. Stoodley CJ, Valera EM, Schmahmann JD (2012): Functional topography of the cerebellum for motor and cognitive tasks: an fMRI study. *Neuroimage* 59: 1560–1570.

53. Brissenden JA, Levin EJ, Osher DE, Halko MA, Somers DC (2016): Functional evidence for a cerebellar node of the dorsal attention network. *J Neurosci* 36: 6083–6096.

54. Brissenden JA, Tobyne SM, Osher DE, Levin EJ, Halko MA, Somers DC (2018): Topographic Cortico-cerebellar networks revealed by visual attention and working memory. *Curr Biol* 28: 3364-3372.e5.

55. Brissenden JA, Tobyne SM, Halko MA, Somers DC (2021): Stimulus-specific visual working memory representations in human cerebellar lobule VIIb/VIIIa. *J Neurosci* 41: 1033–1045.

56. Adamaszek M, D'Agata F, Ferrucci R, Habas C, Keulen S, Kirkby KC, *et al.* (2017): Consensus paper: Cerebellum and emotion. *Cerebellum* 16: 552–576.

57. Schutter DJLG, van Honk J (2005): The cerebellum on the rise in human emotion. *Cerebellum* 4: 290–294.

58. Fatemi SH, Aldinger KA, Ashwood P, Bauman ML, Blaha CD, Blatt GJ, *et al.* (2012): Consensus paper: pathological role of the cerebellum in autism. *Cerebellum* 11: 777–807.

59. Mello D, Crocetti AM, Mostofsky D, Stoodley SH (2015): Cerebellar gray matter and lobular volumes correlate with core autism symptoms. *NeuroImage Clin* 7: 631–639.

60. Crucitti J, Hyde C, Enticott PG, Stokes MA (2020): Are vermal lobules VI-VII smaller in autism spectrum disorder? *Cerebellum* 19: 617–628.

61. Li X, Liu N, Yang C, Zhang W, Lui S (2022): Cerebellar gray matter volume changes in patients with schizophrenia: A voxel-based meta-analysis. *Front Psychiatry* 13: 1083480.

62. Morimoto C, Uematsu A, Nakatani H, Takano Y, Iwashiro N, Abe O, *et al.* (2021): Volumetric differences in gray and white matter of cerebellar Crus I/II across the different clinical stages of schizophrenia. *Psychiatry Clin Neurosci* 75: 256–264.

63. Andreasen NC, O'Leary DS, Cizadlo T, Arndt S, Rezai K, Ponto LL, *et al.* (1996): Schizophrenia and cognitive dysmetria: a positron-emission tomography study of dysfunctional prefrontal-thalamic-cerebellar circuitry. *Proc Natl Acad Sci U S A* 93: 9985–9990.

64. Andreasen NC, Paradiso S, O'Leary DS (1998): "Cognitive dysmetria" as an integrative theory of schizophrenia: a dysfunction in cortical-subcortical-cerebellar circuitry? *Schizophr Bull* 24: 203–218.

65. Cao H, Cannon TD (2019, July 1): Cerebellar dysfunction and schizophrenia: From "cognitive dysmetria" to a potential therapeutic target. *The American Journal of Psychiatry*, vol. 176. American Psychiatric Association Publishing, pp 498–500.

66. Cao H, Chén OY, Chung Y, Forsyth JK, McEwen SC, Gee DG, *et al.* (2018): Cerebello-thalamo-cortical hyperconnectivity as a state-independent functional neural signature for psychosis prediction and characterization. *Nat Commun* 9: 3836.

67. Xiao Y, Kandala S, Huang J, Liu J, McGonigle T, Barch D, *et al.* (2025): The involvement of the cerebellar vermis across the psychotic-affective spectrum in enriched samples of recent-onset schizophrenia, bipolar disorder, and major depressive disorder. *J Psychiatr Res* 181: 14–22.

68. Dusi N, Esposito CM, Delvecchio G, Prunas C, Brambilla P (2024): Case report and systematic review of cerebellar vermis alterations in psychosis. *Int Clin Psychopharmacol* 39: 223–231.

69. Bottmer C, Bachmann S, Pantel J, Essig M, Amann M, Schad LR, *et al.* (2005): Reduced cerebellar volume and neurological soft signs in first-episode schizophrenia. *Psychiatry Res* 140: 239–250.

70. Dean DJ, Bernard JA, Orr JM, Pelletier-Baldelli A, Gupta T, Carol EE, Mittal VA (2014): Cerebellar morphology and procedural learning impairment in neuroleptic-naive youth at ultrahigh risk of psychosis. *Clin Psychol Sci* 2: 152–164.

71. Jacobi H, Faber J, Timmann D, Klockgether T (2021): Update cerebellum and cognition. *J Neurol* 268: 3921–3925.

72. Aldinger KA, Thomson Z, Phelps IG, Haldipur P, Deng M, Timms AE, *et al.* (2021): Spatial and cell type transcriptional landscape of human cerebellar development. *Nat Neurosci* 24: 1163–1175.

73. Zhong S, Wang M, Huang L, Chen Y, Ge Y, Zhang J, *et al.* (2023): Single-cell epigenomics and spatiotemporal transcriptomics reveal human cerebellar development. *Nat Commun* 14: 7613.

CHAPTER 1 FIGURE/TABLE LEGENDS

Table 1. Participant characteristics at baseline by group. Baseline demographic, cognitive, and clinical characteristics of typically developing (TD) controls, individuals with 22q11.2 deletion (22qDel), and duplication (22qDup). Group comparison statistics are reported for all measures. The three groups were comparable in sex and age distributions at baseline. Full-Scale IQ was lower in both CNV groups (22qDel < 22qDup < TD). SRS-2 total T-scores, reflecting autism-related traits, were elevated in both CNV groups relative to controls (TD < 22qDel ≈ 22qDup). SIPS positive symptom total scores, reflecting psychosis severity, were higher in 22qDel relative to both TD controls and 22qDup, with no significant difference between TD controls and 22qDup (TD ≈ 22qDup < 22qDel). eTIV was lower in 22qDel participants compared to both TD control and 22qDup groups (22qDel < TD ≈ 22qDup).

Figure 1 Group differences in total and regional cerebellar volumes. (A) Standardized beta coefficients and 95% confidence intervals are shown for 22qDel and 22qDup groups relative to typically developing (TD) controls. (B) Standardized beta coefficients and 95% confidence intervals for the 22qDup group relative to the 22qDel group. Results in both panels were derived from the same linear mixed-effects model specification, with group reference levels varied to estimate the relevant contrasts. Models included fixed effects of sex, mean-centered age (linear and quadratic) and estimated intracranial volume (eTIV), with subject-level random intercepts to account for repeated measures. Asterisks indicate significance after FDR correction for regional volumes: $q < 0.05$ (*), $q < 0.01$ (**), $q < 0.001$ (***). TOTAL refers to total cerebellar

volume and is shown with uncorrected *p*-value, as it was not included in the FDR correction.

Figure 2 Flatmap visualizations of cerebellar volume differences across 22q11.2 CNVs. (**A**) Flatmap indicating widespread cerebellar volume reductions in 22qDel compared to TD, particularly in midline and lateral posterior regions. (**B**) Flatmap indicating more subtle and heterogeneous volume differences in 22qDup compared to TD, including both increases and reductions across subregions. (**C**) Binary map highlighting regions with convergent volume reductions in 22qDel and 22qDup at FDR $q < 0.05$ (Vermis VII). (**D**) Binary map highlighting regions with monotonic gene dosage effects (22qDel < TD < 22qDup) at FDR $q < 0.05$ (no regions). (**E**) Binary map highlighting regions with convergent volume reductions in 22qDel and 22qDup at uncorrected $p < 0.05$ (Vermis VII, Right Lobule VIIIA). (**F**) Binary map highlighting regions with monotonic gene dosage effects (22qDel < TD < 22qDup) at uncorrected $p < 0.05$ (Vermis IX). Regional volumes were derived using the ACAPULCO cerebellar parcellation and mapped to SUIT-defined anatomical regions for visualization. Beta values reflect standardized group effects from linear mixed-effects models, displayed without p-value thresholding on a symmetric scale (blue = negative, red = positive). To align with SUIT's anatomical scheme, beta values of Lobule I–III and Lobule IV from ACAPULCO were averaged to create a single Lobule I–IV region. The corpus medullare was not visualized in these maps. Binary maps show regions where both 22qDel and 22qDup differed significantly from TD at the indicated threshold; gray regions indicate regions that did not meet this criterion. See Supplementary Table S2 for full model results.

Figure 3. Multivariate associations between cerebellar volume and cognitive and social functioning. Partial least squares correlation (PLSC) identified a single significant latent component (FDR-corrected $q < 0.05$) explaining 95.3% of the covariance between cerebellar regional volumes and measures of cognitive ability and reciprocal social behavior. (A) Cerebellar and behavioral composite scores were significantly correlated across participants ($r = 0.41$, $p < 0.001$). (B) Cerebellar loadings showed a distributed pattern of lower volumes across posterior cerebellar regions. (C–D) Behavioral and cerebellar composite scores differed across groups. (E–F) Loadings indicated strongest contributions from posterior cerebellar regions, including bilateral Lobule VIIIA, left Lobule VIIB, and Vermis IX, associated with lower cognitive ability and greater autism-related social difficulties.

Figure 4. Multivariate associations between cerebellar volume and psychosis-risk symptoms. Partial least squares correlation (PLSC) identified a single significant latent component (FDR-corrected $q < 0.05$) explaining 94.0% of the covariance between cerebellar regional volumes and psychosis-risk symptoms. (A) Cerebellar and behavioral composite scores were significantly correlated across participants ($r = 0.28$, $p < 0.001$). (B) Cerebellar loadings showed a distributed pattern of lower volumes across medial and hemispheric regions. (C–D) Behavioral and cerebellar composite scores differed across groups. (E–F) Loadings indicated strongest contributions from bilateral Crus II, the corpus medullare, and Vermis IX, associated with greater severity of positive psychosis-risk symptoms.

CHAPTER 1 TABLES

Table 1. Participant characteristics at baseline by group

Measure	TD Controls	22qDel	22qDup	Group Comparisons [a]
Participant (n)	167	111	37	
Age, Mean (SD), years	16.2 (6.9)	16.2 (9.4)	18.2 (13.5)	*KW* $\chi^2(2) = 1.79.0$, $p = 0.408$
Age Range, years	6–45	5–55	5–49	
Sex (% female)	51.5	55.0	48.6	$\chi^2(2) = 0.55$, $p = 0.758$
eTIV, mean (SD)	1,541,862 (159,072)	1,429,772 (179,795)	1,543,068 (162,409)	$F(2, 312) = 16.25$, $p < 0.001$; 22qDel < TD ≈ 22qDup
FSIQ, mean (SD)	112.12 (19.64)	79.34 (12.36)	97.32 (17.24)	*KW* $\chi^2(2) = 86.8$, $p < 0.001$; 22qDel < 22qDup < TD
SRS-2 Total T-score, mean (SD)	47.5 (10.3)	70.5 (14.3)	66.8 (16.2)	*KW* $\chi^2(2) = 66.88$, $p < 0.001$; TD < 22qDel ≈ 22qDup
SIPS P Total, mean (SD)	1.24 (1.84)	5.99 (6.54)	2.62 (3.09)	*KW* $\chi^2(2) = 38.4$, $p < 0.001$; TD ≈ 22qDup < 22qDel

TD Controls = Typically Developing Controls; 22qDel = 22q11.2 Deletion; 22qDup = 22q11.2 Duplication; eTIV = estimated Total Intracranial Volume; FSIQ = Full Scale IQ; SRS-2 Total T-score = Social Responsiveness Scale-2 Total T-score; SIPS P Total = Structured Interview for Psychosis-Risk Syndromes Positive Symptom Total Score.

a Group differences in continuous variables were tested using one-way ANOVA (eTIV) or Kruskal–Wallis tests (Age, FSIQ, SRS-2 Total T-score, SIPS P Total), depending on normality and variance. Chi-square tests were used for categorical variables (sex). Post hoc pairwise comparisons used Tukey's HSD (ANOVA) or Wilcoxon rank-sum tests with Bonferroni correction (non-parametric).

CHAPTER 1 FIGURES

Figure 1 Group differences in total and regional cerebellar volumes.

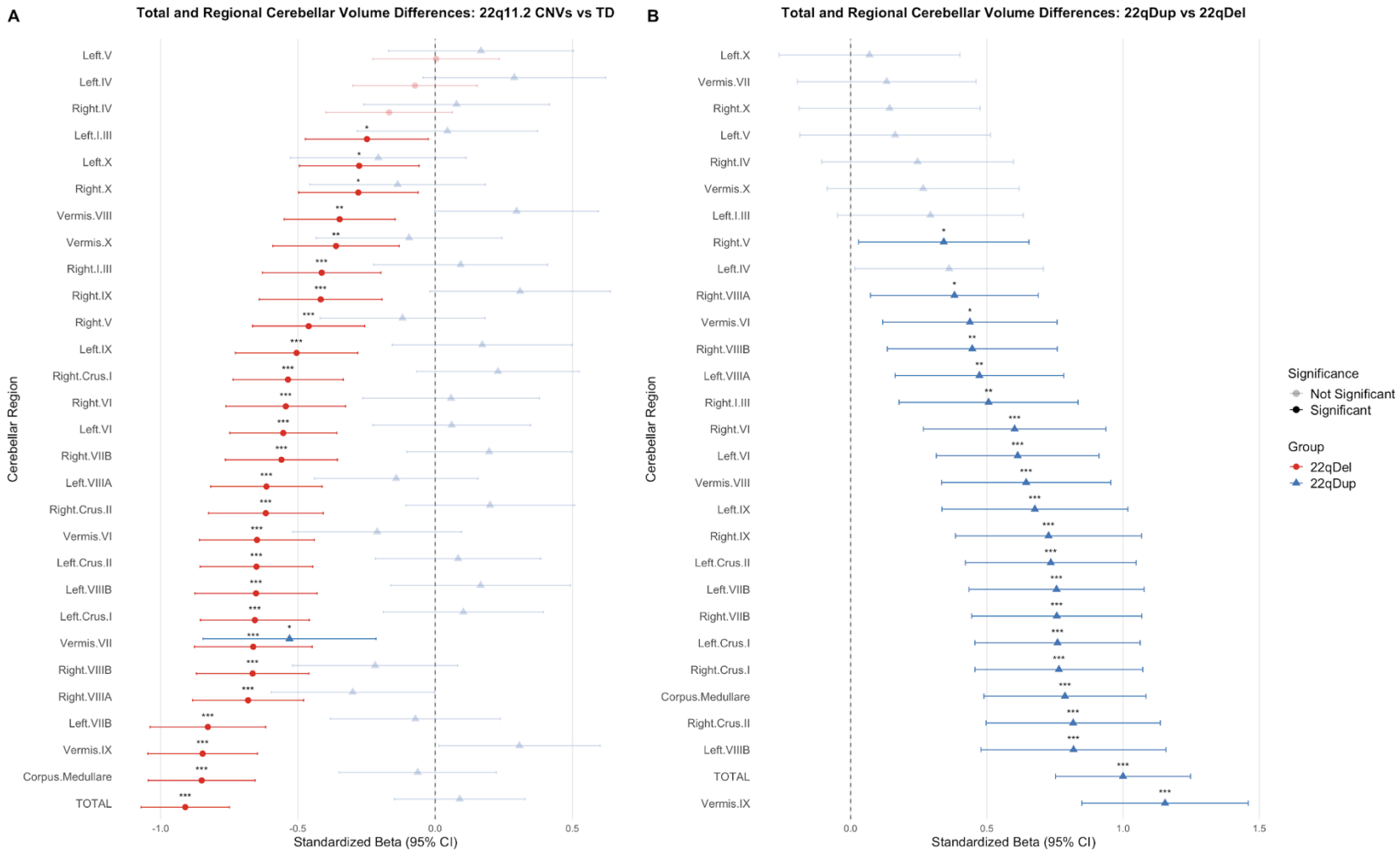

Figure 2 Flatmap visualizations of cerebellar volume differences across 22q11.2 CNVs.

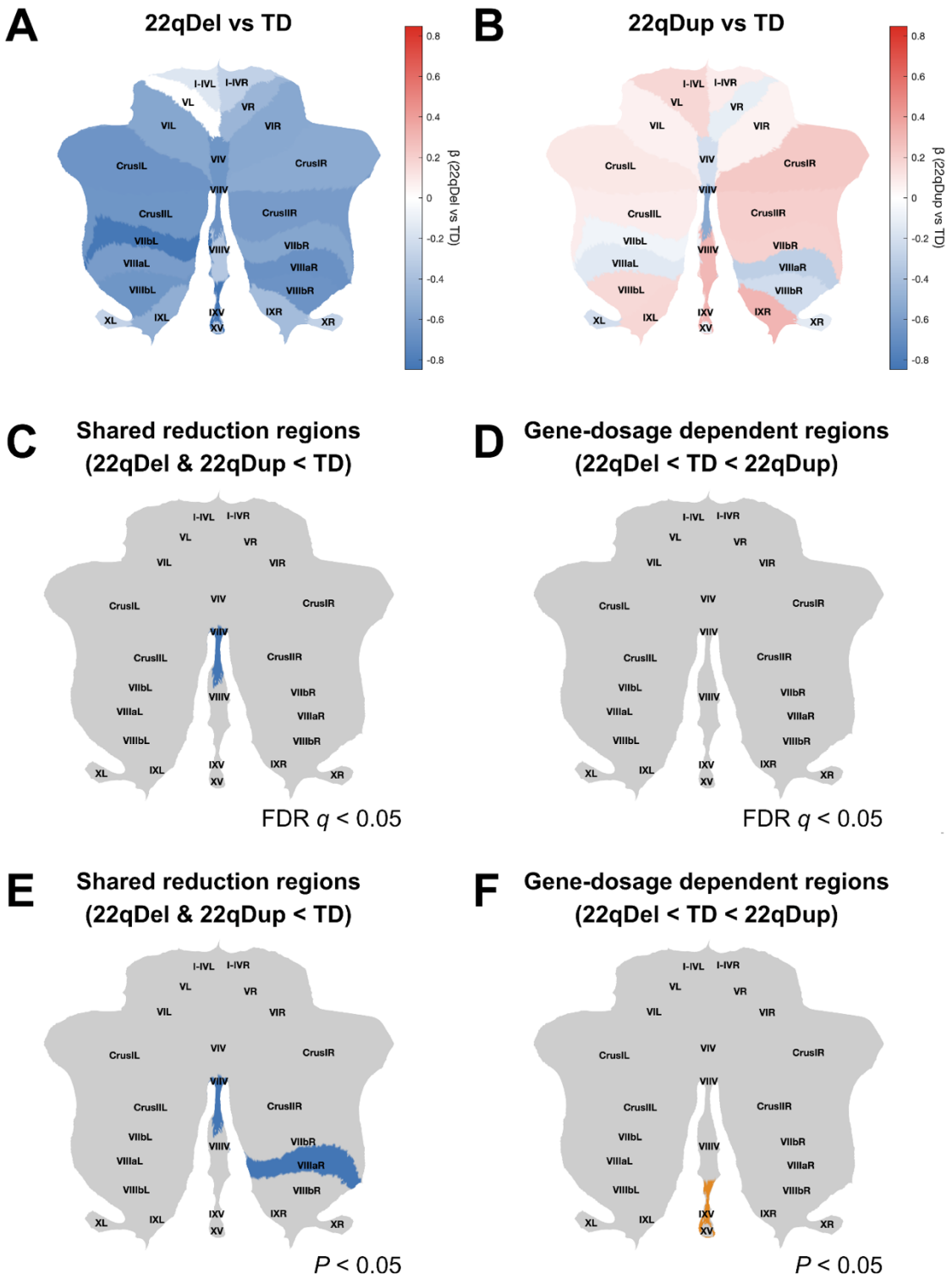

Figure 3 Multivariate associations between cerebellar volume and cognitive and social functioning.

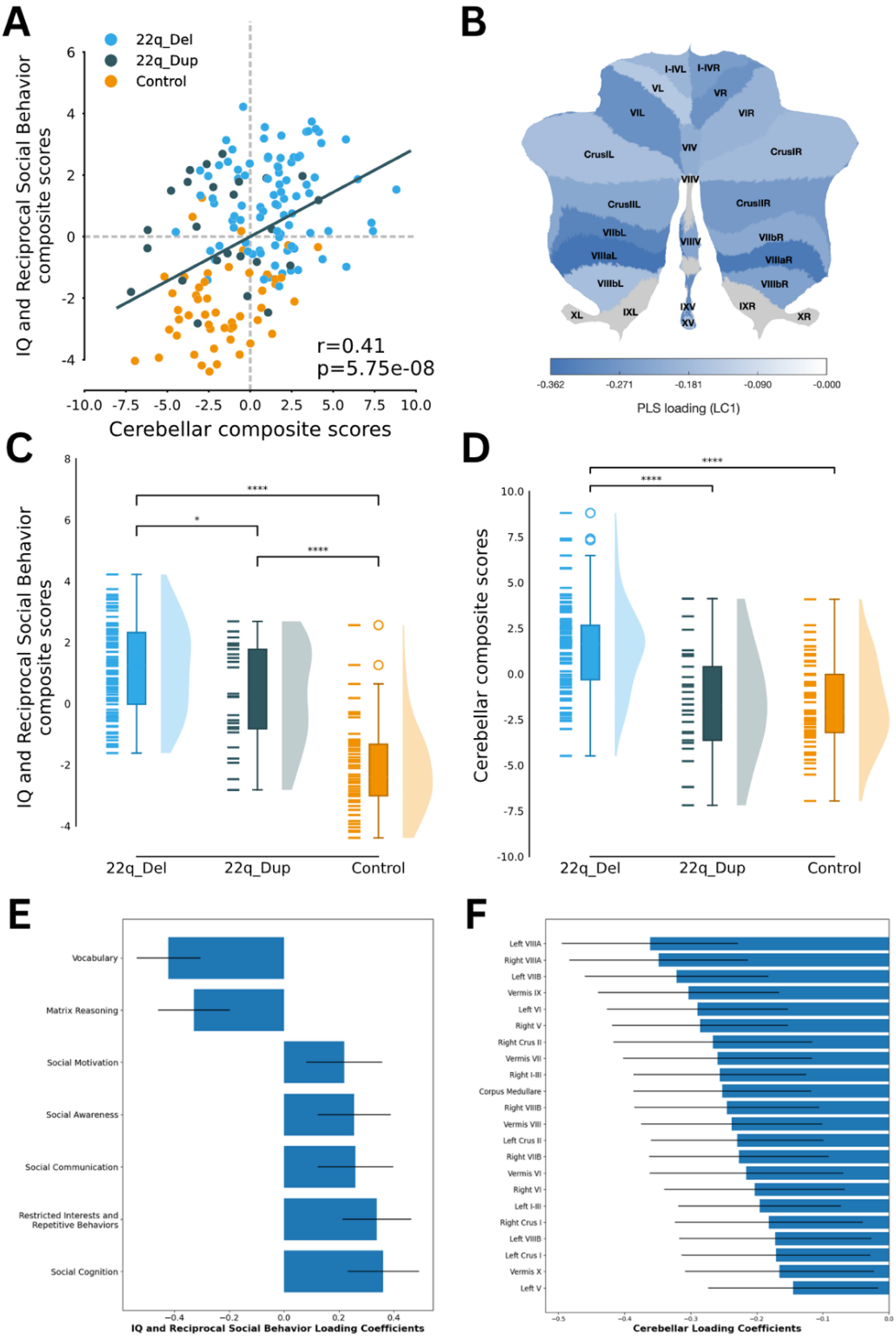

Figure 4 Multivariate associations between cerebellar volume and psychosis-risk symptoms.

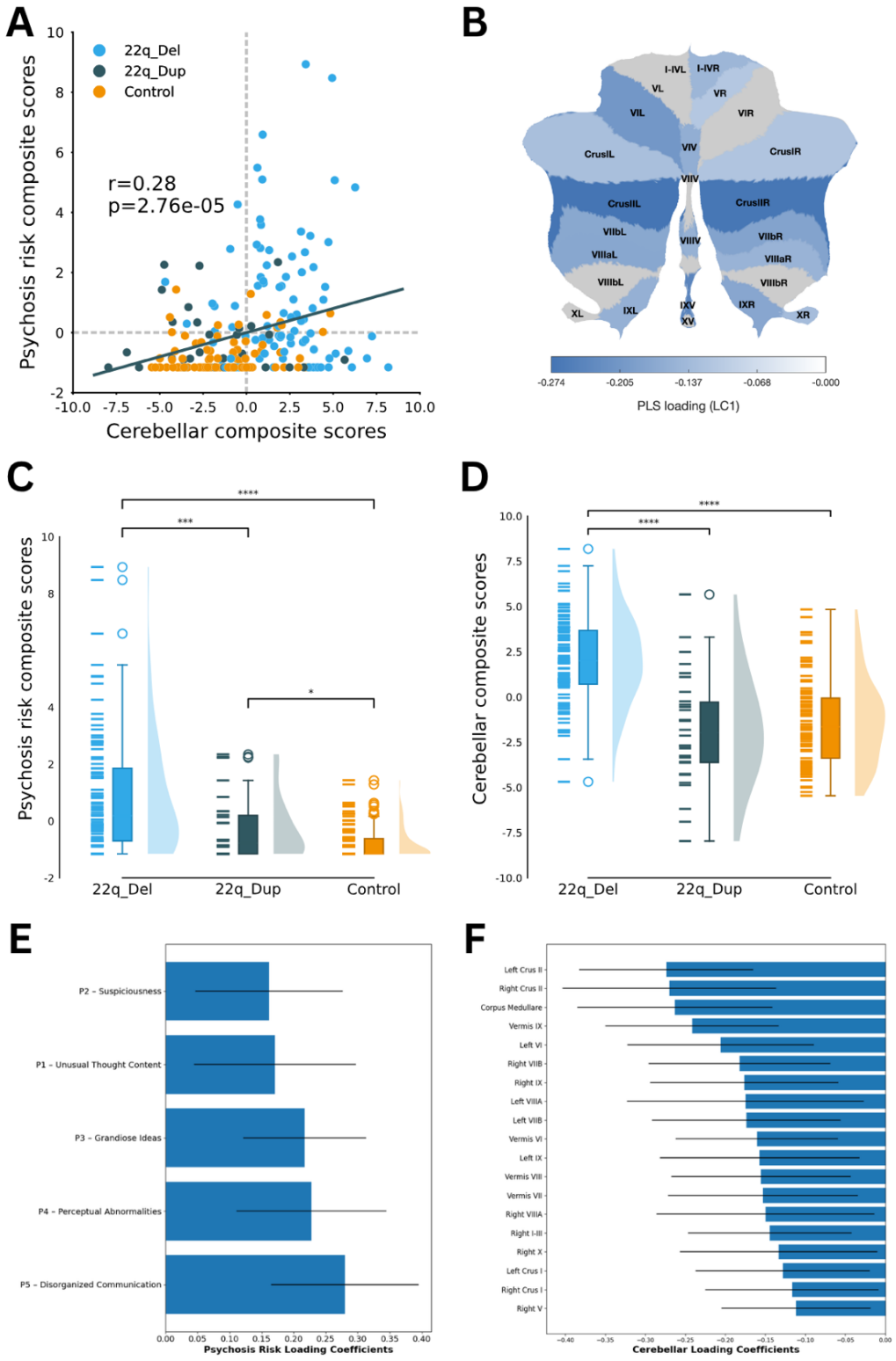

CHAPTER 1 SUPPLEMENTAL MATERIAL

Supplementary Methods

1. Participants and Study Design (Expanded recruitment/exclusion details)

Recruitment occurred through clinical referrals, community outreach, and research registries. TD controls were screened to exclude any personal or family history of psychosis, major neurological disorders, or known genetic conditions. Additional exclusion criteria for all participants included history of significant head trauma, contraindications to MRI, or severe sensorimotor impairments precluding valid assessment. Further details on inclusion and exclusion criteria, recruitment procedures, scanning protocol, and clinical measures have been reported previously (1,2).

2. Behavioral and Clinical Measures

2.1 Cognitive Ability

Overall cognitive ability was assessed using age-appropriate standardized measures of IQ, the *Wechsler Abbreviated Scale of Intelligence* (WASI) (3) or the *Wechsler Abbreviated Scale of Intelligence – Second Edition* (WASI-II) (4). Vocabulary and Matrix Reasoning subtest scores were used as measures of verbal and nonverbal cognitive ability, respectively, and were also combined to derive an estimated Full-Scale IQ (FSIQ) score based on established scoring procedures (3). Testing was conducted by trained research staff under the supervision of licensed psychologists.

2.2 Autism-related Traits

Autism-related traits were measured using the *Social Responsiveness Scale 2nd edition* (SRS-2) (5), a well-validated parent-report questionnaire that quantifies impairments in reciprocal social behavior. Age- and sex-normed T-scores from the SRS-2 subscales—Social Awareness, Social Cognition, Social Communication, Social Motivation and Restricted Interests and Repetitive Behaviors—were used as outcome variables to capture dimensional variation across core domains of autism-related symptomatology across the sample. The SRS-2 Total T-score is reported descriptively in baseline demographic tables and was not used as a primary outcome measure.

2.3 Psychosis Risk Symptoms

Psychosis risk symptoms were assessed in participants over the age of ten using the *Structured Interview for Psychosis-Risk Syndromes* (SIPS) (6), administered by trained Master's-level clinicians with supervision from a licensed clinical psychologist. Severity ratings of five individual positive symptoms—unusual thought content/delusional ideas, suspiciousness/persecutory ideas, grandiose ideas, perceptual abnormalities/hallucinations, and disorganized communication—were used in subsequent analyses. The SIPS positive symptom total score is reported descriptively in baseline demographic tables.

3. MRI Acquisition

Structural MRI data were collected at UCLA using three 3T Siemens MRI scanners: a Trio system at the Ahmanson-Lovelace Brain Mapping Center (BMC), and the Trio and Prisma systems at the Staglin Center for Cognitive Neuroscience (CCN). High-

resolution T1-weighted images were acquired using standardized magnetization-prepared rapid gradient echo (MPRAGE) sequences (7) using comparable parameters across scanners (TR = 2,300–2,400 ms, TE = 2.22–2.89 ms, TI = 900–1,060 ms, flip angle = 8–9°, voxel size = 1.0 × 1.0 × 1.2 mm or 0.8 mm^3 isotropic, and field of view = 240 × 256 mm^2). Data were subsequently harmonized to reduce scanner-related variability, as described in the Data Harmonization section.

4. T1 Image Processing and Quality Control

Prior to processing, all T1-weighted structural images were visually inspected for motion, artifacts, and acquisition errors. High-quality raw images were then used as input to ACAPULCO (version 3.0) (8) for cerebellar segmentation. ACAPULCO is a deep learning-based parcellation tool that divides the cerebellum into 28 anatomically defined subregions and includes its own internal preprocessing pipeline. The ACAPULCO pipeline was run in a containerized environment to ensure consistency across systems. Following segmentation, outputs were visually reviewed for quality, and scans with failed or poor parcellations were excluded from further analysis. Estimated total intracranial volume (eTIV) was derived from the T1-weighted images using FreeSurfer (versions 5.3.0 or 6.0.0) (9), and used as a covariate in all volumetric analyses.

5. Data Harmonization

To address scanner-related variability in volume measures, we applied Longitudinal ComBat (LongComBat) harmonization (10) to eTIV and cerebellar volumes.

LongComBat adjusts for scanner-related effects in multi-site longitudinal data while aiming to preserve biologically meaningful variance (10).

6. Statistical Analysis

6.1 Group Differences in Cerebellar Volume

6.1.1 Primary Analysis

To examine group differences in cerebellar volume, we fit linear mixed-effects models. Separate models were run for total cerebellar volume and for each of 28 anatomically defined cerebellar subregions (see Supplementary Table S2 for the full list). Each model included fixed effects for group (TD, 22qDel, 22qDup), sex, age (mean centered linear and quadratic terms), and eTIV, with a random intercept for subject to account for repeated measures across visits. TD controls were used as the reference group for primary analyses, and planned pairwise contrasts were specified to directly compare the 22qDel and 22qDup groups. To account for multiple comparisons, False Discovery Rate (FDR) correction was applied across the 28 regional volume models.

6.1.2 Sensitivity Analyses

To evaluate the robustness of group differences in cerebellar volume, we conducted a series of sensitivity analyses.

Sensitivity Analysis for Medication Use

First, the primary linear mixed-effects models were repeated with the inclusion of current psychiatric medication use as an additional covariate. Medication classes were

modeled separately and included antipsychotics, antidepressants, psychostimulants, and any psychiatric medication use.

Sensitivity Analysis by Age Group

Second, to assess potential developmental effects, the full dataset was stratified by age into pediatric (<18 years) and adult (≥18 years) subgroups, and the same modeling framework was applied within each age group.

6.2 Brain–Behavior Associations

To examine multivariate associations between cerebellar structure and clinical features, we employed partial least squares correlation analysis (PLSC) to identify latent components (LCs) that maximized covariation between regional cerebellar volumes and neurobehavioral measures. Because PLSC does not accommodate within-subject random effects or missing data, analyses were restricted to a single time point per participant with complete data.

Prior to PLSC, sex, age, and quadratic age effects were regressed out from both brain and behavioral variables using ordinary least squares regression. The PLSC methodology was consistent with our previous work (11).

Based on prior evidence of convergent alterations in cognition and social functioning in 22q11.2 CNVs (i.e., lower IQ and elevated autism-related traits (12)) and established gene-dosage–dependent patterns of psychosis risk (i.e., elevated risk in 22qDel carriers

and lower risk in 22qDup carriers (13,14)), separate PLSC models were specified for (i) cognitive and social functioning and (ii) psychosis-risk symptoms.

For all PLSC models, the brain matrix consisted of 28 ACAPULCO-derived cerebellar volumes that were harmonized and residualized as described above. PLSC decomposes the brain and behavioral data matrices into pairs of latent components capturing maximal covariance between the two domains. Statistical significance of LCs was assessed using permutation testing (5,000 permutations), with false discovery rate (FDR) correction applied across LCs ($q < 0.05$). Individual composite scores were calculated by projecting subject-level data onto significant LCs, and brain and behavioral loadings were computed as Pearson correlations between composite scores and the original variables. Post hoc analyses examined group differences in LC composite scores while accounting for age, quadratic age, and sex (11).

Cognitive and Social Functioning Model

One PLSC model examined associations between cerebellar volumes and cognitive and social functioning. The behavioral matrix included Vocabulary and Matrix Reasoning subtest scores from the WASI/WASI-II and age- and sex-normed T-scores from the SRS-2 Social Awareness, Social Cognition, Social Communication, and Social Motivation subscales. This model was designed to capture shared cerebellar contributions to variation in cognitive ability and reciprocal social functioning across groups. This analysis included 51 TD controls, 89 individuals with 22q11.2 deletion, and 25 individuals with 22q11.2 duplication.

Psychosis-Risk Symptoms Model

A separate PLSC model examined associations between cerebellar volumes and psychosis-risk symptoms. The behavioral matrix included severity ratings of the five SIPS positive symptom items: unusual thought content/delusional ideas, suspiciousness/persecutory ideas, grandiose ideas, perceptual abnormalities/hallucinations, and disorganized communication. This model was motivated by established gene-dosage–dependent differences in psychosis risk across 22q11.2 CNV groups. This analysis included 93 TD controls, 91 individuals with 22q11.2 deletion, and 30 individuals with 22q11.2 duplication.

7. Data Scaling and Visualization

All statistical models reported in text and tables were fitted using raw, unstandardized values to preserve interpretability in native units (e.g., mm^3 for brain volumes, points for behavioral scores). For visualization purposes, some figures (e.g., forest plots, flatmaps) display standardized values to facilitate comparison across regions and groups. Please refer to individual figure legends for details.

Supplementary Results

1. Sensitivity Analyses for Group Differences in Cerebellar Volume

1.1 Sensitivity Analysis for Medication Use

Participant counts for each psychotropic medication class by group at baseline are provided in Table S4. Bonferroni-corrected pairwise Fisher's exact tests did not reveal

significant differences between any individual groups. Group differences in cerebellar volume remained robust after accounting for psychotropic medication use. Specifically, repeating the primary linear mixed-effects models with current medication use included as an additional covariate—modeled separately for antipsychotics, antidepressants, psychostimulants, and any psychiatric medication use—did not alter the pattern, direction, or statistical significance of the total cerebellar volume results (Table S5). Regional cerebellar volume findings were consistent with the primary analyses, with no changes in effect direction or statistical significance.

1.2 Sensitivity Analysis by Age Group

Group differences in cerebellar volume were largely consistent when analyses were conducted separately in pediatric (<18 years; n = 191 participants) and adult (≥18 years; n = 137 participants) subgroups, with subject- and session-level sample sizes for each diagnostic group reported in Table S6. Total cerebellar volume results were consistent with the primary analysis across age strata (Table S6). At the regional level, a small number of effects no longer reached statistical significance after FDR correction in the age-stratified analyses (Figures S1-S2); however, the overall pattern and interpretation of regional findings remained consistent with the primary results. We note that the adult 22q11.2 duplication subgroup was small (n = 12 participants; 21 total sessions). Age-stratified results involving this subgroup should therefore be interpreted with caution.

2. PLSC: Cognitive Ability and Autism-Related Traits

2.1 Latent Component

Within-group correlations were not statistically significant, consistent with reduced dynamic range and limited power when stratifying by CNV group.

2.2 Cerebellar Loadings

Cerebellar loadings for the significant latent component (LC) revealed a distributed pattern of negative associations across multiple regions, indicating that higher LC scores were characterized by smaller regional cerebellar volumes. A total of 22 cerebellar regions showed significant loadings after correction (Figure 3F). The strongest loadings were observed in posterior cerebellar regions, including Left Lobule VIIIA ($r=-0.36$), Right Lobule VIIIA ($r=-0.35$), Left Lobule VIIB ($r=-0.32$), Vermis IX ($r=-0.30$), and Left Lobule VI ($r=-0.29$). Notably, all significant cerebellar loadings were negative, consistent with a multiregional pattern of cerebellar volume reduction associated with the LC. This spatially distributed loading profile suggests that the identified LC reflects a global cerebellar signature rather than effects driven by a single focal region.

2.3 Behavioral Loadings

Behavioral loadings indicated that the LC was characterized by lower cognitive ability and greater autism-related social difficulties (Figure 3E). Vocabulary and Matrix Reasoning subtest scores loaded negatively on the LC, whereas SRS-2 subscales—including Social Awareness, Social Cognition, Social Communication, Social Motivation, and Restricted Interests and Repetitive Behaviors—showed positive loadings. Together,

these loadings indicate that higher LC scores capture a cognitive–social profile marked by reduced cognitive functioning and increased challenges in reciprocal social behavior.

3. PLSC: Psychosis-Risk Symptoms

3.1 Latent Component

Within-group correlations were not statistically significant, consistent with reduced dynamic range and limited power when stratifying by CNV group.

3.2 Cerebellar Loadings

Cerebellar loadings for the significant latent component (LC) revealed a distributed pattern of negative associations across multiple regions, indicating that higher LC scores were characterized by smaller regional cerebellar volumes. A total of 19 cerebellar regions showed significant loadings after correction (Figure 4F). The strongest loadings were observed in Left Crus II ($r=-0.27$), Right Crus II ($r=-0.27$), Corpus Medullare ($r=-0.26$) and Vermis IX ($r=-0.24$). Notably, all significant cerebellar loadings were negative, consistent with a multiregional pattern of cerebellar volume reduction associated with the LC. This spatially distributed loading profile suggests that the identified LC reflects a global cerebellar signature rather than effects driven by a single focal region.

3.3 Behavioral Loadings

Behavioral loadings indicated that the LC was characterized by greater severity of psychosis-risk symptoms (Figure 4E). All five SIPS positive symptom items loaded

positively onto the LC, with the strongest contributions from disorganized communication (P5), followed by perceptual abnormalities/hallucinations (P4), grandiose ideas (P3), unusual thought content/delusional ideas (P1), and suspiciousness/persecutory ideas (P2). Together, these loadings indicate that higher LC scores capture a broad profile of elevated positive psychosis-risk symptoms, rather than being driven by a single symptom domain.

Supplementary Tables

Supplementary Table S1. Full model output for primary total cerebellar volume analysis.

Term	Estimate (B)	CI (2.5%)	CI (97.5%)	SE	t	p-value
(Intercept)	89467.99	79003.05	99932.93	5326.20	16.80	<0.001
Group_22qDel	-16072.03	-18916.36	-13227.71	1445.74	-11.12	<0.001
Group_22qDup	1579.76	-2620.60	5780.13	2134.78	0.74	0.46
Sex	9423.80	6619.64	12227.96	1425.96	6.61	<0.001
Age	53.98	-98.75	206.71	77.73	0.69	0.49
Age^2	-11.22	-19.53	-2.91	4.23	-2.65	0.01
eTIV	0.03	0.02	0.04	0.00	8.67	<0.001

Linear mixed-effects model results for total cerebellar volume. The model includes fixed effects for group (TD, 22qDel, 22qDup), sex, mean-centered age (linear and quadratic), and estimated

Supplementary Table S2. Full model results for primary regional cerebellar volume analyses (TD as reference).

	22qDel vs. TD							22qDup vs. TD						
Region	**B**	**CI (2.5%)**	**CI (97.5%)**	**SE**	**t**	**p-value**	**FDR q**	**B**	**CI (2.5%)**	**CI (97.5%)**	**SE**	**t**	**p-value**	**FDR q**
Corpus Medullare	-2268.34	-2788.14	-1748.53	264.22	-8.59	<0.001	<0.001	-169.75	-932.97	593.46	387.93	-0.44	0.66	0.73
Left Lobules I-III	-59.80	-113.68	-5.92	27.37	-2.18	0.03	0.03	10.67	-68.40	89.74	40.17	0.27	0.79	0.79
Right Lobules I-III	-99.59	-151.56	-47.62	26.41	-3.77	<0.001	<0.001	22.34	-53.93	98.60	38.75	0.58	0.56	0.73
Left Lobule IV	-46.63	-190.42	97.17	73.08	-0.64	0.52	0.54	182.88	-28.32	394.08	107.33	1.70	0.09	0.42
Right Lobule IV	-107.65	-255.33	40.02	75.05	-1.43	0.15	0.16	49.99	-167.02	266.99	110.28	0.45	0.65	0.73
Left Lobule V	1.82	-123.17	126.81	63.51	0.03	0.98	0.98	90.78	-92.66	274.21	93.21	0.97	0.33	0.61
Right Lobule V	-275.43	-397.72	-153.14	62.15	-4.43	<0.001	<0.001	-71.09	-250.75	108.58	91.30	-0.78	0.44	0.68
Vermis VI	-180.60	-238.78	-122.42	29.57	-6.11	<0.001	<0.001	-58.77	-144.31	26.77	43.47	-1.35	0.18	0.47
Left Lobule VI	-922.26	-1247.30	-597.21	165.20	-5.58	<0.001	<0.001	99.97	-378.17	578.11	242.98	0.41	0.68	0.73
Right Lobule VI	-823.46	-1153.26	-493.65	167.61	-4.91	<0.001	<0.001	87.32	-399.34	573.98	247.29	0.35	0.72	0.75
Vermis VII	-124.98	-165.40	-84.56	20.54	-6.08	<0.001	<0.001	-100.05	-159.49	-40.61	30.21	-3.31	<0.001	0.03
Left Crus I	-1559.62	-2030.02	-1089.22	239.09	-6.52	<0.001	<0.001	243.62	-448.29	935.52	351.65	0.69	0.49	0.72
Left Crus II	-1082.77	-1423.91	-741.62	173.38	-6.25	<0.001	<0.001	138.72	-362.42	639.86	254.67	0.54	0.59	0.73
Left Lobule VIIB	-1178.50	-1477.88	-879.13	152.14	-7.75	<0.001	<0.001	-102.85	-542.91	337.21	223.61	-0.46	0.65	0.73
Right Crus I	-1194.20	-1641.53	-746.86	227.38	-5.25	<0.001	<0.001	508.82	-150.46	1168.10	335.08	1.52	0.13	0.47
Right Crus II	-927.54	-1241.89	-613.19	159.77	-5.81	<0.001	<0.001	300.52	-161.57	762.61	234.84	1.28	0.20	0.47
Right Lobule VIIB	-850.42	-1160.84	-540.00	157.77	-5.39	<0.001	<0.001	298.59	-157.35	754.52	231.72	1.29	0.20	0.47

Vermis VIII	-132.02	-208.78	-55.27	39.02	-3.38	<0.001	<0.001	112.50	-0.70	225.70	57.54	1.96	0.05	0.36
Left Lobule VIIIA	-923.42	-1228.22	-618.61	154.92	-5.96	<0.001	<0.001	-213.28	-660.78	234.22	227.44	-0.94	0.35	0.61
Left Lobule VIIIB	-527.12	-706.95	-347.30	91.40	-5.77	<0.001	<0.001	133.60	-130.41	397.61	134.19	1.00	0.32	0.61
Right Lobule VIIIA	-812.62	-1053.90	-571.33	122.64	-6.63	<0.001	<0.001	-358.09	-712.17	-4.00	179.97	-1.99	0.05	0.36
Right Lobule VIIIB	-544.22	-711.95	-376.48	85.26	-6.38	<0.001	<0.001	-178.91	-425.06	67.24	125.12	-1.43	0.15	0.47
Vermis IX	-168.46	-208.21	-128.71	20.20	-8.34	<0.001	<0.001	61.02	2.61	119.44	29.69	2.06	0.04	0.36
Left Lobule IX	-389.11	-560.71	-217.51	87.22	-4.46	<0.001	<0.001	131.92	-120.57	384.41	128.33	1.03	0.30	0.61
Right Lobule IX	-319.26	-490.19	-148.33	86.88	-3.67	<0.001	<0.001	236.69	-14.66	488.03	127.74	1.85	0.06	0.36
Vermis X	-22.88	-37.46	-8.31	7.41	-3.09	<0.001	<0.001	-6.02	-27.46	15.41	10.90	-0.55	0.58	0.73
Left Lobule X	-24.71	-44.17	-5.24	9.89	-2.50	0.01	0.02	-18.50	-47.06	10.06	14.52	-1.27	0.20	0.47
Right Lobule X	-28.50	-50.70	-6.30	11.28	-2.53	0.01	0.01	-13.93	-46.50	18.65	16.56	-0.84	0.40	0.66

Results from linear mixed-effects models assessing group differences across 28 anatomically defined cerebellar subregions. Each model included fixed effects for sex, mean-centered age (linear and quadratic), estimated intracranial volume (eTIV), and group (TD, 22qDel, 22qDup), with a subject-level random intercept to account for repeated measures. In these models, TD controls served as the reference group, and results are reported for 22qDel vs. TD (left) and 22qDup vs. TD (right) comparisons.

Supplementary Table S3. Full model results for primary regional cerebellar volume analyses (22qDel as reference).

	22qDup vs. 22qDel						
Region	B	CI (2.5%)	CI (97.5%)	SE	t	p-value	FDR q
Corpus Medullare	2098.59	1305.56	2891.61	403.06	5.21	<0.001	<0.001
Left Lobules I-III	70.47	-11.47	152.41	41.63	1.69	0.09	0.12
Right Lobules I-III	121.93	42.80	201.06	40.20	3.03	<0.001	<0.001
Left Lobule IV	229.50	9.97	449.04	111.56	2.06	0.04	0.05
Right Lobule IV	157.64	-68.04	383.32	114.68	1.37	0.17	0.20
Left Lobule V	88.96	-101.44	279.35	96.74	0.92	0.36	0.40
Right Lobule V	204.34	17.54	391.15	94.93	2.15	0.03	0.05
Vermis VI	121.83	32.85	210.81	45.21	2.69	0.01	0.01
Left Lobule VI	1022.22	524.70	1519.75	252.83	4.04	<0.001	<0.001
Right Lobule VI	910.78	403.97	1417.58	257.53	3.54	<0.001	<0.001
Vermis VII	24.93	-36.91	86.78	31.43	0.79	0.43	0.44
Left Crus I	1803.24	1083.31	2523.17	365.88	4.93	<0.001	<0.001
Left Crus II	1221.49	700.48	1742.50	264.75	4.61	<0.001	<0.001
Left Lobule VIIB	1075.66	617.93	1533.38	232.57	4.63	<0.001	<0.001
Right Crus I	1703.01	1016.61	2389.42	348.85	4.88	<0.001	<0.001
Right Crus II	1228.06	747.41	1708.72	244.26	5.03	<0.001	<0.001
Right Lobule VIIB	1149.01	675.06	1622.95	240.85	4.77	<0.001	<0.001

Vermis VIII	244.53	126.65	362.40	59.91	4.08	<0.001	<0.001
Left Lobule VIIIA	710.14	245.24	1175.04	236.26	3.01	<0.001	0.01
Left Lobule VIIIB	660.72	386.42	935.02	139.40	4.74	<0.001	<0.001
Right Lobule VIIIA	454.53	87.28	821.78	186.64	2.44	0.02	0.02
Right Lobule VIIIB	365.31	110.08	620.54	129.73	2.82	0.01	0.01
Vermis IX	229.48	168.73	290.23	30.87	7.43	<0.001	<0.001
Left Lobule IX	521.03	258.27	783.78	133.54	3.90	<0.001	<0.001
Right Lobule IX	555.95	294.46	817.44	132.89	4.18	<0.001	<0.001
Vermis X	16.86	-5.44	39.16	11.34	1.49	0.14	0.17
Left Lobule X	6.20	-23.42	35.83	15.05	0.41	0.68	0.68
Right Lobule X	14.57	-19.23	48.38	17.18	0.85	0.40	0.43

Results from linear mixed-effects models assessing group differences across 28 anatomically defined cerebellar subregions. Each model included fixed effects for sex, mean-centered age (linear and quadratic), estimated intracranial volume (eTIV), and group (TD, 22qDel, 22qDup), with a subject-level random intercept to account for repeated measures. In these models, 22qDel was the reference group, and results for the 22qDup vs. 22qDel comparison are reported here.

Supplementary Table S4. Psychotropic medication use by group at baseline.

Medication Class	TD Controls (n=167)	22qDel (n=111)	22qDup (n=37)	Group Comparisons [a]
Antipsychotics, N (%)	0 (0)	11 (9.9)	1 (2.7)	$p < 0.001$
Antidepressants, N (%)	0 (0)	15 (13.5)	2 (5.4)	$p < 0.001$
Psychostimulants, N (%)	2 (1.2)	6 (5.41)	6 (16.2)	$p < 0.001$
Any psychotropic medication, N (%)	3 (1.8)	37 (33.3)	11 (29.7)	$p < 0.001$

Values represent the number of participants receiving each medication class. Counts for "Any psychotropic medication" include antipsychotics, antidepressants, psychostimulants, and other psychotropic medications.

[a] Group differences in medication use were assessed using Fisher's exact tests. Although omnibus tests were significant, Bonferroni-corrected post hoc pairwise Fisher's exact tests did not identify significant differences between individual groups, consistent with sparse cell counts.

Supplementary Table S5. Sensitivity analysis results for total cerebellar volume with adjustment for medication use.

	Antipsychotics				Antidepressants			
Term	**B**	**CI (2.5%)**	**CI (97.5%)**	**p-value**	**B**	**CI (2.5%)**	**CI (97.5%)**	**p-value**
(Intercept)	89604.17	79085.65	100122.68	<0.001	89116.8	78654.96	99578.64	<0.001
Group_22qDel	-16132.58	-19023.1	-13242.05	<0.001	-15822.18	-18680.49	-12963.88	<0.001
Group_22qDup	1569.34	-2637.66	5776.33	0.464	1845.65	-2362.42	6053.73	0.389
Sex	9435.8	6626.91	12244.69	<0.001	9411.24	6611.23	12211.25	<0.001
Age	55.46	-97.79	208.71	0.477	53.09	-99.47	205.64	0.494
Age^2	-11.28	-19.61	-2.95	0.008	-11.5	-19.81	-3.19	0.007
eTIV	0.03	0.02	0.04	<0.001	0.03	0.02	0.04	<0.001
Medication Use	576.59	-4209.63	5362.81	0.813	-1801.35	-4156.23	553.54	0.133

	Antipsychotics				Antidepressants			
Term	**B**	**CI (2.5%)**	**CI (97.5%)**	**p-value**	**B**	**CI (2.5%)**	**CI (97.5%)**	**p-value**
(Intercept)	89604.17	79085.65	100122.68	<0.001	89116.8	78654.96	99578.64	<0.001
Group_22qDel	-16132.58	-19023.1	-13242.05	<0.001	-15822.18	-18680.49	-12963.88	<0.001
Group_22qDup	1569.34	-2637.66	5776.33	0.464	1845.65	-2362.42	6053.73	0.389
Sex	9435.8	6626.91	12244.69	<0.001	9411.24	6611.23	12211.25	<0.001
Age	55.46	-97.79	208.71	0.477	53.09	-99.47	205.64	0.494
Age^2	-11.28	-19.61	-2.95	0.008	-11.5	-19.81	-3.19	0.007
eTIV	0.03	0.02	0.04	<0.001	0.03	0.02	0.04	<0.001
Medication Use	576.59	-4209.63	5362.81	0.813	-1801.35	-4156.23	553.54	0.133

Sensitivity analysis for medication use. Linear mixed-effects models identical to the primary analysis were refitted with an additional medication use covariate. Separate models were fitted for antipsychotics, antidepressants, psychostimulants, and any medication use. Inclusion of medication covariates did not alter the primary results.

Supplementary Table S6. Sensitivity analysis results for total cerebellar volume stratified by age.

	Pediatric (<18 years)				Adult (≥18 years)			
Term	**B**	**CI (2.5%)**	**CI (97.5%)**	**p-value**	**B**	**CI (2.5%)**	**CI (97.5%)**	**p-value**
(Intercept)	82952.05	67802.69	98101.42	<0.001	112546.96	98607.48	126486.45	<0.001
Group_22qDel	-14114.36	-17732.17	-10496.56	<0.001	-19859.29	-24221.55	-15497.03	<0.001
Group_22qDup	-462.95	-5525.59	4599.69	0.857	4942.79	-2676.06	12561.64	0.202
Sex	8843.43	5107.47	12579.39	<0.001	12010.8	7701.29	16320.3	<0.001
Age	312.77	-64.1	689.65	0.103	-233.34	-452.86	-13.82	0.037
Age^2	-93.99	-185.66	-2.31	0.045	1.1	-12.87	15.07	0.876
eTIV	0.03	0.02	0.05	<0.001	0.01	0.01	0.02	0.002

Sensitivity analysis for age stratification. Linear mixed-effects models identical to the primary analysis were refitted separately in pediatric (<18 years) and adult (≥18 years) subgroups. Total cerebellar volume results were consistent with the primary analysis. Sample sizes: Pediatric subgroup (<18 years): TD (n = 92 participants; 148 sessions), 22qDel (n = 74; 118 sessions), 22qDup (n = 25; 42 sessions); Adult subgroup (≥18 years): TD (n = 77; 86 sessions), 22qDel (n = 48; 99 sessions), 22qDup (n = 12; 21 sessions).

Supplementary Figures

Figure S1. Age-stratified group differences in regional cerebellar volume (<18 years).

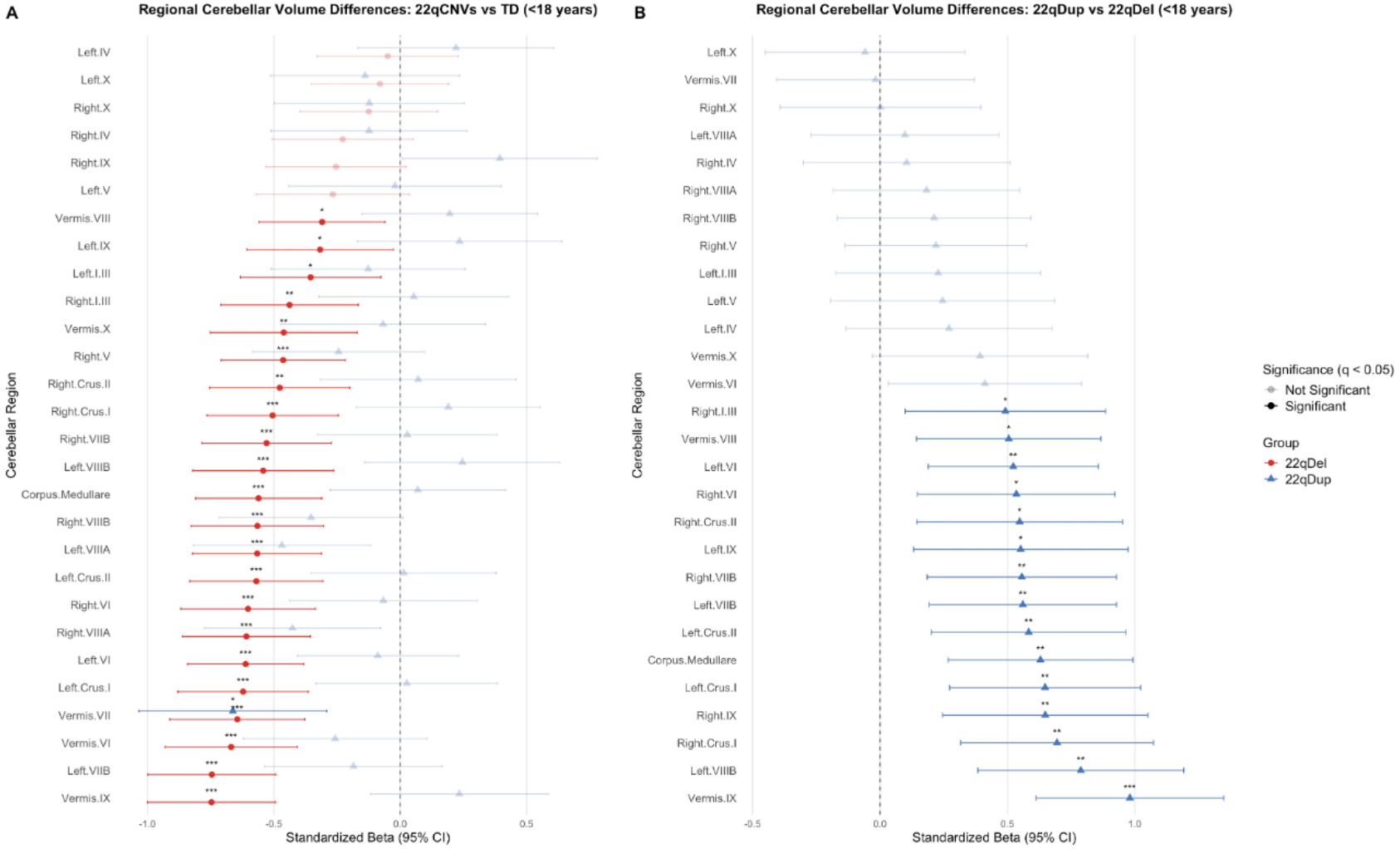

Figure S2. Age-stratified group differences in regional cerebellar volume (≥18 years).

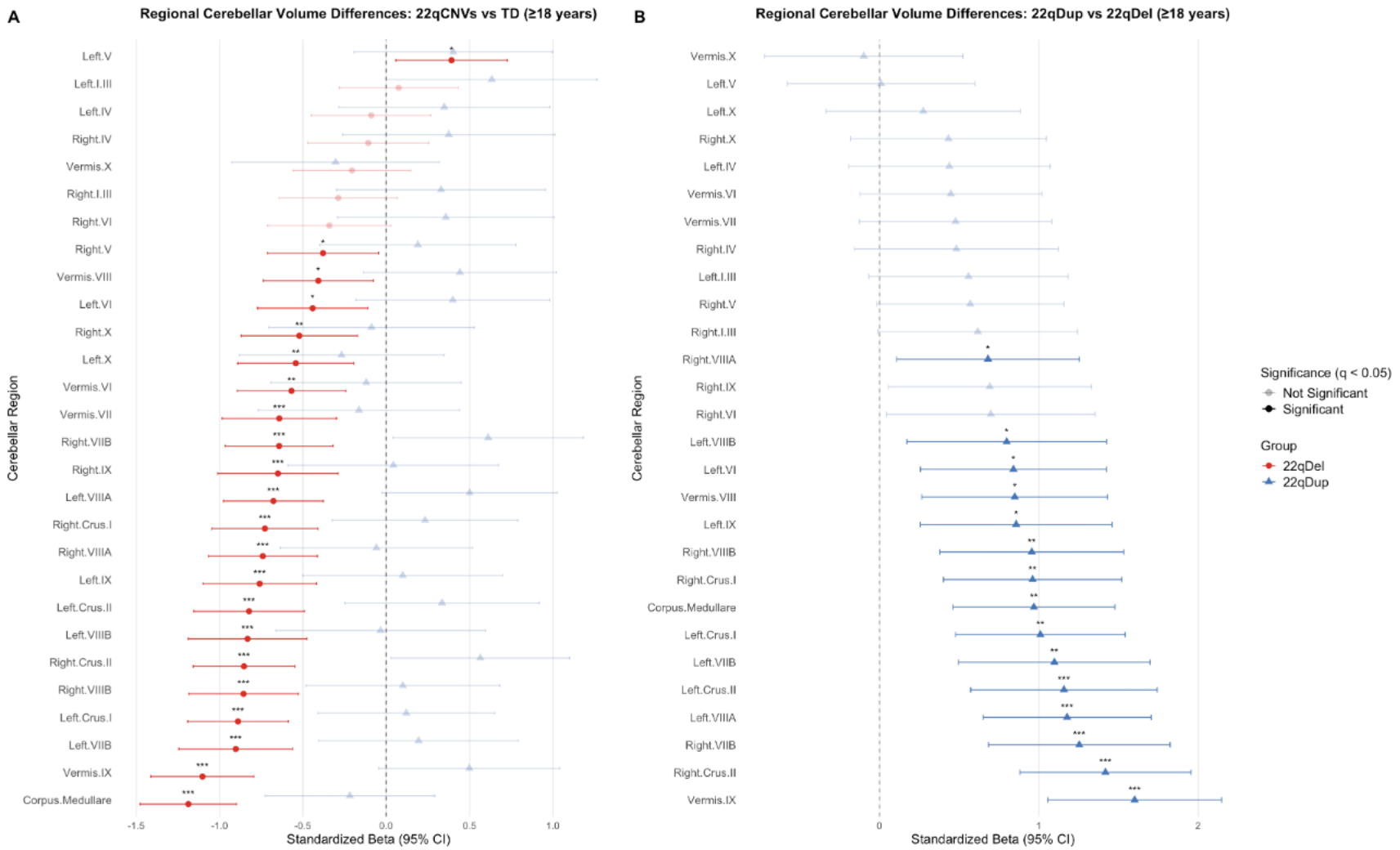

Supplementary References

1. Jalbrzikowski M, Lin A, Vajdi A, Grigoryan V, Kushan L, Ching CRK, *et al.* (2022): Longitudinal trajectories of cortical development in 22q11.2 copy number variants and typically developing controls. *Mol Psychiatry* 27: 4181–4190.

2. Schleifer CH, O'Hora KP, Fung H, Xu J, Robinson T-A, Wu AS, *et al.* (2024): Effects of gene dosage and development on subcortical nuclei volumes in individuals with 22q11.2 copy number variations. *Neuropsychopharmacology*. https://doi.org/10.1038/s41386-024-01832-3

3. Wechsler D (1999): *Manual for the Wechsler Abbreviated Intelligence Scale (WASI)*. San Antonio, TX: The Psychological Corporation.

4. Wechsler D (2011): *Wechsler Abbreviated Scale of Intelligence, Second Edition*. San Antonio, TX: Pearson.

5. Constantino JN, Gruber CP (2005): Social Responsiveness Scale 2nd ed: Western Psychological Services.

6. McGlashan TH, Miller TJ, Woods SW, Hoffman RE, Davidson L (2001): Instrument for the assessment of prodromal symptoms and states. *Early Intervention in Psychotic Disorders*. Dordrecht: Springer Netherlands, pp 135–149.

7. Mugler JP 3rd, Brookeman JR (1990): Three-dimensional magnetization-prepared rapid gradient-echo imaging (3D MP RAGE). *Magn Reson Med* 15: 152–157.

8. Han S, Carass A, He Y, Prince JL (2020): Automatic cerebellum anatomical parcellation using U-Net with locally constrained optimization. *Neuroimage* 218: 116819.

9. Fischl B (2012): FreeSurfer. *Neuroimage* 62: 774–781.

10. Beer JC, Tustison NJ, Cook PA, Davatzikos C, Sheline YI, Shinohara RT, *et al.* (2020): Longitudinal ComBat: A method for harmonizing longitudinal multi-scanner imaging data. *Neuroimage* 220: 117129.

11. Wang HR, Liu Z-Q, Nakua H, Hegarty CE, Thies MB, Patel PK, *et al.* (2025): Decoding early psychoses: Unraveling stable microstructural features associated with psychopathology across independent cohorts. *Biol Psychiatry* 97: 167–177.

12. Lin A, Vajdi A, Kushan-Wells L, Helleman G, Hansen LP, Jonas RK, *et al.* (2020): Reciprocal Copy Number Variations at 22q11.2 Produce Distinct and Convergent Neurobehavioral Impairments Relevant for Schizophrenia and Autism Spectrum Disorder. *Biol Psychiatry* 88: 260–272.

13. Rees E, Walters JTR, Georgieva L, Isles AR, Chambert KD, Richards AL, *et al.* (2014): Analysis of copy number variations at 15 schizophrenia-associated loci. *British Journal of Psychiatry* 204: 108–114.

14. Marshall CR, Howrigan DP, Merico D, Thiruvahindrapuram B, Wu W, Greer DS, *et al.* (2017): Contribution of copy number variants to schizophrenia from a genome-wide study of 41,321 subjects. *Nat Genet* 49: 27–35.

CHAPTER 2: MULTIMODAL CEREBELLAR ALTERATIONS REVEAL DISTINCT EFFECTS OF 22q11.2 DELETION AND DUPLICATION

Hoki Fung[1,2], Charles H. Schleifer[1,2], Kathleen P. O'Hora[1,2], Rune Boen[1], Tyler E. Dietterich[1,2], Haley R. Wang[1,3], Jee Won Kang[1,3], Priyanka Sigar[1,2], Jason S. Nomi[1], Zhen-Qi Liu[4,5], Leila Kushan-Wells[1], Paul J. Mathews[6,7], Leanna Hernandez[1,8], Lucina Q. Uddin[1,3], Carrie E. Bearden[1,3]

1. Department of Psychiatry and Biobehavioral Sciences, Semel Institute for Neuroscience and Human Behavior, University of California, Los Angeles, CA, USA.
2. Neuroscience Interdepartmental Program, University of California Los Angeles, Los Angeles, CA, USA.
3. Department of Psychology, University of California, Los Angeles, CA, USA.
4. Department of Psychiatry, University of Cambridge, Cambridge, UK.
5. Wolfson College, University of Cambridge, Cambridge, UK.
6. Department of Neurology, University of California, Los Angeles School of Medicine, Los Angeles, CA, USA.
7. The Lundquist Institute at Harbor-UCLA, Torrance, CA, USA.
8. Center for Autism Research and Treatment, University of California, Los Angeles, Los Angeles, CA, USA.

A version of this chapter is in preparation for journal submission.

ABSTRACT

Background

Reciprocal 22q11.2 copy number variants (CNVs) provide a powerful gene-dosage model for investigating neurodevelopmental mechanisms. Prior work identified widespread cerebellar volume reductions in 22q11.2 deletion (22qDel) but comparatively preserved cerebellar volume in 22q11.2 duplication (22qDup). Whether this asymmetry extends to cerebellar white matter microstructure and functional connectivity remains unknown.

Methods

Cerebellar white matter microstructure was assessed using diffusion MRI (n=119) and resting-state functional connectivity (FC) in an overlapping sample (n=218), across 22qDel, 22qDup, and typically developing (TD) controls. Regional cerebellar volumes from our prior study were integrated with diffusion and FC metrics to characterize multimodal CNV signatures and their associations with cognitive, social, and psychosis-risk phenotypes.

Results

In contrast to the volumetric pattern, 22qDup showed widespread white matter microstructural alterations across all three cerebellar peduncles, characterized by lower fractional anisotropy and axial diffusivity and higher radial diffusivity. 22qDel showed more selective, opposite-direction alterations in the superior cerebellar peduncle. Cerebellar FC alterations were comparatively limited: 22qDel showed selective

cerebellar-cortical and cerebellar-subcortical hypoconnectivity, whereas no significant FC differences were detected in 22qDup. Multimodal features robustly distinguished 22qDel from 22qDup, with cerebellar volume contributing most strongly to 22qDel-related distinctions and white matter microstructure to 22qDup-related distinctions. A multimodal cerebellar pattern was significantly associated with cognitive and social functioning; associations with psychosis-risk symptoms were nominal but did not survive multiple-comparison correction.

Conclusions

22q11.2 copy number exerts dissociable effects across levels of cerebellar organization: macrostructural alterations are most pronounced in 22qDel, whereas white matter microstructural alterations are unexpectedly widespread in 22qDup, with more limited effects on functional connectivity. These findings demonstrate that cerebellar volume alone does not capture the neurodevelopmental impact of 22q11.2 gene dosage and suggest that distinct dosage-sensitive mechanisms may shape cerebellar morphology and circuit architecture.

INTRODUCTION

Reciprocal 22q11.2 copy number variants (CNVs)—deletions (22qDel) and duplications (22qDup) of the same multi-gene region on chromosome 22—provide a powerful human model for investigating gene-dosage effects on neurodevelopment Both CNVs confer elevated rates of autism spectrum disorder (ASD) and intellectual disability (1–4), yet schizophrenia risk is markedly increased in 22qDel, whereas 22qDup does not share this elevated risk and may instead be protective relative to the general population (5). This combination of shared neurodevelopmental liability and divergent psychosis risk positions reciprocal 22q11.2 CNVs as a powerful genetics-first model for dissecting convergent and divergent neurobiological mechanisms underlying cognition, social functioning, and psychosis risk (6,7).

The cerebellum, traditionally associated with motor coordination, is now understood to be a key hub for cognition, affect, and social processing (8–10), and has been implicated in both schizophrenia (11,12) and ASD (13,14). In our prior lobule-level analysis of cerebellar morphology in 22q11.2 CNVs, 22qDel showed widespread volumetric reductions across nearly all cerebellar subregions relative to typically developing (TD) controls, whereas 22qDup carriers showed comparatively mild and regionally selective alterations, with Vermis VII emerging as a shared site of vulnerability (7). This marked asymmetry raises an important question: does 22qDel exert a greater impact on cerebellar development overall, or do the relative effects of 22qDel and 22qDup depend on the biological feature being measured?

One of the largest between-CNV differences we observed was in the corpus medullare, the central white matter core of the cerebellum, which was substantially

smaller in 22qDel relative to both TD controls and 22qDup (7). The corpus medullare is continuous with the cerebellar peduncles, the three paired white matter tracts linking the cerebellum with the cerebral cortex, subcortex, brainstem, and spinal cord (15). The superior cerebellar peduncle (SCP) is predominantly efferent, carrying output from the cerebellum to the cerebral cortex via the thalamus. The middle cerebellar peduncle (MCP) is exclusively afferent, relaying cortical input to the cerebellum via the corticopontocerebellar pathway, and the inferior cerebellar peduncle (ICP) contains mixed afferent and efferent fibers connecting the cerebellum to the brainstem, spinal cord, and vestibular system (16). However, corpus medullare volume cannot determine which cerebellar pathways are affected or whether reduced volume reflects altered white-matter microstructure.

Diffusion MRI (dMRI) provides complementary information about white-matter organization that cannot be inferred from regional volume. (17). Diffusion tensor imaging (DTI), the most widely used model of the diffusion process, represents water diffusion at each voxel as a three-dimensional tensor (18). In white matter tracts, the directionality of this tensor is influenced by underlying fiber organization, yielding indices from which microstructural properties can be inferred (19). Commonly derived DTI indices include fractional anisotropy (FA), reflecting how strongly water diffusion is constrained along the dominant fiber orientation, and axial, radial, and mean diffusivity (AD, RD, MD), which respectively capture the rate of diffusion along, perpendicular to, and averaged across all directions. FA is broadly associated with fiber density, myelination, and coherence; AD with axonal integrity; and RD with myelin integrity, though none of these

indices is specific to a single microstructural feature, and they are best interpreted together (20).

While individual cerebellar tracts have occasionally been examined in broader whole-brain DTI studies of the 22qDel (21,22), no study has systematically examined all three cerebellar peduncles across both reciprocal CNVs. In prior work from our group using partially overlapping samples, 22qDel and 22qDup showed opposing alterations in supratentorial white matter microstructure: DTI-derived anisotropy was higher in 22qDel and lower in 22qDup relative to TD controls (23), while neurite orientation dispersion and density imaging (NODDI) analyses similarly identified higher intracellular volume fraction in 22qDel and lower intracellular volume fraction in 22qDup (24). These findings motivated the present anatomically targeted test of whether reciprocal copy-number effects on white-matter microstructure extend to the cerebellar output and input pathways, particularly given the contrasting morphological pattern of widespread cerebellar volume reductions in 22qDel but comparatively preserved volume in 22qDup. Structural and microstructural findings, however, do not necessarily imply altered functional communication. Resting-state functional connectivity (rsFC) quantifies functional coupling between brain regions from the temporal correlation of their blood-oxygen-level-dependent (BOLD) signal, a proxy for neural activity, while an individual is at rest (25). Dysconnectivity, reflected as either increased (hyperconnectivity) or decreased (hypoconnectivity) correlation strength relative to baseline or typical development, is thought to indicate atypical functional communication between regions, allowing us to ask whether anatomical and microstructural abnormalities are accompanied by alterations in functional circuitry. rsFC studies in 22qDel have identified

widespread dysconnectivity involving cortical, thalamic and hippocampal circuits, though the direction and anatomical distribution of these effects has varied across studies (26–29). Far less is known about 22qDup, although limited prior evidence from our group suggests that the reciprocal CNVs may show opposing connectivity effects in selected circuits (29). Cerebellar FC has not been systematically characterized across reciprocal 22q11.2 CNVs, leaving unknown whether functional alterations parallel the volumetric phenotype, the predicted reciprocal white-matter phenotype, or neither.

Together, these observations motivate a multimodal test of whether 22q11.2 dosage exerts a common effect across levels of cerebellar organization. Regional volume indexes cerebellar macrostructure, diffusion MRI characterizes white-matter microstructure, and rsFC measures functional coupling. Examining these modalities jointly can therefore determine whether deletion and duplication produce parallel effects across biological scales or preferentially affect distinct dimensions of cerebellar organization (30). Multimodal integration may additionally reveal whether these complementary features jointly distinguish CNV groups and relate to cognitive and clinical phenotypes.

Building on our prior volumetric study (7), we characterized cerebellar white matter microstructure and resting-state functional connectivity in 22qDel and 22qDup relative to TD controls, and integrated these measures with regional cerebellar volume. Based on opposing white-matter abnormalities previously observed outside the cerebellum, we hypothesized that cerebellar white matter microstructure would show reciprocal gene-dosage effects, with opposing alterations in 22qDel and 22qDup relative to TD controls. Based on prior evidence for dosage-sensitive functional dysconnectivity,

we further hypothesized that cerebellar FC would differ between reciprocal CNVs, although the extent to which these effects would parallel structural or microstructural abnormalities was unknown. Finally, we tested whether multimodal cerebellar profiles distinguished CNV groups and captured variation in cognitive ability, social functioning, and psychosis-risk symptoms.

METHODS AND MATERIALS

Participants and Study Design

Participants were drawn from the same longitudinal 22q11.2 CNV study at the University of California, Los Angeles (UCLA) described in our prior volumetric report (7). Resting-state fMRI (rs-fMRI) was acquired across three 3T Siemens scanners, specifically two Trio and one Prisma, in 218 participants (366 scans; baseline 22qDel n=86, 22qDup n=33, TD n=99). Diffusion MRI (dMRI) was acquired across all three scanners, but the cerebellum fell outside the field of view on the two Trio scanners. Only dMRI scans acquired on the Prisma scanner were therefore included in the present study. The resulting dMRI subsample comprised 154 scans from 119 participants at baseline (22qDel n=47; 22qDup n=21; TD n=51). Groups did not differ significantly in age or sex distribution within either modality-specific subsample (Table 1). Recruitment, consent, Institutional Review Board procedures, and inclusion/exclusion criteria were identical to those described previously (7).

Behavioral and Clinical Measures

Cognitive ability, autism-related traits, and psychosis-risk symptoms were assessed using the Wechsler Abbreviated Scale of Intelligence (WASI or WASI-II) (31,32), the Social Responsiveness Scale, Second Edition (SRS-2) (33), and the Structured Interview for Psychosis-Risk Syndromes (SIPS) (34), respectively. Full instrument descriptions and scoring procedures are provided in the Supplementary Methods of our prior report (7).

Diffusion MRI Acquisition and Processing

Multi-shell dMRI data were acquired at UCLA using a previously described protocol (24). Preprocessing was performed using the Human Connectome Project Minimal Preprocessing Pipeline (HCP-MPP) (35). The three cerebellar peduncles, the superior cerebellar peduncle (SCP), middle cerebellar peduncle (MCP), and inferior cerebellar peduncle (ICP), were segmented using the Johns Hopkins University (JHU) white matter atlas (36). The JHU atlas provides separate left and right regions for SCP and ICP, but represents MCP as a single, unified region, yielding five peduncle regions of interest in total. Four diffusion tensor imaging (DTI) metrics were derived for each region: fractional anisotropy (FA), mean diffusivity (MD), radial diffusivity (RD), and axial diffusivity (AD).

Resting-State fMRI Acquisition and Processing

Resting-state fMRI data were acquired at UCLA and preprocessed using the HCP-MPP. Full acquisition and preprocessing details are provided in Supplementary Methods 1. Functional connectivity was computed using the Cole-Anticevic Brain

Network Parcellation (CAB-NP) (37), which assigns 718 cortical, subcortical, and cerebellar parcels to 12 canonical resting-state networks. Ten of the 12 networks contain cerebellar parcels; thus, analyses focused on within-network intra-cerebellar, cerebellar-cortical, and cerebellar-subcortical FC across these 10 networks, yielding 30 connectivity measures in total. Because the rs-fMRI data were acquired on three scanners, rs-fMRI-derived measures were harmonized using Longitudinal ComBat (38), following the same approach used in our prior volumetric study (7).

Multimodal Feature Integration

To construct a multimodal cerebellar feature set, we combined 28 regional cerebellar volumes derived using ACAPULCO (39) in our prior study (7), 20 peduncular DTI metrics (SCP-L, SCP-R, MCP, ICP-L, ICP-R × FA, MD, RD, AD), and 30 within-network cerebellar FC measures (intra-cerebellar, cerebellar–subcortical, and cerebellar–cortical × 10 canonical resting-state networks), yielding 78 features in total. Analyses were restricted to sessions with complete data across all three modalities. For participants with multiple eligible sessions, the earliest session was retained (n=93).

Statistical Analysis

Group Differences

Group differences in DTI and FC measures were examined separately using linear mixed-effects models on all eligible sessions per modality, with fixed effects for group, sex, and mean-centered age (linear and quadratic; FC models additionally included mean framewise displacement), and a random intercept for subject. False

discovery rate (FDR) correction was applied separately for each group contrast within each metric.

Multimodal CNV Classification

To test whether multimodal cerebellar features could classify CNV group membership, we trained four supervised classifiers: Support Vector Machine (SVM, RBF kernel), Random Forest, Elastic Net logistic regression, and Light Gradient Boosting Machine (LightGBM), with hyperparameters detailed in Supplementary Methods 2.1. Classifiers were trained on ComBat-harmonized volume and functional connectivity measures, along with DTI metrics (single-scanner acquisition, so harmonization was not required). Analyses used complete-case data from each subject's earliest fully-sampled visit (three-way, n=93: TD=36, 22qDel=39, 22qDup=18; pairwise, n=75/54/57), with train/test splits per classification task detailed in Supplementary Methods 2.2. Features were z-scored and classifiers used balanced class weights. Performance was evaluated on a stratified, held-out 20% test set (accuracy, balanced accuracy, AUC), with repeated 5-fold cross-validation (10 repeats) and permutation testing (1,000 permutations) to assess significance. Feature importance was averaged across Random Forest and LightGBM.

Multivariate Brain-Behavior Associations

Multivariate brain-behavior associations were examined for the combined 78-feature multimodal set using PLSC (40). Analyses were restricted to the earliest session per participant with complete multimodal imaging and behavioral data. Following our

prior study (1), two separate behavioral models were tested: one comprising cognitive ability and social functioning (n=42), and a second comprising psychosis-risk symptoms (n=91). Prior to PLSC, features were residualized for sex and mean-centered age (linear and quadratic), with FC additionally residualized for mean framewise displacement; each modality block was z-scored and scaled to unit Frobenius norm to ensure equal contribution across modalities. Full PLSC modeling details are provided in Supplementary Methods 3.

Exploratory Diagnostic Classification

An additional exploratory analysis examined whether multimodal cerebellar features could classify binary clinical diagnostic status (ASD and psychosis; see Supplementary Methods 4).

RESULTS

Participant Characteristics

Participant demographic and clinical characteristics for the full sample (i.e., all subjects with a T1-weighted scan) and the subsamples with usable dMRI and rs-fMRI sequences are summarized in Table 1. No significant group differences in age or sex were observed in the full sample or either imaging subsample. As previously reported in this cohort (7), both CNV groups showed lower IQ and elevated autism-related traits relative to TD controls. whereas psychosis-risk symptoms were significantly higher in 22qDel relative to both TD and 22qDup, who did not differ from each other.

Group Differences in Cerebellar White Matter Microstructure

Across the three cerebellar peduncles, superior cerebellar peduncle (SCP), middle cerebellar peduncle (MCP), and inferior cerebellar peduncle (ICP), 22qDup showed robust and widespread microstructural alterations relative to TD controls, with lower FA and AD and higher RD across all three tracts (all $q<0.05$; Figure 1). In contrast, 22qDel showed more circumscribed alterations in white matter microstructure, largely restricted to the SCP, characterized by higher FA and lower RD relative to TD controls ($q<0.05$). The direction of group differences in the SCP was opposite between the two CNVs, consistent with a gene-dosage-dependent effect on this cerebellar white matter tract. Full model output is provided in Supplementary Table S1.

Group Differences in Cerebellar Functional Connectivity

Relative to TD controls, 22qDel showed selective hypoconnectivity across cerebellar-cortical and cerebellar-subcortical networks, most consistently within the posterior-multimodal, language, and somatomotor networks ($q<0.05$; Figure 2), with no significant differences in within-network intra-cerebellar FC. 22qDup did not differ significantly from TD controls on any within-network FC measure. Full model output is provided in Supplementary Table S2.

Multimodal Classification of CNV Group Membership

Three-Group Classification

Of the four focal classifiers, SVM performed best (AUC=0.80, permutation $p<0.001$), followed by LightGBM (AUC=0.78, $p<0.001$), Random Forest (AUC=0.73, $p<0.001$), and Elastic Net (AUC=0.61, $p<0.001$); all four exceeded chance (Figure 3A).

The SVM confusion matrix showed the strongest classification for 22qDel, with most misclassifications occurring between TD and the two CNV groups rather than between 22qDel and 22qDup (Figure 3B). The top-ranked features included fractional anisotropy in the right superior, middle, and right inferior cerebellar peduncles, along with cerebellar volume in right lobule VIIIB, right lobule VIIB, and the corpus medullare. Only one functional connectivity feature, cerebellar-subcortical connectivity within the Visual 2 network, appeared among the top 15 features (Figure 3C).

Pairwise Classification

Multimodal cerebellar features robustly discriminated 22qDel from 22qDup across classifiers (AUC=0.94–1.00; Figure 3D), consistent with the divergent neurobiological profiles of the two CNV groups. Classification of TD vs. 22qDel (AUC=0.71–0.79) and TD vs. 22qDup (AUC=0.61–0.79) was more moderate, with SVM performing best in both comparisons (Figure 3D–G). Feature importance drew on all three modalities, but classification was predominantly structural — cerebellar volume was most informative for distinguishing 22qDel from TD, whereas peduncular fractional anisotropy was more prominent for comparisons involving 22qDup (Figure 3H–J). Full performance metrics by model and comparison, for both three-way and pairwise classification, are provided in Supplementary Table S3.

Multimodal Cerebellar Signatures and Neurobehavioral Outcomes

PLSC: Cognitive Ability and Autism-Related Traits

A multimodal PLSC model identified a significant first latent component (LC; p=0.008; FDR q<0.05; Figure 4A) capturing the majority of shared covariance between multimodal cerebellar features and cognitive ability/social functioning, in a subsample with complete multimodal and behavioral data (N=42; TD=10, 22qDel=25, 22qDup=7). Brain and behavioral composite scores were robustly correlated (r=0.716, p<0.0001; Figure 4B–D). Higher IQ and better reciprocal social behavior were associated with a distributed brain pattern characterized by larger cerebellar volumes across multiple regions, greater somatomotor cerebellar-subcortical FC, and lower middle cerebellar peduncle axial diffusivity (Figure 4E–F).

PLSC: Psychosis-Risk Symptoms

A parallel multimodal model examining psychosis-risk symptoms (N=91: TD=35, 22qDel=39, 22qDup=17) identified a first LC capturing the majority of shared covariance between multimodal cerebellar features and psychosis-risk symptoms; this component reached nominal significance (p=0.049) but did not survive FDR correction (q>0.05; Figure 5A). Brain and behavioral composite scores were correlated (r=0.428, p<0.0001; Figure 5B–D). Descriptively, greater psychosis-risk symptom severity, particularly disorganized communication and perceptual abnormalities, was associated with smaller cerebellar volumes across multiple regions, higher fractional anisotropy and lower radial diffusivity in the bilateral superior cerebellar peduncles and middle cerebellar peduncle, and no reliable functional connectivity loadings (Figure 5E–F). Group differences in LC1 brain and behavior scores across TD, 22qDel, and 22qDup, for both models, are reported in Supplementary Table S4.

Multimodal Classification of Diagnostic Status

Exploratory analyses did not support individual-level classification of ASD or psychosis, although these analyses were substantially underpowered (Supplementary Results 1).

DISCUSSION

Our findings reveal a striking dissociation across levels of cerebellar organization in reciprocal 22q11.2 CNVs. Whereas our prior work identified widespread cerebellar volume reductions in 22qDel but relatively preserved morphology in 22qDup (7), the present study revealed the opposite asymmetry in white-matter microstructure: 22qDup showed large, widespread abnormalities across all three cerebellar peduncles, while 22qDel effects were more selective and concentrated in the superior cerebellar peduncle. Functional connectivity showed a third pattern, with comparatively limited alterations overall and significant hypoconnectivity detected only in 22qDel. Thus, the effects of 22q11.2 copy number are not uniformly expressed across cerebellar macrostructure, microstructure, and functional coupling. Instead, deletion and duplication appear to preferentially affect distinct dimensions of cerebellar organization.

22q11.2 Gene Dosage Effects on Cerebellar White Matter Microstructure

In our prior study, cerebellar gray matter volume alterations were more pronounced and widespread in 22qDel than 22qDup, with the corpus medullare showing among the largest regional reductions relative to TD controls and 22qDup (7). The present findings indicate that this pattern does not generalize to peduncular white matter microstructure: here, 22qDup showed lower fractional anisotropy (FA) and axial

diffusivity (AD) and higher radial diffusivity (RD) across all three cerebellar peduncles, while 22qDel showed the opposite pattern for FA and RD, confined to the superior cerebellar peduncle (SCP), the cerebellum's principal efferent pathway to the subcortex and cortex, consistent with our hypothesized, gene-dosage-dependent effect based on prior reports in extra-cerebellar white matter (23,24).

While providing an informative first look at cerebellar peduncle white matter differences in 22q11.2 CNVs, DTI metrics cannot directly reveal the cellular basis of these differences, as multiple biological factors, including axonal density and myelination, jointly influence these metrics (41). Prior cortical white matter and animal model studies, however, can shed light on plausible mechanistic explanations. The higher FA and lower RD pattern seen in 22qDel's SCP has similarly been reported in cortical white matter, where it has been linked to smaller, densely packed axons (42) and higher axonal density (24), consistent with reduced axon growth and branching in 22q11.2 deletion mouse models (43). 22qDup's alteration, by contrast, spanned all three metrics (FA, AD, and RD) across all three peduncles, not just the efferent pathways, suggesting a less specific disruption than in 22qDel. Lower axonal density in 22qDup could contribute to the FA pattern specifically, consistent with reduced cortical axonal density reported in 22qDup using NODDI (24), but would not obviously account for the lower AD or elevated RD, the latter of which is more often linked to demyelination. Whether a myelin-related process contributes to the 22qDup pattern, however, remains unexplored in the literature.

Limited and Selective Alterations in Cerebellar Functional Connectivity

Relative to the structural and microstructural findings, cerebellar functional connectivity was comparatively spared after correction for multiple comparisons: within-network intra-cerebellar FC did not differ across groups, and only 22qDel showed reductions in cerebellar-cortical and cerebellar-subcortical connectivity, spanning both higher-order and primary sensory and motor networks. Notably, nominal effects across all three FC domains followed the reciprocal, gene-dosage-dependent pattern we hypothesized, with 22qDel trending toward hypoconnectivity and 22qDup toward hyperconnectivity, directionally consistent with prior findings (29), raising the possibility that this sparing reflects reduced statistical power rather than a true absence of effect.

A few factors may further limit sensitivity here. We speculate that the cerebellum's largely parallel, closed-loop circuit architecture (44) means functional coupling between cerebellar subregions could be intrinsically weaker than cerebello-cortical coupling, making intra-cerebellar group differences harder to detect. Separately, our cerebellar-subcortical estimate aggregated across multiple subcortical structures rather than isolating the thalamus, potentially diluting thalamus-specific effects reported by prior seed-based work in 22qDel (28).

While 22qDel showed significant FC alterations, their extent was more limited than the widespread volume reductions, and 22qDup showed minimal FC alterations despite pervasive white matter differences. Together, this indicates that structural, microstructural, and functional cerebellar measures index dissociable aspects of copy-number-related neurobiology, consistent with FC contributing minimally to the classification and PLSC models below.

The dissociation between pronounced volumetric alterations in 22qDel and widespread white-matter microstructural alterations in 22qDup raises the possibility that distinct dosage-sensitive genes or molecular pathways within the 22q11.2 locus contribute to different aspects of cerebellar development. Candidate genes implicated in neuronal maturation, axonal growth, and membrane or synaptic biology include DGCR8, ZDHHC8, RTN4R, and PI4KA (45–48), whereas recent experimental evidence implicates TBX1 in regional cerebellar morphogenesis (49). Future integration with developmental cerebellar transcriptomic and cell-type-resolved expression resources may help distinguish molecular pathways associated with cerebellar morphology from those associated with white-matter organization.

Multimodal Cerebellar Profiles Distinguish CNV Groups and Reveal Domain-Specific Brain-Behavior Associations

Combining cerebellar volume, white matter, and FC features into a single multimodal profile provided a non-linear perspective on group separability. All three modalities contributed, suggesting they capture complementary information about distinct biological processes. Consistent with the single-modality group differences reported here and in our prior study, 22qDel and 22qDup were more distinguishable from each other than either CNV was from TD controls, demonstrating that the relative similarity of 22qDup to TD depends strongly on the biological dimension examined: duplication carriers showed comparatively preserved cerebellar volume and FC but pronounced white-matter microstructural alterations.

The multimodal PLSC analyses revealed two domain-specific cerebellar-behavior profiles with dissociable neural substrates. The cognitive/social model showed a stronger brain-behavior association than the volume-only model from our prior study (r=0.716 vs. r=0.41), suggesting that FC, particularly somatomotor cerebellar-cortical connectivity, captures complementary information beyond structure alone for cognitive-social phenotypes. In contrast, the nominally significant psychosis-risk model in 22qDel was dominated by volumetric and white matter features with no reliable FC contribution. This may partly reflect a restricted range in psychosis-risk symptom scores: the SIPS scale has a floor of zero, precluding differentiation of 22qDup from the general population despite its hypothesized protective effect, which may limit the detectable variance available to any brain measure, including FC.

Lastly, despite success in distinguishing CNV groups and capturing brain-behavior associations, multimodal cerebellar features did not classify ASD or psychosis diagnostic status, likely reflecting limited power given the small number of positive diagnoses in these subgroups rather than a genuine absence of cerebellar signal.

Limitations

Several limitations should be noted. Sample sizes for the dMRI (n=119) and rs-fMRI (n=218) subsamples were smaller than the full volumetric cohort, and multimodal analyses, which required complete data across all included modalities and measures, were further limited to N=42–93, constraining power especially for the PLSC models. For diagnostic classification specifically, only nine psychosis cases were available in the 22qDel multimodal subsample, limiting the robustness of this evaluation. Structure-

function covariance could not be directly examined, as volumetric, DTI, and FC features were derived using different atlases and parcellation schemes; a unified cerebellar atlas across modalities would enable more direct integration in future work. The dMRI subsample was drawn from a single scanner and skewed slightly older than the full cohort, limiting generalizability across the full developmental range. Finally, classification and PLSC analyses were cross-sectional and based on a single timepoint per participant, precluding examination of developmental change in multimodal cerebellar signatures.

Implications and Future Directions

Together, these findings indicate that cerebellar white matter and functional alterations in 22q11.2 CNVs follow copy-number- and modality-specific patterns that are not fully predictable from gray matter volume alone. They further demonstrate that multimodal integration captures complementary aspects of the neurobehavioral phenotype. Future studies in larger, harmonized multimodal samples will be critical for improving power to detect group differences and support within-group prediction of clinical outcomes.

As cerebellum-specific imaging and molecular resources mature, future work could move beyond regional volumetry using higher-resolution, submillimeter cerebellar atlases and more specific diffusion models such as NODDI to better localize and characterize the alterations observed here. Direct structure-function coupling analyses could further test whether cerebellar morphology and white matter microstructure covary with functional connectivity, and whether this differs by copy number. Integrating these

imaging phenotypes with cerebellum-specific transcriptomic and gene-dosage resources may help identify candidate pathways underlying the divergent effects observed in 22qDel and 22qDup, an approach that could extend to other neuropsychiatric CNVs, to delineate shared and CNV-specific mechanisms.

CHAPTER 2 ACKNOWLEDGMENTS AND DISCLOSURES

Author Contributions

HF: Conceptualization, Methodology, Data curation, Formal analysis, Software, Validation, Visualization, Writing – original draft, Writing – review & editing. **CHS:** Methodology, Data curation, Software. **KPO:** Methodology, Data curation. **RB:** Methodology, Data curation. **TED:** Data curation, Software. **HRW:** Methodology, Software. **JWK:** Methodology, Data curation. **PS:** Methodology. **JSN:** Methodology. **Z-QL:** Methodology. **LK-W:** Investigation, Data curation, Project administration. **PJM:** Methodology, Supervision, Writing - review & editing. **LMH:** Methodology, Supervision, Writing - review & editing. **LQU:** Methodology, Supervision, Writing - review & editing. **CEB:** Conceptualization, Methodology, Writing – review & editing, Supervision, Funding acquisition, Resources.

Funding

This work was supported by the National Institute of Mental Health (Grant Nos. R01/R37MH085953, R01MH129858, U01MH101779, U01MH119736, and R21MH116473, all to CEB), the Department of Defense (Grant No. W81XWH-12-1-0081, to CEB), the Simons Foundation Autism Research Initiative Explorer Award (to CEB), the Uytengsu-Hamilton 22q11 Neuropsychiatry Research Award (to CEB), and the Consortium for Neuropsychiatric Phenomics (NIH Roadmap for Medical Research grant UL1-DE019580).

Acknowledgments

We are deeply grateful to the participants and their families for their time, commitment, and invaluable contributions to this study.

Disclosures

All authors reported no biomedical financial interests or potential conflicts of interest.

CHAPTER 2 REFERENCES

1. McDonald-McGinn DM, Sullivan KE, Marino B, Philip N, Swillen A, Vorstman JAS, *et al.* (2015): 22q11.2 deletion syndrome. *Nat Rev Dis Primers* 1: 15072.
2. Portnoï M-F (2009): Microduplication 22q11.2: a new chromosomal syndrome. *Eur J Med Genet* 52: 88–93.
3. Hoeffding LK, Trabjerg BB, Olsen L, Mazin W, Sparsø T, Vangkilde A, *et al.* (2017): Risk of psychiatric disorders among individuals with the 22q11.2 deletion or duplication: A Danish nationwide, register-based study: A danish nationwide, register-based study. *JAMA Psychiatry* 74: 282–290.
4. Olsen L, Sparsø T, Weinsheimer SM, Dos Santos MBQ, Mazin W, Rosengren A, *et al.* (2018): Prevalence of rearrangements in the 22q11.2 region and population-based risk of neuropsychiatric and developmental disorders in a Danish population: a case-cohort study. *Lancet Psychiatry* 5: 573–580.
5. Rees E, Kirov G, Sanders A, Walters JTR, Chambert KD, Shi J, *et al.* (2014): Evidence that duplications of 22q11.2 protect against schizophrenia. *Mol Psychiatry* 19: 37–40.
6. Lin A, Vajdi A, Kushan-Wells L, Helleman G, Hansen LP, Jonas RK, *et al.* (2020): Reciprocal copy number variations at 22q11.2 produce distinct and convergent neurobehavioral impairments relevant for schizophrenia and autism spectrum disorder. *Biol Psychiatry* 88: 260–272.
7. Fung H, O'Hora KP, Boen R, Wang HR, Amir CM, Schleifer CH, *et al.* (2026): Convergent and divergent cerebellar alterations in 22q11.2 copy number variants. *Biol Psychiatry Glob Open Sci* 6: 100718.

8. Stoodley CJ, Schmahmann JD (2009): Functional topography in the human cerebellum: a meta-analysis of neuroimaging studies. *Neuroimage* 44: 489–501.

9. Buckner RL (2013): The cerebellum and cognitive function: 25 years of insight from anatomy and neuroimaging. *Neuron* 80: 807–815.

10. King M, Hernandez-Castillo CR, Poldrack RA, Ivry RB, Diedrichsen J (2019): Functional boundaries in the human cerebellum revealed by a multi-domain task battery. *Nat Neurosci* 22: 1371–1378.

11. Andreasen NC, Pierson R (2008): The role of the cerebellum in schizophrenia. *Biol Psychiatry* 64: 81–88.

12. Moberget T, Doan NT, Alnæs D, Kaufmann T, Córdova-Palomera A, Lagerberg TV, *et al.* (2018): Cerebellar volume and cerebellocerebral structural covariance in schizophrenia: a multisite mega-analysis of 983 patients and 1349 healthy controls. *Mol Psychiatry* 23: 1512–1520.

13. D'Mello AM, Stoodley CJ (2015): Cerebro-cerebellar circuits in autism spectrum disorder. *Front Neurosci* 9: 408.

14. Rodrigues BA, Silva J do N, Kawamoto EM (2025): Cerebellar alterations in autism spectrum disorder: A mini-review. *Cerebellum* 24: 52.

15. Yanamadala V (2026): The cerebellum. *Essential Neuroanatomy*. Cham: Springer Nature Switzerland, pp 79–101.

16. Glickstein M, Doron K (2008): Cerebellum: connections and functions. *Cerebellum* 7: 589–594.

17. Le Bihan D, Breton E, Lallemand D, Grenier P, Cabanis E, Laval-Jeantet M (1986): MR imaging of intravoxel incoherent motions: application to diffusion and perfusion in neurologic disorders. *Radiology* 161: 401–407.

18. Basser PJ, Mattiello J, LeBihan D (1994): MR diffusion tensor spectroscopy and imaging. *Biophys J* 66: 259–267.

19. Beaulieu C (2002): The basis of anisotropic water diffusion in the nervous system - a technical review. *NMR Biomed* 15: 435–455.

20. Alexander AL, Lee JE, Lazar M, Field AS (2007): Diffusion tensor imaging of the brain. *Neurotherapeutics* 4: 316–329.

21. Sundram F, Campbell LE, Azuma R, Daly E, Bloemen OJN, Barker GJ, *et al.* (2010): White matter microstructure in 22q11 deletion syndrome: a pilot diffusion tensor imaging and voxel-based morphometry study of children and adolescents. *J Neurodev Disord* 2: 77–92.

22. Radoeva PD, Coman IL, Antshel KM, Fremont W, McCarthy CS, Kotkar A, *et al.* (2012): Atlas-based white matter analysis in individuals with velo-cardio-facial syndrome (22q11.2 deletion syndrome) and unaffected siblings. *Behav Brain Funct* 8: 38.

23. Seitz-Holland J, Lyons M, Kushan L, Lin A, Villalon-Reina JE, Cho KIK, *et al.* (2021): Opposing white matter microstructure abnormalities in 22q11.2 deletion and duplication carriers. *Transl Psychiatry* 11: 580.

24. Boen R, Villalón-Reina JE, Kushan L, O'Hora KP, Fung H, Parker N, *et al.* (2026): Gene dosage effects of 22q11.2 copy number variants on in-vivo measures of white matter axonal density and dispersion. *Mol Psychiatry* 31: 3687–3698.

25. Biswal B, Yetkin FZ, Haughton VM, Hyde JS (1995): Functional connectivity in the motor cortex of resting human brain using echo-planar MRI. *Magn Reson Med* 34: 537–541.

26. Debbané M, Lazouret M, Lagioia A, Schneider M, Van De Ville D, Eliez S (2012): Resting-state networks in adolescents with 22q11.2 deletion syndrome: associations with prodromal symptoms and executive functions. *Schizophr Res* 139: 33–39.

27. Mattiaccio LM, Coman IL, Schreiner MJ, Antshel KM, Fremont WP, Bearden CE, Kates WR (2016): Atypical functional connectivity in resting-state networks of individuals with 22q11.2 deletion syndrome: associations with neurocognitive and psychiatric functioning. *J Neurodev Disord* 8: 2.

28. Schleifer C, Lin A, Kushan L, Ji JL, Yang G, Bearden CE, Anticevic A (2019): Dissociable disruptions in thalamic and hippocampal resting-state functional connectivity in youth with 22q11.2 deletions. *J Neurosci* 39: 1301–1319.

29. Moreau CA, Urchs SGW, Kuldeep K, Orban P, Schramm C, Dumas G, *et al.* (2020): Mutations associated with neuropsychiatric conditions delineate functional brain connectivity dimensions contributing to autism and schizophrenia. *Nat Commun* 11: 5272.

30. Fung H, Hoftman GD (2024): Are you maximizing your multimodal, longitudinal dataset? Toward an integrated framework for advancing psychosis research. *Biol Psychiatry Cogn Neurosci Neuroimaging* 9: 849–851.

31. Wechsler D (1999): *Manual for the Wechsler Abbreviated Intelligence Scale (WASI)*. San Antonio, TX: The Psychological Corporation.

32. Wechsler D (2011): *Wechsler Abbreviated Scale of Intelligence, Second Edition*. San Antonio, TX: Pearson.

33. Constantino JN, Gruber CP (2005): Social Responsiveness Scale 2nd ed: Western Psychological Services.

34. McGlashan TH, Miller TJ, Woods SW, Hoffman RE, Davidson L (2001): Instrument for the assessment of prodromal symptoms and states. *Early Intervention in Psychotic Disorders*. Dordrecht: Springer Netherlands, pp 135–149.

35. Glasser MF, Sotiropoulos SN, Wilson JA, Coalson TS, Fischl B, Andersson JL, *et al.* (2013): The minimal preprocessing pipelines for the Human Connectome Project. *Neuroimage* 80: 105–124.

36. Mori S, Oishi K, Jiang H, Jiang L, Li X, Akhter K, *et al.* (2008): Stereotaxic white matter atlas based on diffusion tensor imaging in an ICBM template. *Neuroimage* 40: 570–582.

37. Ji JL, Spronk M, Kulkarni K, Repovš G, Anticevic A, Cole MW (2019): Mapping the human brain's cortical-subcortical functional network organization. *Neuroimage* 185: 35–57.

38. Beer JC, Tustison NJ, Cook PA, Davatzikos C, Sheline YI, Shinohara RT, *et al.* (2020): Longitudinal ComBat: A method for harmonizing longitudinal multi-scanner imaging data. *Neuroimage* 220: 117129.

39. Han S, Carass A, He Y, Prince JL (2020): Automatic cerebellum anatomical parcellation using U-Net with locally constrained optimization. *Neuroimage* 218: 116819.

40. Moser DA, Doucet GE, Lee WH, Rasgon A, Krinsky H, Leibu E, *et al.* (2018): Multivariate associations among behavioral, clinical, and multimodal imaging phenotypes in patients with psychosis. *JAMA Psychiatry* 75: 386–395.

41. Villalón-Reina JE, Martínez K, Qu X, Ching CRK, Nir TM, Kothapalli D, *et al.* (2020): Altered white matter microstructure in 22q11.2 deletion syndrome: a multisite diffusion tensor imaging study. *Mol Psychiatry* 25: 2818–2831.

42. Raven EP, Veraart J, Kievit RA, Genc S, Ward IL, Hall J, *et al.* (2023): In vivo evidence of microstructural hypo-connectivity of brain white matter in 22q11.2 deletion syndrome. *Mol Psychiatry* 28: 4342–4352.

43. Fernandez A, Meechan DW, Karpinski BA, Paronett EM, Bryan CA, Rutz HL, *et al.* (2019): Mitochondrial dysfunction leads to cortical under-connectivity and cognitive impairment. *Neuron* 102: 1127-1142.e3.

44. Buckner RL, Krienen FM, Castellanos A, Diaz JC, Yeo BTT (2011): The organization of the human cerebellum estimated by intrinsic functional connectivity. *J Neurophysiol* 106: 2322–2345.

45. Fénelon K, Mukai J, Xu B, Hsu P-K, Drew LJ, Karayiorgou M, *et al.* (2011): Deficiency of Dgcr8, a gene disrupted by the 22q11.2 microdeletion, results in altered short-term plasticity in the prefrontal cortex. *Proc Natl Acad Sci U S A* 108: 4447–4452.

46. Mukai J, Tamura M, Fénelon K, Rosen AM, Spellman TJ, Kang R, *et al.* (2015): Molecular substrates of altered axonal growth and brain connectivity in a mouse model of schizophrenia. *Neuron* 86: 680–695.

47. Hsu R, Woodroffe A, Lai W-S, Cook MN, Mukai J, Dunning JP, *et al.* (2007): Nogo Receptor 1 (RTN4R) as a candidate gene for schizophrenia: analysis using human and mouse genetic approaches. *PLoS One* 2: e1234.

48. Verdura E, Rodríguez-Palmero A, Vélez-Santamaria V, Planas-Serra L, de la Calle I, Raspall-Chaure M, *et al.* (2021): Biallelic PI4KA variants cause a novel neurodevelopmental syndrome with hypomyelinating leukodystrophy. *Brain* 144: 2659–2669.

49. Eom T-Y, Schmitt JE, Li Y, Davenport CM, Steinberg J, Bonnan A, *et al.* (2024): Tbx1 haploinsufficiency leads to local skull deformity, paraflocculus and flocculus dysplasia, and motor-learning deficit in 22q11.2 deletion syndrome. *Nat Commun* 15: 10510.

CHAPTER 2 FIGURE/TABLE LEGENDS

Table 1. Participant characteristics at baseline by group and imaging subsample. Demographic, cognitive, and clinical characteristics of typically developing (TD) controls, individuals with 22q11.2 deletion (22qDel), and individuals with 22q11.2 duplication (22qDup) are shown separately for the T1w full sample, diffusion MRI (dMRI) subsample, and resting-state fMRI (rs-fMRI) subsample. The three groups were comparable in sex and age distributions within each subsample. FSIQ was lower in both CNV groups relative to TD controls. SRS-2 total T-scores, reflecting autism-related traits, were elevated in both CNV groups relative to TD controls. SIPS-P total scores, reflecting psychosis severity, were higher in individuals with 22qDel relative to both TD controls and individuals with 22qDup, with no significant difference between TD controls and individuals with 22qDup. eTIV was lower in the 22qDel group compared with both the TD control and 22qDup groups. Mean framewise displacement did not differ significantly across groups in the rs-fMRI subsample.

Figure 1. Cerebellar peduncle microstructural differences in 22q11.2 CNV carriers relative to typically developing controls. Forest plots show group-difference effect sizes (β ± 95% CI) for fractional anisotropy (FA), radial diffusivity (RD), axial diffusivity (AD), and mean diffusivity (MD) across cerebellar peduncle regions defined by the JHU ICBM-DTI-81 atlas. Outcome variables were z-scored prior to model fitting; β therefore represents the group difference in SD units of each DTI metric, adjusting for covariates (see Methods). Red = 22qDel vs. TD; Blue = 22qDup vs. TD. Filled markers indicate effects surviving false discovery rate correction (FDR $q < 0.05$); transparent markers

indicate q > 0.05. Asterisks denote uncorrected significance: *p < 0.05, **p < 0.01, ***p < 0.001. Abbreviations: FA, fractional anisotropy; RD, radial diffusivity; AD, axial diffusivity; MD, mean diffusivity; SCP, superior cerebellar peduncle; MCP, middle cerebellar peduncle; ICP, inferior cerebellar peduncle; TD, typically developing; FDR, false discovery rate.

Figure 2. Within-network cerebellar functional connectivity differences in 22q11.2 CNV carriers relative to typically developing controls. Forest plots show group-difference effect sizes (β ± 95% CI) for within-network resting-state functional connectivity, organized separately for intra-cerebellar (left), cerebellar-subcortical (middle), and cerebellar-cortical (right) connections. Networks are defined by the Cole-Anticevic Brain-wide Network Partition (CAB-NP; Ji et al., 2019 (37)) and ordered along the y-axis by network number as in the original partition; only 10 of the 12 CAB-NP networks are represented in the cerebellum. Outcome variables were z-scored prior to model fitting; β therefore represents the group difference in SD units of within-network connectivity, adjusting for covariates (see Methods). Red = 22qDel vs. TD; Blue = 22qDup vs. TD. Filled markers indicate effects surviving false discovery rate correction (FDR q < 0.05); transparent markers indicate q > 0.05. Asterisks denote uncorrected significance: *p < 0.05, **p < 0.01, ***p < 0.001. Abbreviations: rsFC, resting-state functional connectivity; CAB-NP, Cole-Anticevic Brain-wide Network Partition; TD, typically developing; FDR, false discovery rate.

Figure 3. Multimodal classification of CNV group membership using cerebellar features. All models were trained on complete-case multimodal data (cerebellar volume + DTI + rsFC; 78 features) using an 80/20 train–test split (SEED=42). (A) Three-way classification performance (AUC-ROC; chance=0.50) for SVM, Random Forest (RF), Elastic Net (EN), and LightGBM, classifying TD controls, 22qDel, and 22qDup. (B) Confusion matrix for the best-performing three-way model (SVM; AUC=0.80), showing predicted vs. true group labels with cell proportions and counts. (C) Top 15 features ranked by average importance across RF and LightGBM for the three-way comparison, colored by modality (blue=volume, red=FC, green=DTI). (D) Pairwise binary classification AUC-ROC (test set) for all four models across three group comparisons (TD vs. 22qDel; TD vs. 22qDup; 22qDel vs. 22qDup). (E–G) SVM confusion matrices for each pairwise comparison (AUC=0.79, 0.79, and 1.00, respectively). (H–J) Top 15 features by average importance (RF + LightGBM) for each pairwise comparison, colored by modality. Asterisks in panels A and D denote permutation-based significance vs. chance: *p < 0.05, **p < 0.01, ***p < 0.001; ns = not significant. Abbreviations: SVM, support vector machine; RF, random forest; EN, elastic net; AUC, area under the receiver operating characteristic curve; TD, typically developing; DTI, diffusion tensor imaging; rsFC, resting-state functional connectivity; FA, fractional anisotropy; AD, axial diffusivity; RD, radial diffusivity; SCP, superior cerebellar peduncle; MCP, middle cerebellar peduncle; ICP, inferior cerebellar peduncle.

Figure 4. Multimodal cerebellar brain–behavior associations with cognitive and social functioning. Partial least squares correlation (PLSC) linking 78 multimodal

cerebellar features (28 volume + 30 rsFC + 20 DTI) to Full-Scale IQ and five SRS-2 subscales (N=42 participants with complete brain and behavioral data). (A) Covariance explained by each latent component (LC); LC1 was statistically significant after FDR correction (**p < 0.01; red), with LC2–6 non-significant (gray). (B) Correlation between LC1 brain and behavioral composite scores across participants (r=0.716, p<0.001), colored by CNV group. (C) LC1 brain composite scores by group. (D) LC1 behavioral composite scores by group. (E) LC1 behavioral loadings with 95% bootstrap confidence intervals; all six behavioral features showed reliable loadings (red). Full-Scale IQ loaded positively; all five SRS-2 subscales (Social Cognition, Social Communication, Social Awareness, Restricted Interests and Repetitive Behaviors, Social Motivation) loaded negatively. (F) LC1 brain feature loadings organized by modality: cerebellar volume (left; 21/28 features reliable), within-network cerebellar FC (middle; 1/30 reliable), and cerebellar peduncle DTI (right; 1/20 reliable). Red bars indicate bootstrap-reliable contributions; gray bars indicate non-reliable loadings. Error bars represent 95% bootstrap confidence intervals. Abbreviations: PLSC, partial least squares correlation; LC, latent component; FSIQ, Full-Scale Intelligence Quotient; SRS-2, Social Responsiveness Scale, Second Edition; rsFC, resting-state functional connectivity; DTI, diffusion tensor imaging; FA, fractional anisotropy; RD, radial diffusivity; AD, axial diffusivity; MD, mean diffusivity; SCP, superior cerebellar peduncle; MCP, middle cerebellar peduncle; ICP, inferior cerebellar peduncle; FDR, false discovery rate.

Figure 5. Multimodal cerebellar brain–behavior associations with psychosis-risk symptom severity. Partial least squares correlation (PLSC) linking 78 multimodal

cerebellar features (28 volume + 30 rsFC + 20 DTI) to SIPS positive symptom subscores (P1–P5; N=91 participants with complete brain and behavioral data). (A) Covariance explained by each latent component (LC); LC1 reached nominal significance by permutation test ($p < 0.05$) but did not survive FDR correction ($q > 0.05$); LC2–5 were non-significant (gray). (B) Correlation between LC1 brain and behavioral composite scores across participants ($r=0.428$, $p<0.001$), colored by CNV group. (C) LC1 brain composite scores by group. (D) LC1 behavioral composite scores by group; 22qDel participants showed the widest range and highest behavioral scores, consistent with elevated psychosis-risk symptoms. LC1 behavioral loadings with 95% bootstrap confidence intervals; only P5 (Disorganized Communication) and P4 (Perceptual Abnormalities) showed reliable loadings (red); P1 (Unusual Thought Content), P3 (Grandiosity), and P2 (Suspiciousness) were non-reliable (gray). (F) LC1 brain feature loadings by modality: cerebellar volume (left; 11/28 features reliable), within-network cerebellar FC (middle; 0/30 reliable), and cerebellar peduncle DTI (right; 7/20 reliable). Red bars indicate bootstrap-reliable contributions; gray bars indicate non-reliable loadings. Error bars represent 95% bootstrap confidence intervals. Abbreviations: PLSC, partial least squares correlation; LC, latent component; SIPS, Structured Interview for Psychosis-Risk Syndromes; rsFC, resting-state functional connectivity; DTI, diffusion tensor imaging; FA, fractional anisotropy; RD, radial diffusivity; AD, axial diffusivity; MD, mean diffusivity; SCP, superior cerebellar peduncle; MCP, middle cerebellar peduncle; ICP, inferior cerebellar peduncle; FDR, false discovery rate.

CHAPTER 2 TABLES

Table 1. Participant characteristics at baseline by group

Measure	TD Controls	22qDel	22qDup	Group Comparisons [a]
Full Sample				
Participants (n)	167	111	37	
Age, Mean (SD), years	16.2 (6.9)	16.2 (9.4)	18.2 (13.5)	$F(2,312) = 0.89$, $p = 0.412$
Age range, years	6–45	5–55	5–49	
Sex (% female)	51.5%	55.0%	48.6%	$\chi^2(2) = 0.55$, $p = 0.758$
eTIV, Mean (SD), mm^3	1,541,862 (159,072)	1,429,772 (179,795)	1,543,068 (162,409)	$F(2,312) = 16.25$, $p < .001$; 22qDel < TD ≈ 22qDup
FSIQ, Mean (SD); available n/total N	111.3 (19.2); n=77/167	79.4 (12.3); n=97/111	98.3 (18.1); n=35/37	KW $\chi^2(2) = 95.5$, $p < .001$; 22qDel < 22qDup < TD
SRS-2 Total T-score, Mean (SD); available n/total N	47.5 (10.3); n=51/167	70.5 (14.3); n=89/111	66.8 (16.2); n=27/37	KW $\chi^2(2) = 66.9$, $p < .001$; TD < 22qDup ≈ 22qDel
SIPS Positive Symptom Total, Mean (SD); available n/total N	1.2 (1.8); n=83/167	6.0 (6.5); n=77/111	2.6 (3.1); n=26/37	KW $\chi^2(2) = 38.4$, $p < .001$; TD < 22qDup < 22qDel
dMRI Subsample				
Participants (n)	51	47	21	
Age, Mean (SD), years	17.7 (7.6)	20.6 (10.2)	22.5 (13.8)	$F(2,116)=2.08$, $p=0.129$
Age range, years	7–45	9–55	8–49	
Sex (% female)	68.6	66	47.6	$\chi^2=2.99$, $p=0.224$
FSIQ, Mean (SD); available n/total N	113.9 (19.8); n=36/51	82.7 (13.8); n=43/47	99.2 (18.7); n=20/21	KW $\chi^2(2) = 42.2$, $p < .001$; 22qDel < 22qDup < TD
SRS-2 Total T-score, Mean (SD); available n/total N	46.4 (14.2); n=14/51	72.0 (14.4); n=30/47	59.4 (12.3); n=9/21	KW $\chi^2(2) = 20.4$, $p < .001$; TD < 22qDup ≈ 22qDel
SIPS P Total, Mean (SD); available n/total N	1.3 (2.0); n=42/51	5.0 (6.5); n=46/47	2.2 (2.8); n=20/21	KW $\chi^2(2) = 12.2$, $p = .002$; TD ≈ 22qDup < 22qDel
rs-fMRI Subsample				
Participants (n)	99	86	33	
Age, Mean (SD), years	15.6 (7.0)	17.1 (8.8)	19.0 (12.3)	$F(2,215) = 2.04$, $p = 0.132$
Age range, years	6–45	6–55	6–45	
Sex (% female)	56.6	60.5	42.4	$\chi^2(2) = 3.18$, $p = 0.204$
Framewise Displacement, Mean (SD), mm	0.19 (0.17)	0.24 (0.19)	0.24 (0.18)	KW $\chi^2(2) = 7.2$, $p = 0.027$; TD ≈ 22qDup ≈ 22qDel
FSIQ, Mean (SD); available n/total N	112.9 (20.4); n=89/99	79.3 (13.7); n=82/86	97.6 (20.7); n=31/33	KW $\chi^2(2) = 88.7$, $p < .001$; 22qDel < 22qDup < TD

SRS-2 Total T-score, Mean (SD); available n/total N	47.0 (10.6); n=52/99	70.7 (14.3); n=74/86	65.1 (15.9); n=22/33	KW $\chi^2(2) = 64.2$, $p < .001$; TD < 22qDup ≈ 22qDel
SIPS P Total, Mean (SD); available n/total N	1.2 (1.9); n=78/99	5.5 (5.9); n=75/86	2.4 (2.7); n=29/33	KW $\chi^2(2) = 44.2$, $p < .001$; TD < 22qDup < 22qDel

TD Controls = Typically Developing Controls; 22qDel = 22q11.2 Deletion; 22qDup = 22q11.2 Duplication; T1w = T1-weighted (structural MRI); dMRI = diffusion MRI; rs-fMRI = resting-state functional MRI; eTIV, estimated total intracranial volume; FSIQ = Full-Scale IQ (WASI/WASI-II); SRS-2 = Social Responsiveness Scale, Second Edition; SIPS = Structured Interview for Psychosis-Risk Syndromes.

[a] Group differences were assessed using one-way ANOVA (age, eTIV), Kruskal-Wallis (KW) tests (FSIQ, SRS-2 Total T-score, SIPS-P Total score), or χ^2 tests (sex), depending on variable distribution. Post-hoc pairwise comparisons for significant KW tests used Wilcoxon rank-sum tests with Bonferroni correction.

CHAPTER 2 FIGURES

Figure 1 Cerebellar peduncle microstructural differences in 22q11.2 CNV carriers relative to typically developing controls.

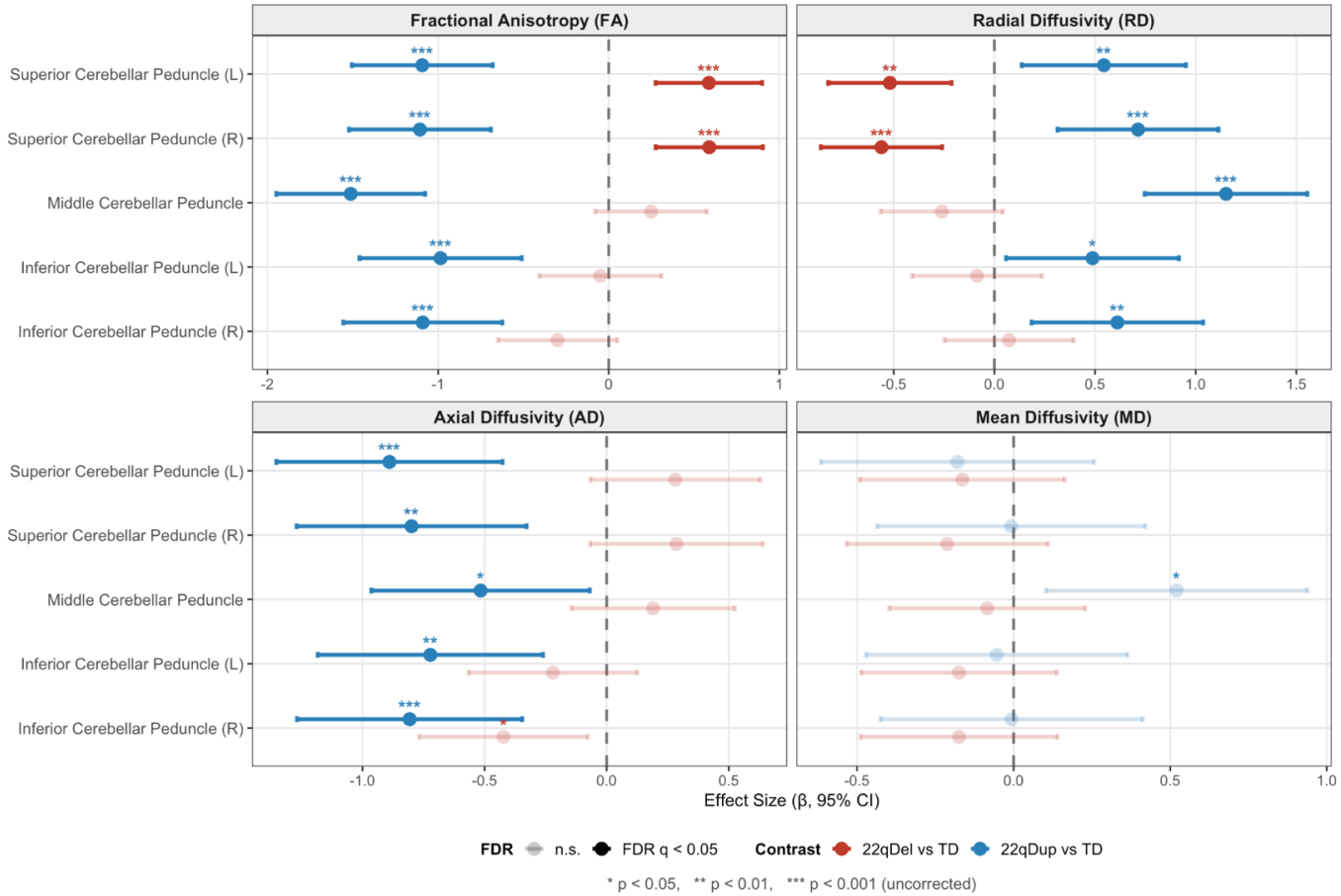

Figure 2 Within-network cerebellar functional connectivity differences in 22q11.2 CNV carriers relative to typically developing controls.

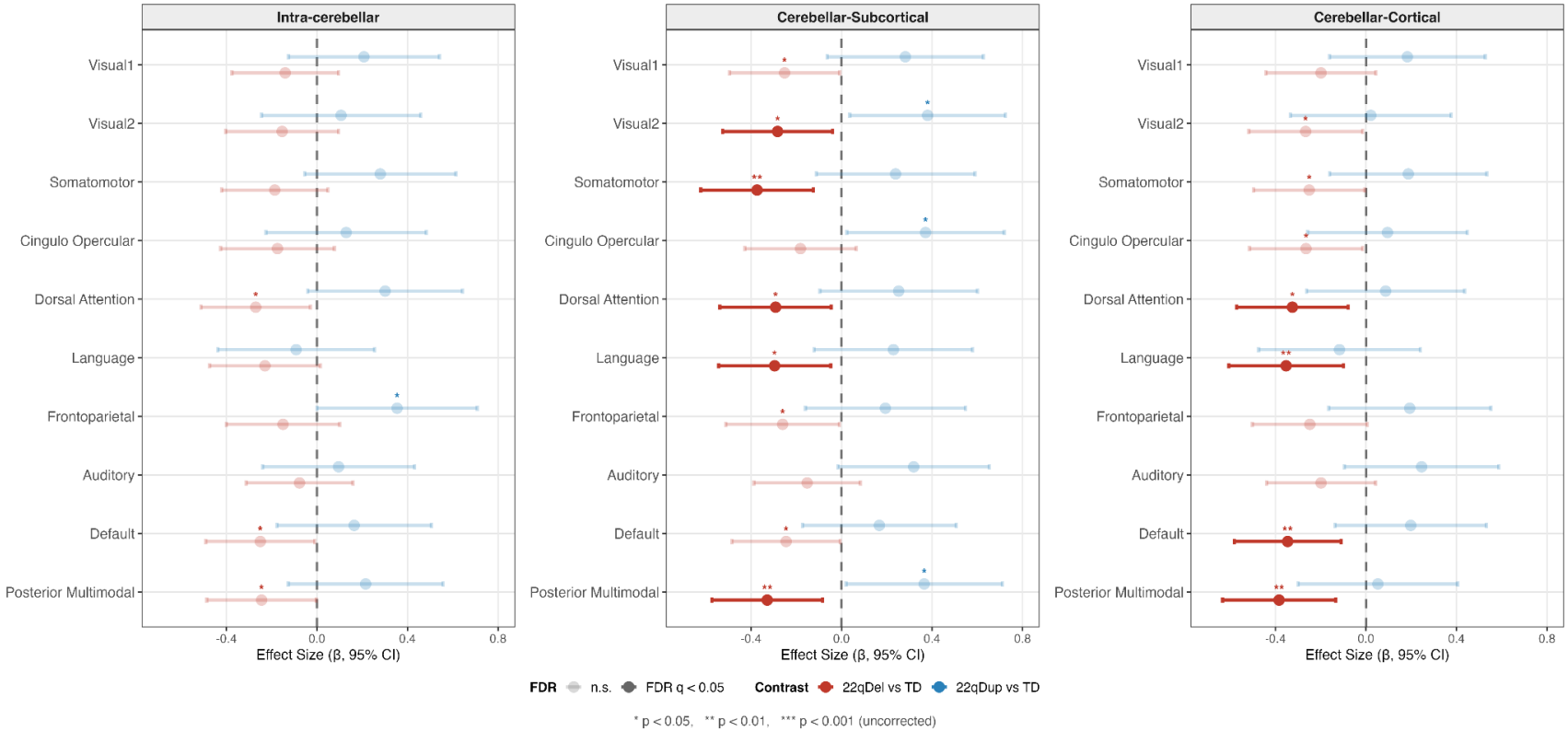

Figure 3 Multimodal classification of CNV group membership using cerebellar features.

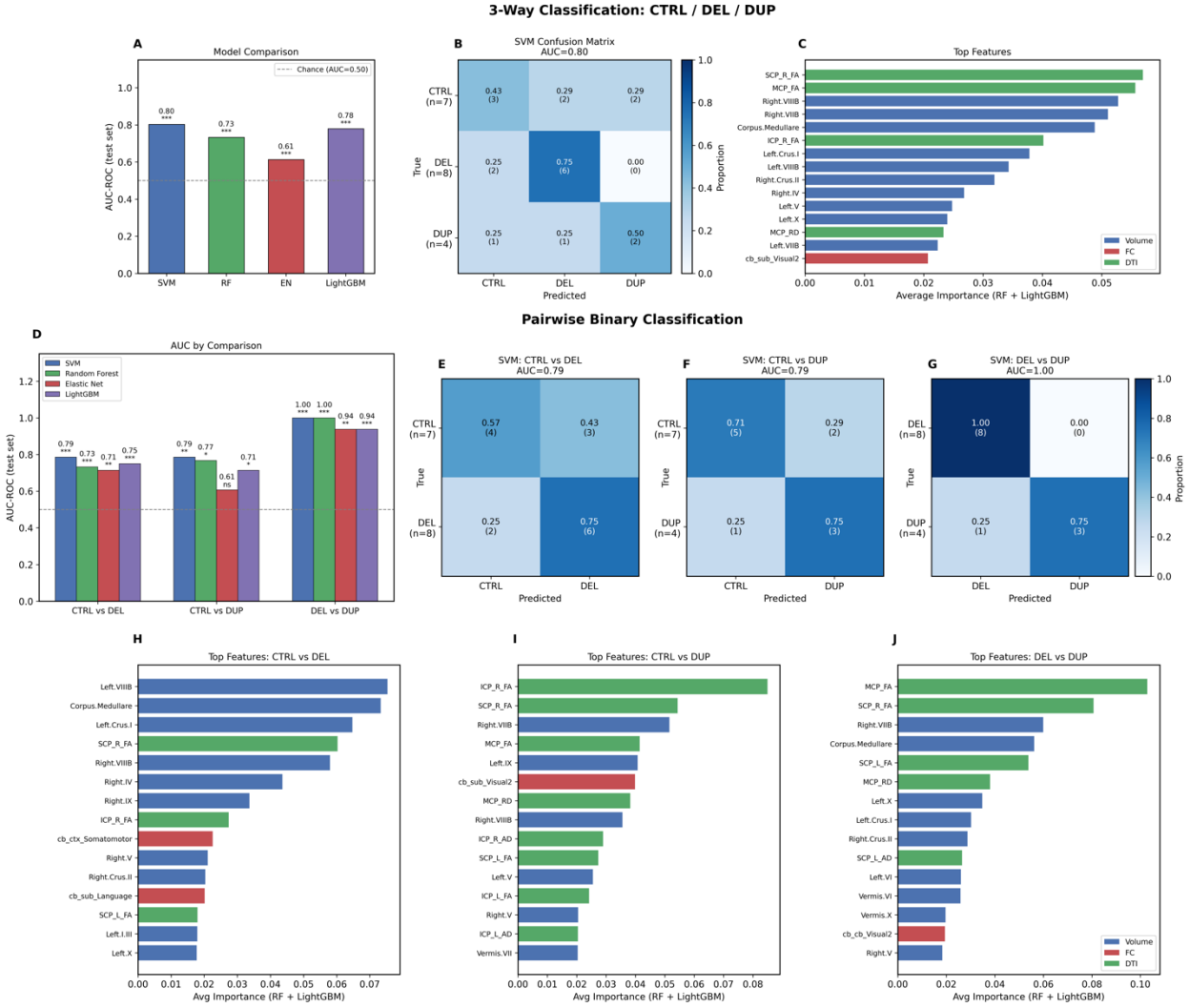

Figure 4 Multimodal cerebellar brain–behavior associations with cognitive and social functioning.

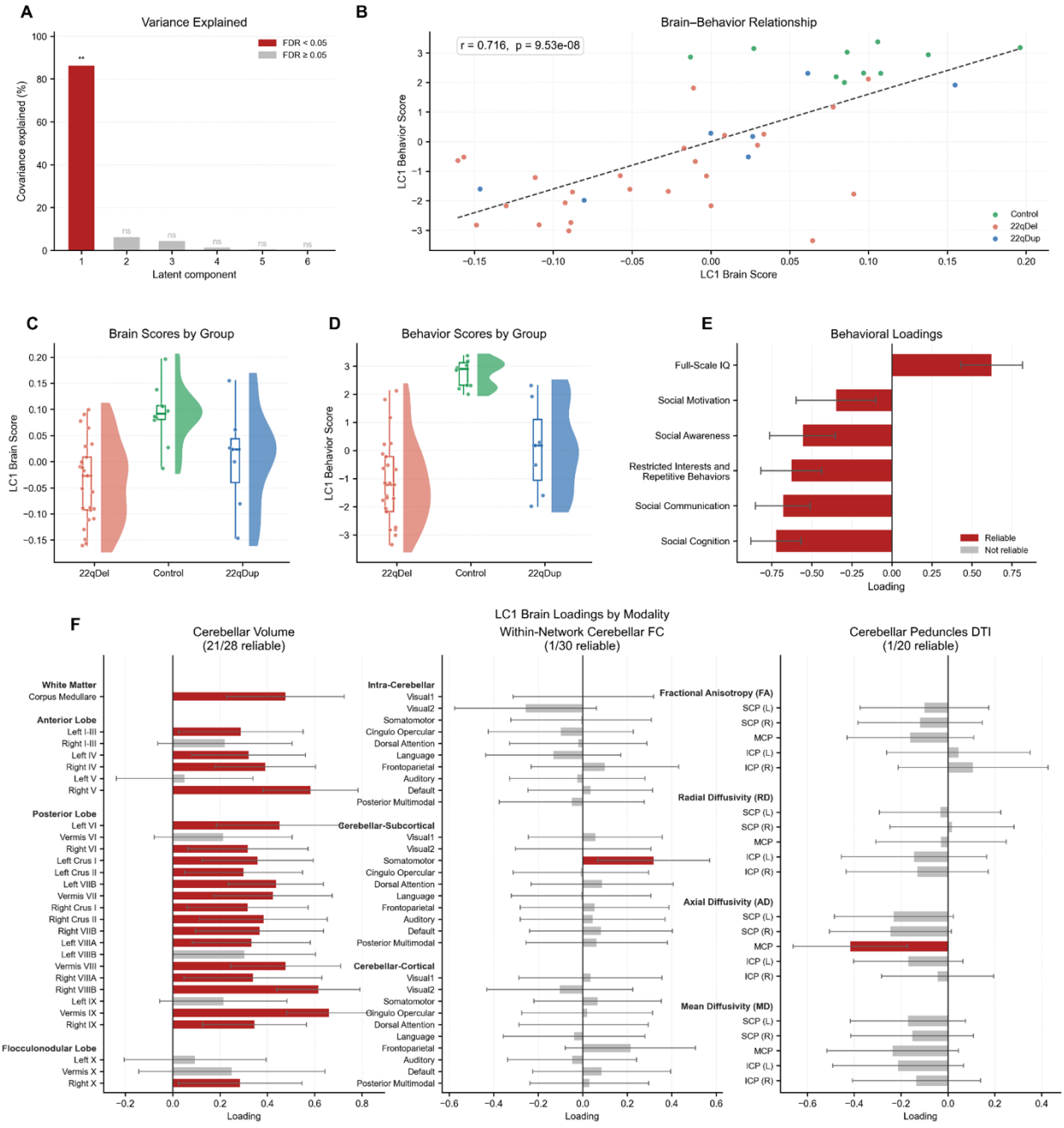

Figure 5 Multimodal cerebellar brain–behavior associations with psychosis-risk symptom severity.

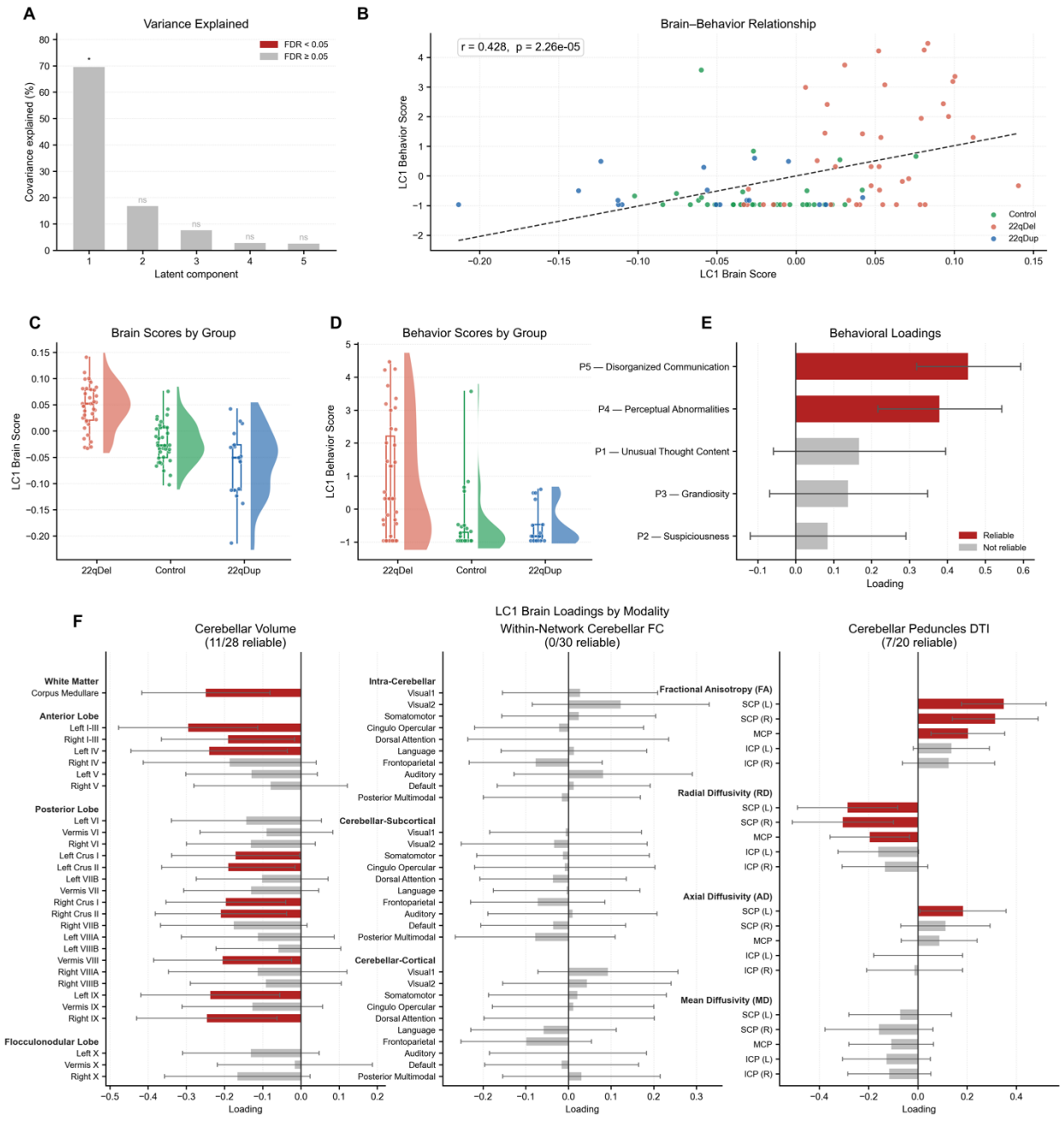

CHAPTER 2 SUPPLEMENTAL MATERIAL

Supplementary Methods

1. Resting-State fMRI Acquisition and Preprocessing

Resting-state fMRI data were acquired and preprocessed following a previously described protocol (1), using the Human Connectome Project Minimal Preprocessing Pipeline (HCP-MPP) with additional bandpass filtering, motion scrubbing for frames exceeding a framewise displacement or signal change threshold, spatial smoothing, and regression of mean signal from ventricles, deep white matter, and mean gray matter. Scans with excessive motion (>50% of frames flagged) or poor cerebellar registration were excluded.

2. Multimodal CNV Classification

2.1 Classifier hyperparameters

Hyperparameters were fixed a priori (not tuned via grid search) and a single random seed (42) was applied.

Model Settings

Model	**Settings**
SVM	RBF kernel, C=1.0, gamma=scale, class_weight=balanced
Random Forest	100 trees, max_depth=10, class_weight=balanced
Elastic Net	l1_ratio=0.5, C=1.0, solver=saga, class_weight=balanced
LightGBM	100 estimators, max_depth=6, learning_rate=0.1, class_weight=balanced, min_child_samples=10 (pairwise) / 20 (three-way, default)

2.2 Train/test splits

Classification	Training set (n)	Test set (n)
Three-way	74	19
TD vs. 22qDel	60	15
TD vs. 22qDup	43	11
22qDel vs. 22qDup	45	12

3. Multivariate Brain-Behavior Associations (PLSC)

3.1 PLSC estimation

Latent components were estimated with the behavioral PLS implementation in `pyls`. Component significance was assessed with 10,000 permutations, and loading stability with 10,000 bootstrap resamples (random seed = 42; no train/test split). A loading was considered reliable if its bootstrap 95% confidence interval did not cross zero.

3.2 Brain loadings

Because the behavioral block was specified as the primary block in the initial PLS analysis, brain loadings and their confidence intervals were obtained by re-running the analysis with the brain and behavioral blocks swapped, with bootstrapping retained. Permutations were omitted because latent variable significance had already been assessed in the primary analysis.

3.3 Behavioral measures per model

The cognitive/social model comprised Full-Scale IQ (FSIQ) and five SRS-2 T-score subdomains: Social Awareness, Social Cognition, Social Communication, Social Motivation, and Autistic Mannerisms. The psychosis-risk model comprised five SIPS positive-symptom severity items: P1 (Unusual Thought Content / Delusional Ideas), P2

(Suspiciousness / Persecutory Ideas), P3 (Grandiosity), P4 (Perceptual Abnormalities / Hallucinations), and P5 (Disorganized Communication).

4. Exploratory Diagnostic Classification

As an exploratory analysis, we additionally tested whether multimodal cerebellar features could classify binary clinical diagnostic status: ASD (within 22qDel, within 22qDup, and across the combined 22q11.2 CNV sample) and psychosis (within 22qDel). Given the limited number of positive diagnoses in these clinical subgroups, gradient-boosting classifiers (XGBoost, LightGBM) were used, as these methods accommodate missing data and maximize available sample size. Models were evaluated via repeated stratified 5-fold cross-validation (10 repeats).

Supplementary Results

1. Exploratory Diagnostic Classification

Multimodal cerebellar features did not reliably classify ASD diagnostic status within 22qDel (N=87, ASD=47), within 22qDup (N=32, ASD=14), or across the combined 22q sample (N=119, ASD=61), with AUC at or below chance across all comparisons. Within 22qDel, psychosis diagnostic status was similarly not classifiable above chance (XGBoost: AUC=0.48; LightGBM: AUC=0.51; N=100, psychosis=9), with apparent high raw accuracy (~87%) reflecting class imbalance rather than true discriminability. Across all classifiers and subgroups, no model exceeded AUC=0.55 after averaging across cross-validation folds.

Supplementary Tables

Supplementary Table S1. Group differences in cerebellar white matter microstructure.

Metric	Region	22qDel vs. TD							22qDup vs. TD						
		B	CI (2.5%)	CI (97.5 %)	SE	t	p-value	FDR q	B	CI (2.5%)	CI (97.5 %)	SE	t	p-value	FDR q
FA	Left SCP	0.59	0.27	0.90	0.16	3.73	<0.001	<0.001	-1.09	-1.51	-0.68	0.21	-5.25	<0.001	<0.001
	Right SCP	0.59	0.28	0.90	0.16	3.72	<0.001	<0.001	-1.11	-1.52	-0.69	0.21	-5.27	<0.001	<0.001
	MCP	0.25	-0.08	0.58	0.17	1.50	0.14	0.17	-1.51	-1.95	-1.08	0.22	-6.88	<0.001	<0.001
	Left ICP	-0.05	-0.41	0.31	0.18	-0.28	0.78	0.78	-0.99	-1.46	-0.51	0.24	-4.11	<0.001	<0.001
	Right ICP	-0.30	-0.65	0.05	0.18	-1.70	0.09	0.15	-1.09	-1.56	-0.62	0.24	-4.64	<0.001	<0.001
MD	Left SCP	-0.16	-0.49	0.16	0.16	-0.99	0.32	0.40	-0.18	-0.62	0.26	0.22	-0.81	0.42	0.98
	Right SCP	-0.21	-0.53	0.11	0.16	-1.31	0.19	0.40	-0.01	-0.44	0.42	0.22	-0.04	0.97	0.98
	MCP	-0.08	-0.40	0.23	0.16	-0.53	0.59	0.59	0.52	0.10	0.94	0.21	2.47	0.01	0.07
	Left ICP	-0.17	-0.49	0.14	0.16	-1.11	0.27	0.40	-0.05	-0.47	0.36	0.21	-0.26	0.80	0.98
	Right ICP	-0.17	-0.49	0.14	0.16	-1.10	0.28	0.40	-0.01	-0.43	0.41	0.21	-0.03	0.98	0.98
RD	Left SCP	-0.52	-0.83	-0.21	0.15	-3.36	0.001	0.003	0.54	0.14	0.95	0.21	2.65	0.01	0.01
	Right SCP	-0.56	-0.86	-0.26	0.15	-3.69	<0.001	0.002	0.71	0.31	1.11	0.20	3.54	<0.001	0.001
	MCP	-0.26	-0.56	0.04	0.15	-1.70	0.09	0.15	1.15	0.75	1.55	0.20	5.65	<0.001	<0.001
	Left ICP	-0.09	-0.41	0.24	0.16	-0.53	0.60	0.65	0.49	0.06	0.92	0.22	2.25	0.03	0.03
	Right ICP	0.07	-0.25	0.39	0.16	0.45	0.65	0.65	0.61	0.19	1.04	0.21	2.84	0.01	0.01
AD	Left SCP	0.28	-0.07	0.63	0.18	1.60	0.11	0.19	-0.89	-1.35	-0.43	0.23	-3.81	<0.001	0.001
	Right SCP	0.29	-0.07	0.64	0.18	1.60	0.11	0.19	-0.80	-1.27	-0.33	0.24	-3.36	0.001	0.002
	MCP	0.19	-0.14	0.52	0.17	1.13	0.26	0.26	-0.52	-0.96	-0.07	0.23	-2.29	0.02	0.02
	Left ICP	-0.22	-0.57	0.13	0.17	-1.26	0.21	0.26	-0.72	-1.18	-0.26	0.23	-3.10	0.002	0.003
	Right ICP	-0.42	-0.77	-0.08	0.17	-2.43	0.02	0.08	-0.81	-1.27	-0.35	0.23	-3.47	<0.001	0.002

Note. Linear mixed-effects models per DTI metric and peduncle region; B = unstandardized fixed-effect estimate for group (outcome z-scored; SE, t, and CI in the same units). FDR q computed within each metric (FA = fractional anisotropy, MD = mean diffusivity, RD = radial diffusivity, AD = axial diffusivity) across the 5 peduncle regions and 2 group contrasts. SCP = superior cerebellar peduncle; MCP = middle cerebellar peduncle; ICP = inferior cerebellar peduncle.

Supplementary Table S2. Group differences in cerebellar functional connectivity (CAB-NP networks).

Connection Type	Network	22qDel vs. TD							22qDup vs. TD						
		B	CI (2.5%)	CI (97.5%)	SE	t	p-value	FDR q	B	CI (2.5%)	CI (97.5%)	SE	t	p-value	FDR q
Intra-cerebellar	Visual 1	-0.14	-0.38	0.09	0.12	-1.18	0.24	0.27	0.21	-0.13	0.54	0.17	1.23	0.22	0.44
	Visual 2	-0.15	-0.40	0.09	0.13	-1.22	0.22	0.27	0.11	-0.25	0.46	0.18	0.60	0.55	0.60
	Somatomotor	-0.19	-0.42	0.05	0.12	-1.57	0.12	0.24	0.28	-0.05	0.61	0.17	1.65	0.10	0.33
	Cingulo-Opercular	-0.17	-0.43	0.08	0.13	-1.37	0.17	0.27	0.13	-0.23	0.48	0.18	0.72	0.47	0.60
	Dorsal Attention	-0.27	-0.51	-0.03	0.12	-2.21	0.03	0.16	0.30	-0.04	0.64	0.17	1.74	0.08	0.33
	Language	-0.23	-0.47	0.01	0.12	-1.85	0.07	0.16	-0.09	-0.44	0.25	0.18	-0.53	0.60	0.60
	Frontoparietal	-0.15	-0.40	0.10	0.13	-1.18	0.24	0.27	0.35	0.00	0.71	0.18	1.98	0.05	0.33
	Auditory	-0.08	-0.31	0.16	0.12	-0.65	0.52	0.52	0.10	-0.24	0.43	0.17	0.56	0.58	0.60
	Default	-0.25	-0.49	-0.01	0.12	-2.05	0.04	0.16	0.16	-0.18	0.51	0.17	0.95	0.34	0.57
	Posterior Multimodal	-0.24	-0.49	-0.00	0.12	-2.00	0.05	0.16	0.21	-0.13	0.56	0.17	1.24	0.22	0.44
Cerebellar-Cortical	Visual 1	-0.20	-0.44	0.04	0.12	-1.61	0.11	0.11	0.18	-0.16	0.53	0.17	1.05	0.30	0.59
	Visual 2	-0.27	-0.52	-0.01	0.13	-2.09	0.04	0.06	0.02	-0.33	0.38	0.18	0.12	0.91	0.91
	Somatomotor	-0.25	-0.50	-0.01	0.12	-2.02	0.05	0.06	0.19	-0.16	0.53	0.18	1.06	0.29	0.59
	Cingulo-Opercular	-0.27	-0.51	-0.02	0.13	-2.09	0.04	0.06	0.09	-0.26	0.45	0.18	0.53	0.60	0.78
	Dorsal Attention	-0.33	-0.57	-0.08	0.12	-2.60	0.01	0.03	0.09	-0.26	0.44	0.18	0.49	0.62	0.78
	Language	-0.35	-0.61	-0.10	0.13	-2.75	0.01	0.02	-0.12	-0.47	0.24	0.18	-0.65	0.52	0.78
	Frontoparietal	-0.25	-0.50	0.01	0.13	-1.93	0.06	0.07	0.19	-0.17	0.55	0.18	1.06	0.29	0.59
	Auditory	-0.20	-0.44	0.04	0.12	-1.64	0.10	0.11	0.25	-0.10	0.59	0.17	1.43	0.16	0.59
	Default	-0.35	-0.58	-0.11	0.12	-2.90	0.004	0.02	0.20	-0.14	0.53	0.17	1.17	0.25	0.59
	Posterior Multimodal	-0.38	-0.63	-0.13	0.13	-3.03	0.003	0.02	0.05	-0.30	0.40	0.18	0.29	0.77	0.86
Cerebellar-Subcortical	Visual 1	-0.25	-0.50	-0.01	0.12	-2.03	0.04	0.06	0.28	-0.06	0.63	0.17	1.61	0.11	0.22
	Visual 2	-0.28	-0.53	-0.04	0.12	-2.29	0.02	0.05	0.38	0.04	0.72	0.17	2.18	0.03	0.13
	Somatomotor	-0.37	-0.62	-0.12	0.13	-2.96	0.003	0.03	0.24	-0.11	0.59	0.18	1.34	0.18	0.25
	Cingulo-Opercular	-0.18	-0.43	0.06	0.12	-1.45	0.15	0.16	0.37	0.02	0.72	0.18	2.10	0.04	0.13
	Dorsal Attention	-0.29	-0.54	-0.05	0.12	-2.34	0.02	0.05	0.25	-0.10	0.60	0.18	1.43	0.15	0.25
	Language	-0.30	-0.54	-0.05	0.13	-2.35	0.02	0.05	0.23	-0.12	0.58	0.18	1.29	0.20	0.25

	Frontoparietal	-0.26	-0.51	-0.01	0.13	-2.05	0.04	0.06	0.19	-0.16	0.55	0.18	1.08	0.28	0.31
	Auditory	-0.15	-0.39	0.08	0.12	-1.27	0.21	0.21	0.32	-0.02	0.65	0.17	1.88	0.06	0.15
	Default	-0.24	-0.48	-0.01	0.12	-2.02	0.04	0.06	0.17	-0.17	0.51	0.17	0.97	0.33	0.33
	Posterior Multimodal	-0.33	-0.57	-0.08	0.12	-2.65	0.01	0.04	0.37	0.02	0.71	0.17	2.09	0.04	0.13

Note. Linear mixed-effects models per connection type and network; B = unstandardized fixed-effect estimate for group (outcome z-scored; SE, t, and CI in the same units). FDR q-values were computed separately for each connectivity type (intra-cerebellar, cerebellar-cortical, cerebellar-subcortical) and group contrast, across the 10 networks.

Supplementary Table S3. Full classification performance by model and comparison (three-way and pairwise).

Comparison	Model	Accuracy	Balanced Accuracy	AUC (test set)	Perm. p	N (train/test)
Three-way (TD/Del/Dup)	SVM	0.58	0.56	0.80	<.001	74/19
	Random Forest	0.53	0.48	0.73	<.001	74/19
	Elastic Net	0.37	0.34	0.61	<.001	74/19
	LightGBM	0.53	0.48	0.78	<.001	74/19
TD vs. Del	SVM	0.67	0.66	0.79	<.001	60/15
	Random Forest	0.53	0.52	0.73	<.001	60/15
	Elastic Net	0.60	0.60	0.71	.002	60/15
	LightGBM	0.67	0.66	0.75	<.001	60/15
TD vs. Dup	SVM	0.73	0.73	0.79	.005	43/11
	Random Forest	0.73	0.68	0.77	.027	43/11
	Elastic Net	0.55	0.54	0.61	.157 (ns)	43/11
	LightGBM	0.64	0.66	0.71	.046	43/11
Del vs. Dup	SVM	0.92	0.88	1.00	<.001	45/12
	Random Forest	0.92	0.88	1.00	<.001	45/12
	Elastic Net	0.75	0.69	0.94	.003	45/12
	LightGBM	0.83	0.81	0.94	<.001	45/12

Note. TD = typically developing; Del = 22q11.2 deletion; Dup = 22q11.2 duplication; AUC = area under the curve. Permutation p-values (Perm. p) are based on 1,000 permutations of a separate cross-validated AUC on the training split and are not directly comparable to the held-out test-set AUC. ns = not significant (p > .05).

Supplementary Table S4. PLSC: Group differences underlying LC1 across CNV groups.

Model	Score	ANOVA F	ANOVA p	TD vs. Del	TD vs. Dup	Del vs. Dup
Cognitive/Social	Brain	9.94	.0003	t=4.71, p<.0001	t=2.29, p=.037	t=−1.24, p=.226 (ns)
	Behavior	29.66	<.0001	t=8.05, p<.0001	t=4.92, p=.0002	t=−1.88, p=.070 (ns)
Psychosis-risk	Brain	38.74	<.0001	t=−7.29, p<.0001	t=2.69, p=.010	t=7.38, p<.0001
	Behavior	12.00	<.0001	t=−4.19, p=.0001	t=−0.40, p=.692 (ns)	t=2.92, p=.005

Note. One-way ANOVA followed by pairwise t-tests (uncorrected) on LC1 brain and behavior scores across TD, 22qDel, and 22qDup, separately for each PLSC model (Cognitive/Social: N=42, TD=10, 22qDel=25, 22qDup=7; Psychosis-risk: N=91, TD=35, 22qDel=39, 22qDup=17). ns = not significant (p > .05).

Supplementary References

1. Schleifer CH, Chang SE, Amir CM, O'Hora KP, Fung H, Kang JWD, *et al.* (2025): Unique functional neuroimaging signatures of genetic versus clinical high risk for psychosis. *Biol Psychiatry* 97: 178–187.

CHAPTER 3: CONVERGENT AND DIVERGENT CEREBELLAR ALTERATIONS ACROSS HIGH-RISK NEUROPSYCHIATRIC COPY NUMBER VARIANTS

Hoki Fung[1,2], Leila Kushan-Wells[1], Milin Kim[3], Kuaikuai Duan[4,5], Sarah Shultz[4,5], Jennifer Mulle[6,7], Carrie E. Bearden[1,8]

1. Department of Psychiatry and Biobehavioral Sciences, Semel Institute for Neuroscience and Human Behavior, University of California, Los Angeles, CA, USA.
2. Neuroscience Interdepartmental Program, University of California Los Angeles, Los Angeles, CA, USA.
3. Center for Precision Psychiatry, Division of Mental Health and Addiction, Oslo University Hospital & Institute of Clinical Medicine, University of Oslo, Oslo, Norway.
4. Marcus Autism Center, Children's Healthcare of Atlanta, Emory University School of Medicine, Atlanta, GA, USA.
5. Department of Pediatrics, Emory University School of Medicine, Atlanta, GA, USA.
6. Department of Psychiatry, Robert Wood Johnson Medical School, Rutgers University, New Brunswick, NJ, USA.
7. Center for Advanced Biotechnology and Medicine, Rutgers University, New Brunswick, NJ, USA.
8. Department of Psychology, University of California, Los Angeles, CA, USA.

A version of this chapter is in preparation for journal submission.

ABSTRACT

Background

22q11.2 deletion (22qDel) and 3q29 deletion (3q29Del) are rare, recurrent copy number variants (CNVs) conferring some of the highest known genetic risks for schizophrenia and autism spectrum disorder (ASD). Each has separately been linked to reduced cerebellar volume, but no study has directly compared cerebellar phenotypes across the two CNVs, leaving it unknown whether cerebellar vulnerability and its clinical correlates are shared or distinct.

Methods

T1-weighted MRI scans from 322 participants across two independently recruited cohorts (22qDel n=111, 22qControl n=109; 3q29Del n=24, 3q29Control n=78; mean age 15.2–16.2 ± SD 7.3–9.3 years across groups) were parcellated into 28 cerebellar subregions using ACAPULCO. To compare cerebellar volume between groups despite group-site collinearity, we adapted a previously published normative model to each site, generating deviation scores that were compared between groups using linear regression with FDR correction. In a subset with clinical data (N=77–85 depending on measure), we examined associations between deviation scores and cognitive, psychosis-risk, and social functioning measures.

Results

Both 22qDel (mean z=−1.61, d=−1.26) and 3q29Del mean z=−1.84, d=−1.45) showed substantial reductions in total cerebellar volume relative to normative expectations

(p<.001), with no significant between-CNV difference (β=−.23, p=.416). Regional analyses revealed both convergent and CNV-specific patterns, with reductions observed across most subregions in both groups, while five of 28 subregions differed significantly between CNVs after FDR correction. Exploratory brain-behavior analyses revealed nominal, directionally consistent associations that did not survive FDR correction in either group.

Conclusions

Despite arising from distinct genomic loci, 22qDel and 3q29Del show large and broadly similar cerebellar volume reductions, alongside more circumscribed regional differences. These findings identify the cerebellum as a site of convergent neuroanatomical vulnerability across high-penetrance neuropsychiatric CNVs and demonstrate the utility of normative modeling for comparing rare genetic cohorts collected across independent sites.

INTRODUCTION

Rare, recurrent copy number variants (CNVs) are among the most highly penetrant known genetic risk factors for psychiatric and neurodevelopmental disorders (1). The 22q11.2 deletion (22qDel) and the 3q29 deletion (3q29Del) are two such CNVs, conferring more than 20-fold and 40-fold increased risk for schizophrenia, respectively (2,3), representing some of the largest known genetic risk effects for the disorder. They are also associated with elevated rates of autism spectrum disorder (ASD) and intellectual disability (4,5). The two CNVs arise from microdeletions at entirely distinct genomic loci: 22qDel spans ~3 Mb at the 22q11.2 locus, affecting 46 protein-coding genes (6), whereas 3q29Del spans a smaller, ~1.6 Mb segment at the 3q29 locus, affecting 21 protein-coding genes (7). Because both CNVs act through single, well-defined genomic loci rather than the polygenic architecture typical of idiopathic psychiatric illness (8,9), they offer a genetics-first framework for identifying convergent neurobiological mechanisms underlying shared psychiatric risk, as well as CNV-specific mechanisms that may explain differences in clinical presentation (for an overview of the genetics-first approach, see (10)).

Prior neuroimaging work has begun to characterize brain structure across multiple neuropsychiatric CNVs, including large-scale comparative studies of cortical and subcortical morphometry that suggest both convergent and CNV-specific effects on brain structure (11–14). However, 3q29Del has not been included in any of these cross-CNV comparisons, and these efforts have focused almost exclusively on cortical and subcortical systems, leaving open whether analogous patterns of convergence and divergence extend to 3q29 and the cerebellum.

The cerebellum had long been viewed as a motor structure, but is now recognized as a key hub for cognition, affect, and social processing, with the anterior cerebellum coarsely mapping onto sensorimotor function and the posterior cerebellum onto cognitive and affective processing (15,16). Cerebellar dysfunction has also been implicated across a broad range of neurodevelopmental and psychiatric disorders (17). For example, structural cerebellar abnormalities are among the most consistently replicated brain findings in idiopathic schizophrenia, with meta-analytic evidence pointing to reduced gray matter volume in the posterior cerebellum, including right lobule VI, left Crus II, and right lobule VIII (18). A separate meta-analysis similarly found reduced posterior cerebellar gray matter in ASD, localized to the right Crus I, left lobule VIIIB, and Vermis IX (19). This convergence on posterior cerebellar regions across both conditions underscores the cerebellum's relevance to psychiatric risk beyond its classical motor role.

Cerebellar findings in idiopathic schizophrenia and ASD are drawn from etiologically heterogeneous samples, however, making it difficult to determine whether cerebellar involvement reflects a direct consequence of genetic risk or is confounded by this underlying heterogeneity. CNVs such as 22qDel and 3q29Del, with their well-defined, highly penetrant genetic risk for both conditions, offer a more direct test of this question. In a prior report, we found that 22qDel is associated with widespread reductions in total and regional cerebellar volume relative to typically developing (TD) controls (20). Independently, Sefik and colleagues reported reduced cerebellar volume in 3q29Del relative to their own control group (21). These parallel findings raise the possibility that cerebellar vulnerability may represent a shared neurobiological signature

across recurrent CNVs conferring risk for psychosis and ASD. However, because these findings were generated in separate cohorts, using different control samples, scanners, and processing pipelines, it remains unknown whether cerebellar alterations in 22qDel and 3q29Del are truly convergent, or whether they instead reflect CNV-specific regional patterns of vulnerability, nor whether the magnitude of effect is similar across CNVs.

To directly address this question, we combined the independently recruited 22qDel and 3q29Del cohorts into a single analytic sample. However, because the two cohorts were recruited and scanned at different sites, CNV group is completely collinear with site, and no participants were scanned at both. This precludes standard methods such as linear regression with site as a covariate, or dedicated harmonization tools like ComBat (22), both of which require overlapping data across sites to disentangle CNV-related from site-related variance.

Normative modeling offers a solution to this problem. Rather than directly comparing raw regional volumes across sites, it estimates each individual's expected brain measure based on relevant covariates (e.g., age, sex, site), using a model trained on a large, independent reference sample, and quantifies their deviation from this expectation as a standardized (z) score (23). A recently developed, cerebellum-specific lifespan normative model (24), trained on over 27,000 individuals across 132 sites, can be calibrated using site-matched TD controls to generate deviation scores for each deletion participant, placing 22qDel and 3q29Del on a common, directly comparable metric despite being collected at different sites.

Here, we leverage normative modeling to directly compare total and regional cerebellar volume deviations in 22qDel and 3q29Del, the largest single-site cohorts of

each CNV currently available. Based on prior separate findings, we expected both CNVs to show substantial cerebellar volume reductions. Our primary question was whether the magnitude and regional distribution of these alterations would converge across CNVs when quantified on a common normative scale, or instead reveal CNV-specific patterns of cerebellar vulnerability. Considering the distinct genomic loci, gene sets, and clinical profiles associated with each CNV, we further hypothesized that regional analyses would reveal both convergent and CNV-specific patterns of cerebellar alterations. We additionally examined how these deviations relate to cognitive, social, and psychosis-risk clinical measures within and across groups. However, given the limited sample size for brain-behavior analyses, particularly in 3q29Del, these analyses were considered exploratory and hypothesis-generating rather than confirmatory.

METHODS AND MATERIALS

Figure 1 provides a graphical overview of the study workflow, including data collection across the two cohorts, cerebellar parcellation, normative model application, and statistical comparison of deviation scores, each of which is described in detail below.

Participants and Study Design

Participants included individuals with molecularly confirmed 22qDel, recruited as part of an ongoing study at the University of California, Los Angeles (UCLA; see (20) for full recruitment details), and individuals with molecularly confirmed 3q29Del, recruited as part of an independent study at Emory University (see (21) for full recruitment

details). The combined sample included 322 participants: 111 with 22qDel, 24 with 3q29Del, and 187 typically developing (TD) controls recruited from the same two sites (109 from UCLA, 78 from Emory). Full demographic characteristics are summarized in Table 1. Written informed consent (or assent with parental consent for minors) was obtained from all participants, and all procedures were approved by the relevant Institutional Review Boards.

Behavioral and Clinical Measures

Cognitive ability was assessed using the Wechsler Abbreviated Scale of Intelligence (WASI or WASI-II) (25,26). Autism-related reciprocal social behavior was measured using the Social Responsiveness Scale, Second Edition (SRS-2) (27). Psychosis-risk symptoms were assessed using the Structured Interview for Psychosis-Risk Syndromes (SIPS) (28). Full instrument descriptions and scoring procedures are provided in the Supplementary Methods of our prior report (20). Brain-behavior analyses focused on three primary measures: Full-Scale IQ (FSIQ), the SIPS Positive symptom subscale (SIPS-P), and the SRS-2 Total T-score. Not all participants had complete data for every measure. Sample size and descriptive statistics for the three primary measures are reported in Table 1.

MRI Acquisition and Processing

Structural MRI data were acquired using T1-weighted MPRAGE sequences at each site. At UCLA, 22qDel and TD control data were acquired across three 3T Siemens scanners. At Emory, 3q29Del and TD control data were acquired on a single

scanner. All participants contributed a single scan, except for a subset of TD controls in the 22q sample who had scans acquired on more than one scanner. These additional scans were used only for scanner-specific calibration of the normative model (see Normative Modeling) and are not double-counted in the TD N reported in Participants and Study Design and Table 1. Sample sizes by site, scanner, and group are provided in Supplementary Table S1. Acquisition details are reported in our prior reports (20,21). Cerebellar parcellation was performed using ACAPULCO (29), a deep-learning-based method that segments the cerebellum into 28 anatomically defined subregions, from which regional and total cerebellar volumes were subsequently derived. This pipeline was applied identically to all participants across both sites, following the processing steps described in (20).

Normative Modeling

To address the site-CNV collinearity, we applied normative modeling to obtain standardized volume measures relative to a common normative reference, enabling direct comparison across the two cohorts. Specifically, we used a previously published, pretrained cerebellar volume normative model (the Cerebellum Volume Bayesian Linear Regression [BLR] Lifespan Normative Model (24)), available via PCNportal (30). This model was trained on a large, independent reference sample (N=27,117 individuals; 132 sites; age range 3-85 years) to estimate ACAPULCO-derived regional and total cerebellar volume based on age and sex, correcting for scanning site. To account for differences between our scanners and those in the reference sample, the model was first calibrated to each scanner using all available scanner-matched TD controls

(Supplementary Table S1). For each deletion participant, the corresponding calibrated model then generated standardized z-scores quantifying their deviation from the expected value for total cerebellar volume and each of the 28 subregions.

Statistical Analysis

Group differences in total and regional cerebellar volume deviation scores between 22qDel and 3q29Del were examined using linear regression (deviation score ~ CNV group), with FDR correction applied across the 28 regional models. Regions showing no significant difference between 22qDel and 3q29Del were considered similarly affected. Regions that differed significantly between groups were considered distinctly affected. To further characterize the pattern of deviation within each category, we additionally tested, separately within each group, whether each of the 28 regional deviation scores differed significantly from the common normative reference, using one-sample t-tests with FDR correction applied across the 28 regions within each group.

To characterize the clinical subsample in exploratory brain-behavioral analyses, we first examined group differences in FSIQ, SIPS-P, and SRS-2 Total T-score using Welch's t-tests. We then examined brain-behavior associations in two ways: Spearman correlations between total cerebellar volume deviation scores and each measure were examined within each group, with FDR correction applied across the three measures. Deviation-score-by-group interaction models (clinical score ~ CNV group × deviation score) then tested whether these associations differed between CNVs, with FDR correction applied across the three interaction tests. The same correlation and

interaction models were also examined at the regional level (28 regions × the same three measures) as an exploratory analysis.

RESULTS

Participant Characteristics

Participant characteristics are summarized in Table 1. One-way ANOVA confirmed no significant age difference across the four groups. A chi-square test indicated an overall sex distribution difference ($p=0.035$), reflecting higher female representation in the 22q groups (~53%) relative to the 3q29 groups (~37%), although no post hoc pairwise comparisons were significant. The two deletion groups did not differ significantly on FSIQ, SIPS-P, or SRS-2 Total T-score among participants with available data.

Total Cerebellar Volume

Both 22qDel and 3q29Del showed total cerebellar volume deviation scores significantly below the normative reference, with mean reductions of approximately 1.6–1.8 standard deviations below expected volume in both groups (22qDel: $M=-1.61$, $t(110)=-13.32$, $p<.001$; 3q29Del: $M=-1.84$, $t(23)=-7.12$, $p<.001$; Figure 2). Direct comparison of deviation scores between 22qDel and 3q29Del revealed no significant difference in the magnitude of total cerebellar volume reduction ($\beta=-0.23$, $p=0.416$), indicating a comparable degree of global cerebellar vulnerability across the two CNVs.

Regional Cerebellar Volume

Nearly all cerebellar subregions were significantly smaller relative to the normative mean in 22qDel (28 of 28 regions) and in 3q29Del (24 of 28 regions), indicating widespread cerebellar reduction in both CNVs (Supplementary Tables S2a–S2b). The four regions not significantly reduced in 3q29Del were left Lobule VI ($z=-0.08$), Vermis VI ($z=-0.25$), right Lobule VIIIB ($z=-0.37$), and Vermis IX ($z=-0.30$).

Among the convergently reduced regions (i.e., reduced in both groups with no significant between-group difference), several showed particularly closely matched effect sizes, including right Crus II (22qDel $z=-1.31$, 3q29Del $z=-1.33$), Vermis X (22qDel $z=-0.48$, 3q29Del $z=-0.45$), right Lobule VIIIA (22qDel $z=-0.76$, 3q29Del $z=-0.80$), right Lobule IX (22qDel $z=-0.92$, 3q29Del $z=-1.01$), right Crus I (22qDel $z=-0.86$, 3q29Del $z=-0.96$), and left Lobule VIIIA (22qDel $z=-0.93$, 3q29Del $z=-1.04$).

Despite the broad convergence, five subregions differed significantly between 22qDel and 3q29Del after FDR correction ($q<0.05$): left Lobule IV, left Lobule VI, left Crus I, left Lobule IX, and right Lobule VIIIB (Figure 3). In three of these regions—left Lobule IX, left Lobule IV, and left Crus I—while both CNV groups were below the normative mean, 3q29Del showed significantly greater volume reduction than 22qDel (3q29Del < 22qDel < normative mean; Figure 4). In the remaining two regions—left Lobule VI and right Lobule VIIIB—a different pattern emerged: 22qDel showed significantly greater reduction than 3q29Del, whose volumes approximated the normative mean (22qDel < normative mean ≈ 3q29Del; Figure 4). Full model output for the between-group comparison across all 28 regions is provided in Supplementary Table S3.

Exploratory Brain-Behavior Associations

Descriptively, both deletion groups scored below the population mean for FSIQ (22qDel M=78.48; 3q29Del M=72.67; population M=100) and above the population mean for SRS-2 Total T-score (22qDel M=71.17; 3q29Del M=66.22; population M=50), consistent with elevated rates of cognitive impairment and autism-related traits previously reported in both CNVs. Mean SIPS-P scores in both deletion groups (22qDel M=4.76; 3q29Del M=6.40) were also higher than those previously reported in TD controls (M=1.24, SD=1.84) in our prior study (20).

22qDel and 3q29Del did not differ significantly on any of the three primary clinical measures (Table 1; Figure 5). Within-group correlations and deviation-score-by-group interaction models were non-significant for total cerebellar volume deviation scores, and none of the regional-level analyses survived correction for multiple comparisons; nominal results are reported in full in Supplementary Results 1.

DISCUSSION

This study provides the first direct, dedicated comparison of cerebellar structure between 22qDel and 3q29Del, using a normative modeling framework designed to overcome the site-CNV collinearity inherent to combining independently collected rare-variant cohorts. Both 22qDel and 3q29Del showed substantial, statistically indistinguishable reductions in total cerebellar volume relative to a large normative reference, indicating shared global cerebellar vulnerability across these two etiologically distinct, high-risk CNVs. Regional analyses revealed that this vulnerability was broadly convergent, with the majority of cerebellar subregions significantly reduced in both CNVs, alongside a smaller subset of subregions that diverged between groups.

Shared Global Cerebellar Vulnerability Across High-Risk CNVs

To our knowledge, this is the first study to demonstrate cerebellar structural convergence between 22qDel and 3q29Del specifically. The comparable magnitude of total cerebellar volume reduction in 22qDel and 3q29Del, despite these CNVs arising from entirely distinct genomic loci and affecting largely non-overlapping sets of genes, suggests that cerebellar volume loss may represent a convergent downstream consequence of high-penetrance genetic risk, rather than a locus-specific effect. This pattern is consistent with prior comparative work showing that structural brain alterations in high-risk CNVs can converge on shared brain systems even when the initiating genetic lesions differ (11,13), though the mechanisms underlying such convergence remain poorly understood (14,31). One possible contributing factor is the cerebellum's unusually protracted postnatal developmental trajectory, which may leave it particularly vulnerable to disruption across a wide range of distinct genetic insults occurring at different points during an extended developmental window (32). Notably, this reduction was substantially larger than what has been reported in idiopathic psychiatric samples: one-sample Cohen's d was −1.26 in 22qDel and −1.45 in 3q29Del, versus d=−0.35 for schizophrenia in a large mega-analysis (33). Using the same normative reference model applied here, Kim et al. (24) similarly reported a small but reliable reduction in schizophrenia, and a smaller, more directionally mixed pattern in ASD. This is consistent with a genetics-first approach revealing phenotypes otherwise diluted in etiologically heterogeneous cohorts.

Regionally Convergent and Divergent Cerebellar Signatures

Beyond the shared global reduction, most cerebellar subregions were also similarly reduced in both 22qDel and 3q29Del, indicating that cerebellar vulnerability in these two CNVs is broadly convergent at the regional, and not only the global, level. Among these convergently affected regions, several showed closely matched effect sizes between groups, including right Crus I and right Lobule VIIIA. Notably, right Crus I is among the regions most consistently implicated in idiopathic ASD (19), while right Lobule VIIIA falls within Lobule VIII, among the regions most consistently implicated in idiopathic schizophrenia (18). This suggests that at least part of the shared cerebellar vulnerability observed across these two high-risk CNVs converges on territories also implicated in idiopathic presentations of both conditions.

Despite this broad convergence, regional analyses also revealed that 22qDel and 3q29Del diverge in a small subset of specific cerebellar subregions. Left Lobule IX, left Crus I, and left Lobule IV were more severely reduced in 3q29Del than 22qDel. Left Crus I in particular has been implicated in cognitive deficits in psychotic disorders, with a recent connectivity and Transcranial Magnetic Stimulation (TMS) study linking this region to working memory, verbal ability, and cognitive flexibility (34). Left Crus I was more strongly reduced in 3q29Del than 22qDel. Given the established involvement of Crus I in higher-order cognitive and cerebello-cortical networks, this regional difference identifies a candidate CNV-specific anatomical phenotype for future investigation. Whether it contributes to differences in psychiatric or cognitive outcomes between CNVs remains unknown. In contrast, left Lobule VI and right Lobule VIIIB were uniquely reduced in 22qDel, with 3q29Del volumes approximating the normative mean. Reduced gray matter in right Lobule VIII is among the most consistently replicated cerebellar

findings in schizophrenia (18), and reduced connectivity in this region has separately been linked to impaired social functioning in individuals at clinical high risk for psychosis (35). Its selective reduction in 22qDel may reflect CNV-specific vulnerability relevant to distinct aspects of psychiatric or cognitive impairment in this population.

Together, our findings identify CrusI/II and Lobule VIII as key cerebellar territories showing structural vulnerability across 22qDel and 3q29Del, overlapping with regions previously implicated in idiopathic ASD and schizophrenia. Subregional differences raise the possibility that CNV-specific differential reduction within these territories tracks each CNV's distinct psychiatric risk profile. However, we did not find these regions to be significantly related to the psychosis-risk and social functioning measures examined here, an absence that may reflect limited power rather than a true lack of clinical relevance.

Normative Modeling as a Framework for Cross-Cohort Rare-Variant Comparisons

A central contribution of this study is methodological: by leveraging a large, independent lifespan reference model with site adaptation, normative modeling enabled direct comparison of cerebellar phenotypes across two rare-CNV cohorts that were recruited, scanned, and processed independently, without requiring any participants to be scanned at both sites. This approach circumvents a fundamental limitation of rare-disease neuroimaging research, in which sample sizes at any single site are often too small to support well-powered analyses, and in which combining across sites via standard harmonization methods is not possible when CNV group and site are completely confounded. As more genetically defined patient cohorts are collected

across independent sites, normative modeling approaches like the one used here may offer a scalable framework for cross-cohort comparison in rare-variant neuroimaging research more broadly.

Limitations

Several limitations should be noted. This study was cross-sectional, with a single timepoint per participant, precluding examination of developmental trajectories of cerebellar volume in either CNV. Clinical and cognitive data were limited, with missingness ranging from 40-51% across several measures in 22qDel and an overall small sample size for 3q29Del (n=24). Consequently, the null brain-behavior findings reported here, including the absence of significant deviation-score-by-group interactions, were likely underpowered to detect all but large effects, and should not be interpreted as evidence against a true cerebellar-clinical association in either CNV. Although normative modeling with site adaptation directly addresses the site-CNV collinearity inherent to the structural comparison, residual site-related differences in acquisition protocol, sequence parameters, or sample ascertainment cannot be fully excluded. We could not formally benchmark this approach against a directly harmonized alternative, such as traveling-subject validation or multi-site harmonization, as no participants were scanned at both sites, nor were both CNV groups present at each site. Finally, all available typically developing controls at each site were used for model calibration to maximize the precision of the site adaptation. This came at the cost of retaining an independent sample to directly evaluate where site controls fell relative to the normative reference, or to include controls in the brain-behavior analyses.

Implications and Future Directions

Longitudinal designs will be important for clarifying whether the cerebellar differences identified here reflect static or progressively diverging developmental trajectories across 22qDel and 3q29Del. Extending normative modeling approaches to CNVs with differing psychiatric risk profiles, such as 22q11.2 duplication (which confers relatively lower psychosis risk but elevated ASD risk), may help disentangle which cerebellar signatures track risk for psychosis versus ASD specifically, rather than the shared risk profile examined here. As cerebellar imaging methods continue to advance, incorporating additional phenotypes such as functional connectivity and microstructure may further refine understanding of how these CNVs affect cerebellar structure and function beyond volume alone. Emerging advances in cerebellar gene expression profiling and animal model studies may also help shed light on the molecular mechanisms linking these genetically distinct CNVs to convergent cerebellar phenotypes, a question neuroimaging alone cannot resolve. Larger, better-powered clinical subsamples, supported by harmonized behavioral and cognitive assessment batteries across sites, will also be needed to more definitively test whether these structural signatures relate to shared or distinct patterns of psychosis risk, autism-related traits, and cognitive impairment.

CHAPTER 3 ACKNOWLEDGMENTS AND DISCLOSURES

Author Contributions

HF: Conceptualization, Methodology, Data curation, Formal analysis, Software, Validation, Visualization, Writing – original draft, Writing – review & editing. **LK-W:** Investigation, Data curation, Project administration. **MK:** Methodology, Software. **KD:** Investigation, Data curation, Methodology, Writing – review & editing, Supervision. **SS:** Investigation, Data curation, Methodology, Writing – review & editing, Supervision. **JM:** Conceptualization, Methodology, Writing – review & editing, Supervision, Funding acquisition, Resources. **CEB:** Conceptualization, Methodology, Writing – review & editing, Supervision, Funding acquisition, Resources.

Funding

This work was supported by the National Institute of Mental Health (Grant Nos. R01/R37MH085953, R01MH129858, U01MH101779, U01MH119736, R21MH116473, all to CEB, and R01MH118534 to JM), the Department of Defense (Grant No. W81XWH-12-1-0081, to CEB), the Simons Foundation Autism Research Initiative Explorer Award (to CEB), the Uytengsu-Hamilton 22q11 Neuropsychiatry Research Award (to CEB).

Acknowledgments

We are deeply grateful to the participants and their families for their time, commitment, and invaluable contributions to this study.

Disclosures

All authors reported no biomedical financial interests or potential conflicts of interest.

CHAPTER 3 REFERENCES

1. Torres F, Barbosa M, Maciel P (2016): Recurrent copy number variations as risk factors for neurodevelopmental disorders: critical overview and analysis of clinical implications. *J Med Genet* 53: 73–90.
2. Cleynen I, Engchuan W, Hestand MS, Heung T, Holleman AM, Johnston HR, *et al.* (2021): Genetic contributors to risk of schizophrenia in the presence of a 22q11.2 deletion. *Mol Psychiatry* 26: 4496–4510.
3. Mulle JG (2015): The 3q29 deletion confers >40-fold increase in risk for schizophrenia. *Mol Psychiatry* 20: 1028–1029.
4. Schneider M, Debbané M, Bassett AS, Chow EWC, Fung WLA, van den Bree M, *et al.* (2014): Psychiatric disorders from childhood to adulthood in 22q11.2 deletion syndrome: results from the International Consortium on Brain and Behavior in 22q11.2 Deletion Syndrome. *Am J Psychiatry* 171: 627–639.
5. Mulle JG, Dodd AF, McGrath JA, Wolyniec PS, Mitchell AA, Shetty AC, *et al.* (2010): Microdeletions of 3q29 confer high risk for schizophrenia. *Am J Hum Genet* 87: 229–236.
6. McDonald-McGinn DM, Sullivan KE, Marino B, Philip N, Swillen A, Vorstman JAS, *et al.* (2015): 22q11.2 deletion syndrome. *Nat Rev Dis Primers* 1: 15072.
7. Yilmaz F, Gurusamy U, Mosley TJ, Hallast P, Kim K, Mostovoy Y, *et al.* (2023): High level of complexity and global diversity of the 3q29 locus revealed by optical mapping and long-read sequencing. *Genome Med* 15: 35.
8. Sullivan PF, Daly MJ, O'Donovan M (2012): Genetic architectures of psychiatric disorders: the emerging picture and its implications. *Nat Rev Genet* 13: 537–551.

9. Owen MJ, Bray NJ, Walters JTR, O'Donovan MC (2025): Genomics of schizophrenia, bipolar disorder and major depressive disorder. *Nat Rev Genet* 1–16.

10. Fiksinski AM, Hoftman GD, Vorstman JAS, Bearden CE (2023): A genetics-first approach to understanding autism and schizophrenia spectrum disorders: the 22q11.2 deletion syndrome. *Mol Psychiatry* 28: 341–353.

11. Modenato C, Kumar K, Moreau C, Martin-Brevet S, Huguet G, Schramm C, *et al.* (2021): Effects of eight neuropsychiatric copy number variants on human brain structure. *Transl Psychiatry* 11: 399.

12. Sønderby IE, Ching CRK, Thomopoulos SI, van der Meer D, Sun D, Villalon-Reina JE, *et al.* (2022): Effects of copy number variations on brain structure and risk for psychiatric illness: Large-scale studies from the ENIGMA working groups on CNVs. *Hum Brain Mapp* 43: 300–328.

13. Kumar K, Modenato C, Moreau C, Ching CRK, Harvey A, Martin-Brevet S, *et al.* (2023): Subcortical brain alterations in carriers of genomic copy number variants. *Am J Psychiatry* 180: 685–698.

14. Kopal J, Kumar K, Saltoun K, Modenato C, Moreau CA, Martin-Brevet S, *et al.* (2023): Rare CNVs and phenome-wide profiling highlight brain structural divergence and phenotypical convergence. *Nat Hum Behav* 7: 1001–1017.

15. Buckner RL (2013): The cerebellum and cognitive function: 25 years of insight from anatomy and neuroimaging. *Neuron* 80: 807–815.

16. Stoodley CJ, Schmahmann JD (2009): Functional topography in the human cerebellum: a meta-analysis of neuroimaging studies. *Neuroimage* 44: 489–501.

17. Argyropoulos GPD, Lupo M, Olivito G (2022): Editorial: The cerebellar role in psychiatric disorders: Emerging evidence and future perspectives. *Front Behav Neurosci* 16: 1075679.

18. Li X, Liu N, Yang C, Zhang W, Lui S (2022): Cerebellar gray matter volume changes in patients with schizophrenia: A voxel-based meta-analysis. *Front Psychiatry* 13: 1083480.

19. Stoodley CJ (2014): Distinct regions of the cerebellum show gray matter decreases in autism, ADHD, and developmental dyslexia. *Front Syst Neurosci* 8: 92.

20. Fung H, O'Hora KP, Boen R, Wang HR, Amir CM, Schleifer CH, *et al.* (2026): Convergent and divergent cerebellar alterations in 22q11.2 copy number variants. *Biol Psychiatry Glob Open Sci* 6: 100718.

21. Sefik E, Duan K, Li Y, Sholar B, Evans L, Pincus J, *et al.* (2024): Structural deviations of the posterior fossa and the cerebellum and their cognitive links in a neurodevelopmental deletion syndrome. *Mol Psychiatry* 29: 3395–3411.

22. Fortin J-P, Cullen N, Sheline YI, Taylor WD, Aselcioglu I, Cook PA, *et al.* (2018): Harmonization of cortical thickness measurements across scanners and sites. *Neuroimage* 167: 104–120.

23. Marquand AF, Rezek I, Buitelaar J, Beckmann CF (2016): Understanding heterogeneity in clinical cohorts using normative models: Beyond case-control studies. *Biol Psychiatry* 80: 552–561.

24. Kim M, Leonardsen E, Rutherford S, Selbæk G, Persson K, Steen NE, *et al.* (2024): Mapping cerebellar anatomical heterogeneity in mental and neurological illnesses. *Nat Ment Health* 2: 1196–1207.

25. Wechsler D (1999): *Manual for the Wechsler Abbreviated Intelligence Scale (WASI)*. San Antonio, TX: The Psychological Corporation.

26. Wechsler D (2011): *Wechsler Abbreviated Scale of Intelligence, Second Edition*. San Antonio, TX: Pearson.

27. Constantino JN, Gruber CP (2005): Social Responsiveness Scale 2nd ed: Western Psychological Services.

28. McGlashan TH, Miller TJ, Woods SW, Hoffman RE, Davidson L (2001): Instrument for the assessment of prodromal symptoms and states. *Early Intervention in Psychotic Disorders*. Dordrecht: Springer Netherlands, pp 135–149.

29. Han S, Carass A, He Y, Prince JL (2020): Automatic cerebellum anatomical parcellation using U-Net with locally constrained optimization. *Neuroimage* 218: 116819.

30. Barkema P, Rutherford S, Lee H-C, Kia SM, Savage H, Beckmann C, Marquand A (2023): Predictive Clinical Neuroscience Portal (PCNportal): instant online access to research-grade normative models for clinical neuroscientists. *Wellcome Open Res* 8: 326.

31. Moreau CA, Ching CR, Kumar K, Jacquemont S, Bearden CE (2021): Structural and functional brain alterations revealed by neuroimaging in CNV carriers. *Curr Opin Genet Dev* 68: 88–98.

32. Sathyanesan A, Zhou J, Scafidi J, Heck DH, Sillitoe RV, Gallo V (2019): Emerging connections between cerebellar development, behaviour and complex brain disorders. *Nat Rev Neurosci* 20: 298–313.

33. Moberget T, Doan NT, Alnæs D, Kaufmann T, Córdova-Palomera A, Lagerberg TV, *et al.* (2018): Cerebellar volume and cerebellocerebral structural covariance in schizophrenia: a multisite mega-analysis of 983 patients and 1349 healthy controls. *Mol Psychiatry* 23: 1512–1520.

34. Cao H, Argyelan M, Yan J, Velioglu HA, Fang F, Joanlanne A, *et al.* (2026): Mapping cerebellar connectivity to cognition in psychosis: Convergent evidence from functional magnetic resonance imaging and transcranial magnetic stimulation. *Biol Psychiatry* 99: 134–141.

35. Frosch IR, Damme KSF, Bernard JA, Mittal VA (2022): Cerebellar correlates of social dysfunction among individuals at clinical high risk for psychosis. *Front Psychiatry* 13: 1027470.

CHAPTER 3 FIGURE/TABLE LEGENDS

Table 1. Participant characteristics. Demographic and clinical characteristics of individuals with 22q11.2 deletion (22qDel), 3q29 deletion (3q29Del), and their respective typically developing controls (22qCon, 3q29Con), shown for the full imaging sample and clinical subsample. Groups did not differ significantly in age. Sex distribution differed significantly across the four groups overall, although no post hoc pairwise comparisons were significant. Estimated total intracranial volume (eTIV) was lower in both deletion groups relative to both control groups, which did not differ from one another. Within the clinical subsample, FSIQ, SRS-2 Total T-score, and SIPS-P did not differ significantly between 22qDel and 3q29Del.

Figure 1. Graphical overview of the study workflow. Overview of data collection across the two cohorts, cerebellar parcellation of T1-weighted MRI using ACAPULCO, application of a normative model (with site-specific adaptation) to derive regional deviation scores, and subsequent statistical comparison between 22qDel and 3q29Del.

Figure 2. Total cerebellar volume deviation scores in 22qDel and 3q29Del. Violin and box plots of total cerebellar volume deviation (z) scores, derived from the adapted normative model, in 22qDel and 3q29Del. Both groups showed deviation scores approximately 1.6–1.8 SD below the normative mean; groups did not differ significantly ($\beta = -0.23$, $p = 0.416$).

Figure 3. Regional cerebellar volume deviation scores in 22qDel and 3q29Del. Dot-and-line plot of mean normative deviation (z) scores across 28 ACAPULCO-defined cerebellar subregions in 22qDel (red) and 3q29Del (blue), sorted by 22qDel mean z-score. The dashed vertical line at zero indicates the normative reference mean. Purple connecting lines indicate regions with an FDR-significant group difference ($q<0.05$); gray connecting lines indicate non-significant differences between 22qDel and 3q29Del. Five regions differed significantly between groups: left Lobule IX, left Crus I, left Lobule IV, left Lobule VI, and right Lobule VIIIB.

Figure 4. Anatomical localization and functional relevance of significant cerebellar subregions. Cerebellar flatmap highlighting the five subregions showing significant group differences between 22qDel and 3q29Del (FDR $q<0.05$), colored by directionality: blue regions (left Lobule IV, left Crus I, left Lobule IX) follow the pattern 3q29Del < 22qDel < normative mean; red regions (left Lobule VI, right Lobule VIIIB) follow the pattern 22qDel < 3q29Del ≈ normative mean. Accompanying table summarizes the primary functional domain associated with each region.

Figure 5. Cognitive and neuropsychiatric phenotypes by group and their associations with total cerebellar volume. Raincloud (violin, box, and individual data points) plots of Full-Scale IQ (FSIQ), SIPS Positive symptoms (SIPS-P), and SRS-2 Total T-score in 22qDel (red) and 3q29Del (blue); groups did not differ significantly on any measure (Table 1).

CHAPTER 3 TABLES

Table 1. Participant characteristics by group

Measure	22qDel	22qCon	3q29Del	3q29Con	Group Comparison[a]
Full Imaging Sample					
Participants (n)	111	109	24	78	
Age, Mean (SD), years	16.2 (9.3)	15.2 (7.3)	15.3 (9.1)	15.3 (8.8)	F(3,318)=0.30, p=0.822
Age Range, years	5–55	6–45	5–39	5–41	
Sex (% female)	55.0	52.3	37.5	35.9	$\chi^2(3)=8.59$, p=0.035[b]
Site (n scanners)	UCLA (3)	UCLA (3)	Emory (1)	Emory (1)	
eTIV, Mean (SD), cm^3	1429.8 (179.8)	1540.7 (164.1)	1340.9 (116.1)	1584.7 (130.0)	F(3,318)=24.86, p<.001; 3q29Del ≈ 22qDel < 22qControl ≈ 3q29Control
Clinical Subsample					
FSIQ, Mean (SD) [n]	78.5 (12.4) [61]		72.7 (13.6) [24]		t(38.8) = 1.82, p = 0.077
SRS-2 Total T-score, Mean (SD) [n]	71.2 (14.1) [54]		66.2 (13.9) [23]		t(42.0) = 1.42, p = 0.163
SIPS-P, Mean (SD) [n]	4.8 (5.5) [62]		6.4 (6.9) [15]		t(18.6) = −0.86, p = 0.401

22qDel = 22q11.2 Deletion; 22qCon = 22q11.2 Control; 3q29Del = 3q29 Deletion; 3q29Con = 3q29 Control; eTIV = estimated total intracranial volume; FSIQ = Full-Scale IQ; SRS-2 = Social Responsiveness Scale, Second Edition; SIPS-P = Structured Interview for Psychosis-Risk Syndromes Positive Symptoms.

[a] Group differences in the full imaging sample were assessed using one-way ANOVA (age, eTIV) and a chi-square test (sex). Significant ANOVA results were followed by Tukey's HSD post-hoc tests. A significant χ^2 result for sex was followed by pairwise Fisher's exact tests with Bonferroni correction. Clinical measures in the deletion subsample were compared using Welch's t-tests.

[b] No individual pairwise comparison for sex was statistically significant, though the pattern reflects higher female representation in both 22q groups (~53%) relative to both 3q29 groups (~37%).

CHAPTER 3 FIGURES

Figure 1 Graphical overview of the study workflow.

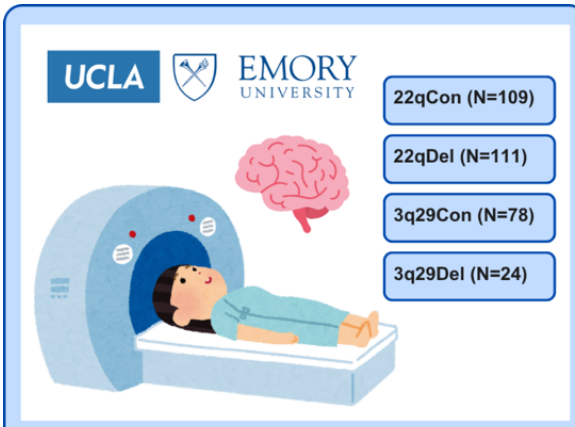

1. Data Collection
High-res T1 structural MRI was acquired from 322 participants. 22q scans were collected at UCLA. 3q29 scans were collected at Emory University.

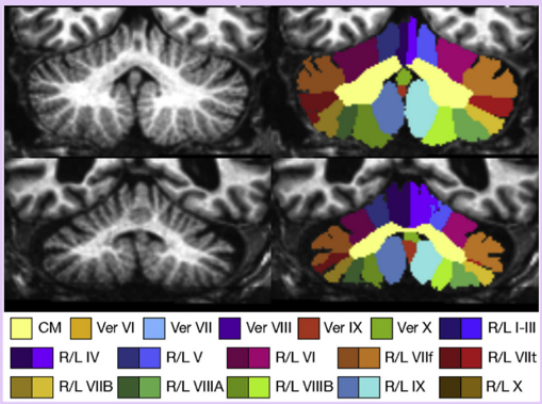

2. Cerebellum Parcellation
The cerebellum was parcellated into 28 anatomical regions using ACAPULCO, a convolutional neural network-based cerebellar parcellation pipeline [6].

3. Normative Modeling (PCNportal)
We used an existing cerebellar volume normative model trained on a large multi-site healthy sample [7], calibrated it to our data using site-specific controls, and then estimated age-, sex-, and site-adjusted regional cerebellar volume deviations for 22qDel and 3q29Del participants.

REFERENCE MODEL
Existing cerebellar BLR lifespan model trained on multi-site healthy controls [7]

SITE ADAPTATION
Calibrated the model to our data using site-specific controls

DEVIATION ESTIMATION
Z-scores were computed for deletion participants relative to the adapted model

4. Statistical Analysis (R)
We compared normative deviation scores between 22qDel and 3q29Del groups at both total and regional cerebellar levels, with FDR correction applied across regional analyses. We also tested whether each group deviated significantly from the normative mean.

DELETION GROUP COMPARISON
Linear models (Z ~ group) were used to compare total and regional cerebellar Z-scores between deletion groups, with FDR correction applied across regions.

NORMATIVE DEVIATION
Group Z-scores were compared to zero (the normative mean) to characterize deviations from normative expectations and contextualize group differences.

Figure 2 Total cerebellar volume deviation scores in 22qDel and 3q29Del.

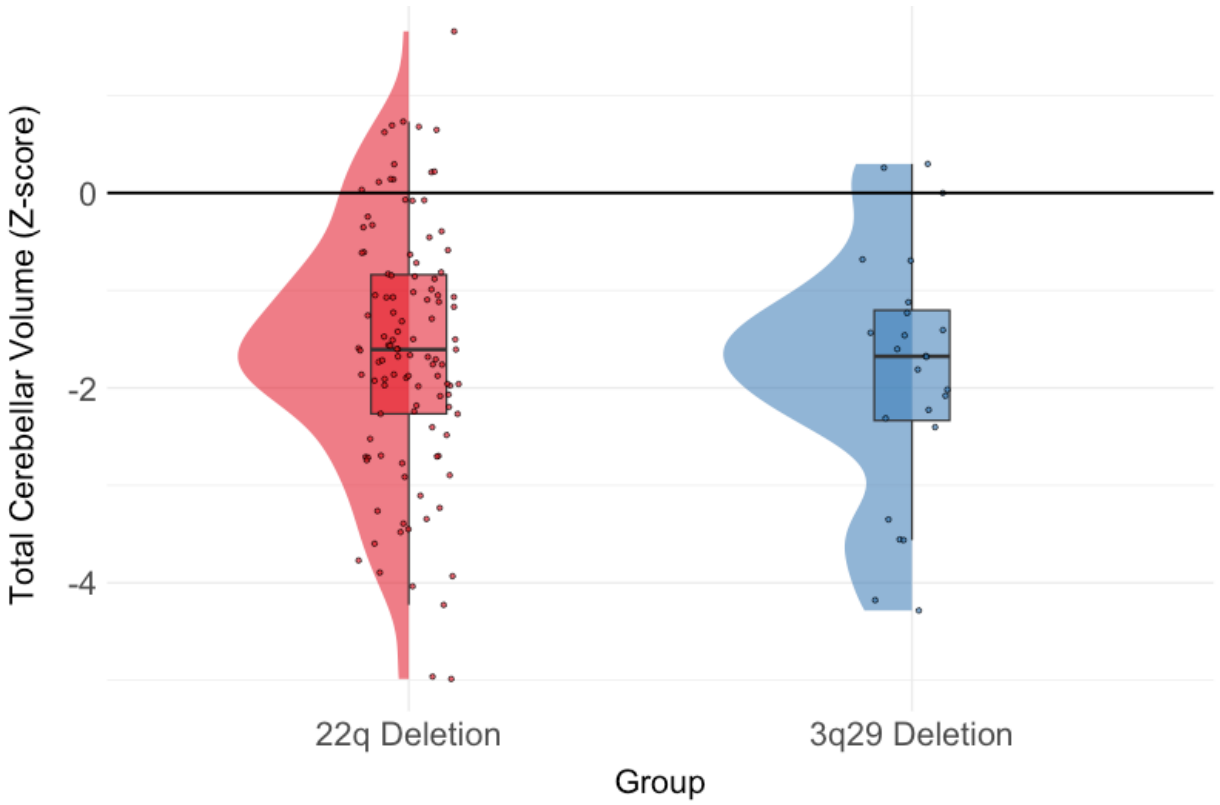

Figure 3 Regional cerebellar volume deviation scores in 22qDel and 3q29Del.

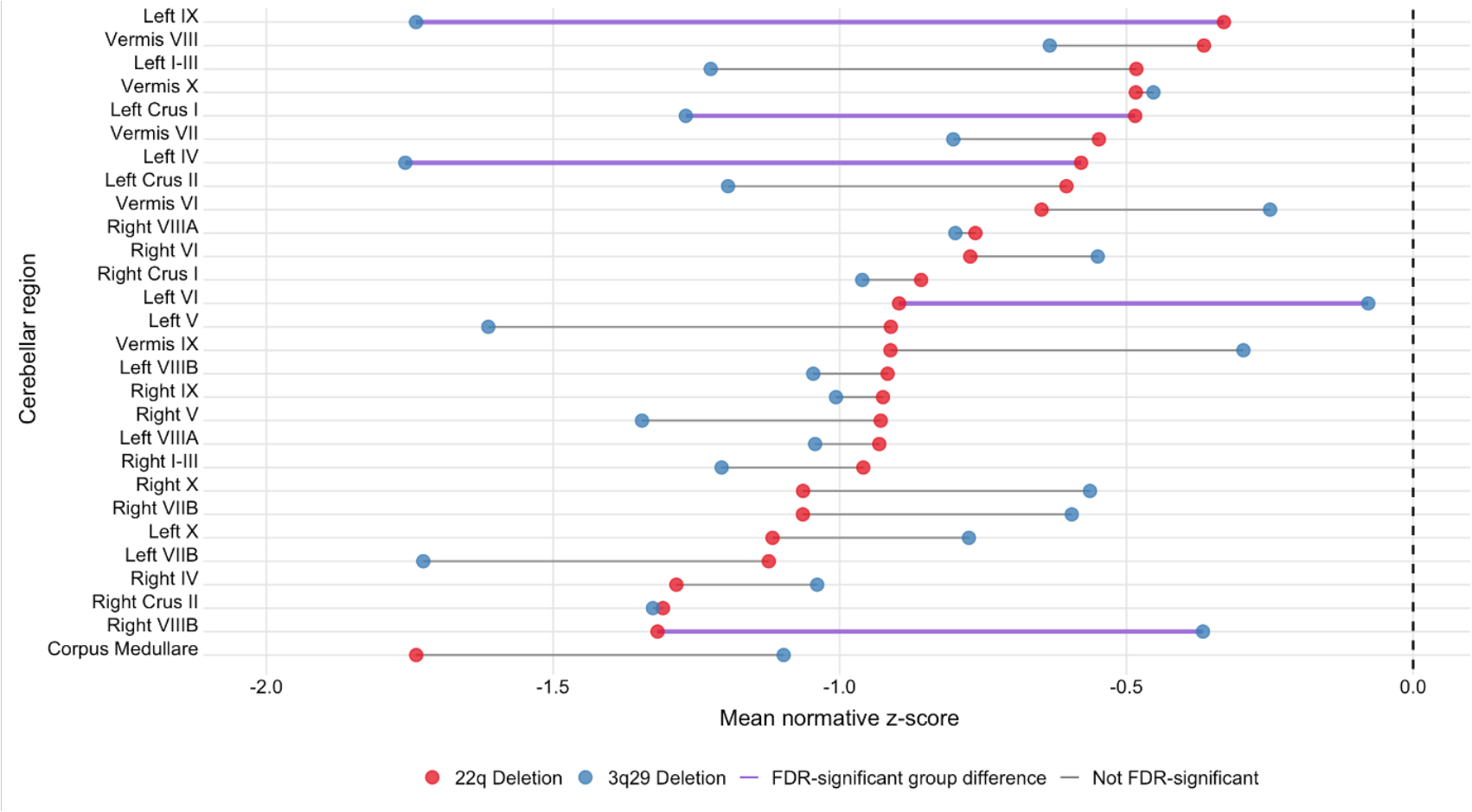

Figure 4 Anatomical localization and functional relevance of significant cerebellar subregions.

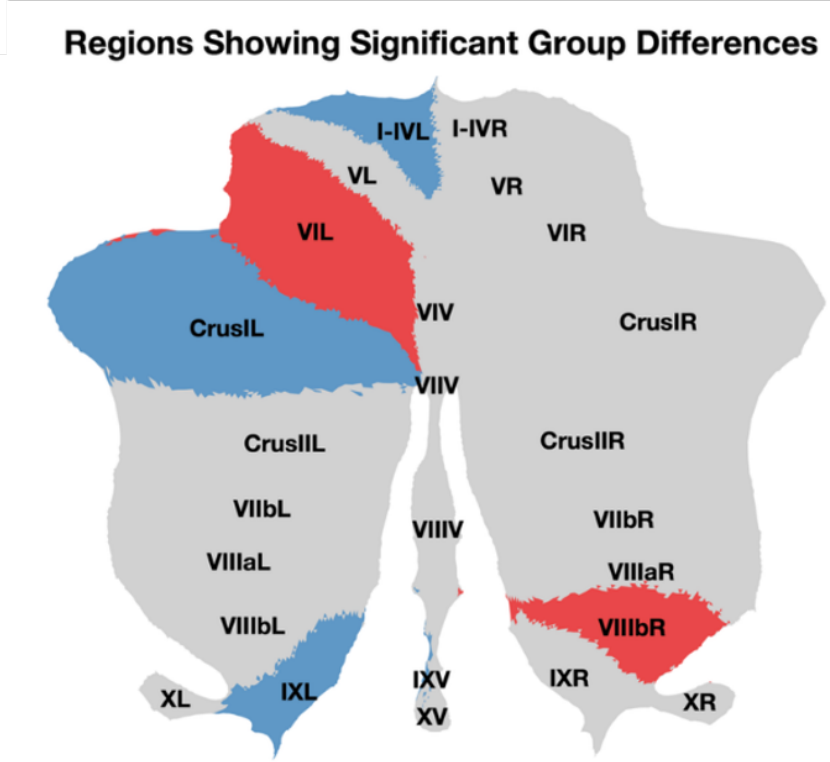

Region	Associated Functions
Left IV	Motor control, proprioception
Left VI	Motor-cognitive integration
Left Crus I	Executive function, working memory, and language
Right VIIIB	Sensorimotor processing and working memory
Left IX	Cognitive, social, and emotional processing

Colored regions ($q < 0.05$)

3q29Del < 22qDel < Normative Mean

22qDel < 3q29Del ≈ Normative Mean

Figure 5 Cognitive and neuropsychiatric phenotypes by group and their associations with total cerebellar volume.

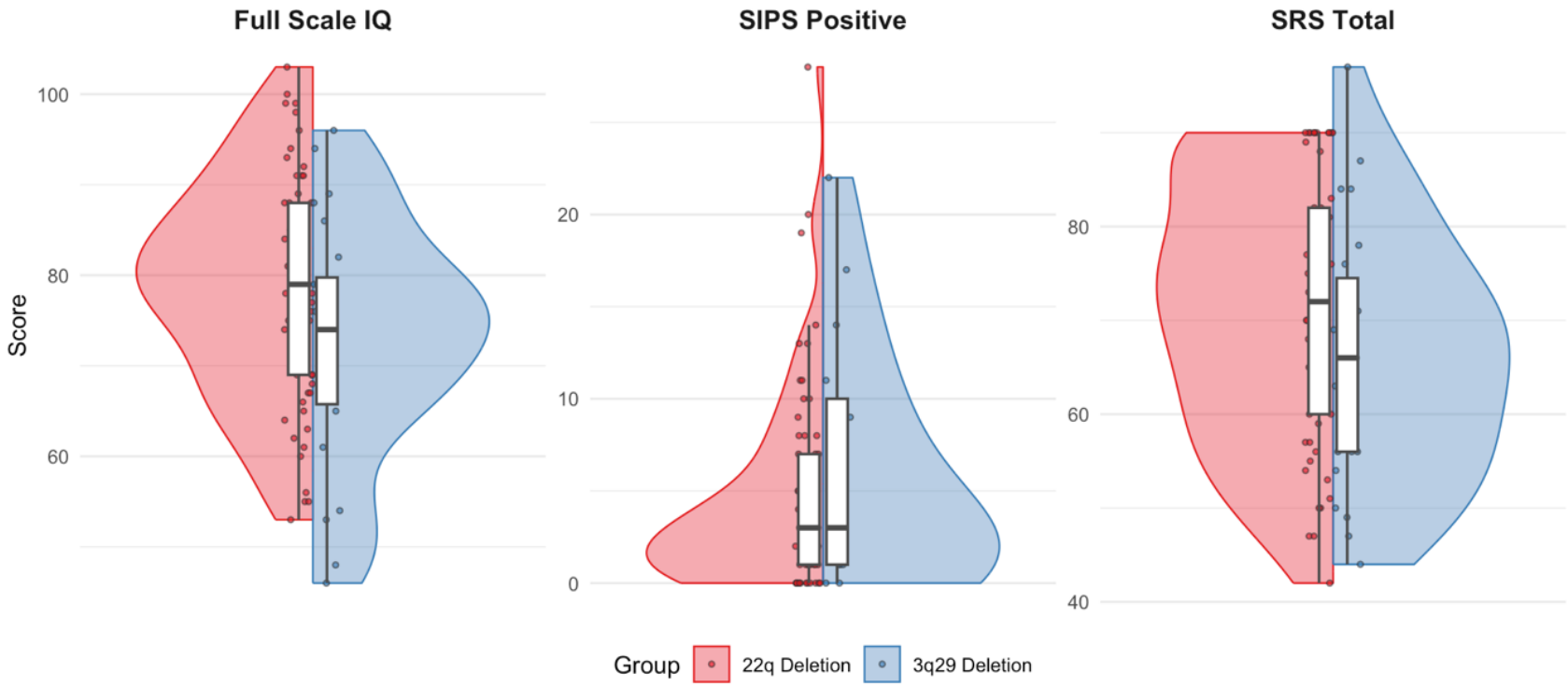

CHAPTER 3 SUPPLEMENTAL MATERIAL

Supplementary Results

1. Full Exploratory Brain-Behavior Association Results

Within-group Spearman correlations between total cerebellar volume deviation scores and the three primary clinical measures were weak and non-significant in both groups. In 22qDel, FSIQ ρ=0.09, SIPS-P ρ=−0.11, and SRS-2 Total ρ=−0.12. In 3q29Del, FSIQ ρ=0.28, SIPS-P ρ=−0.11, and SRS-2 Total ρ=−0.17 (Supplementary Figure S1). Though not statistically significant, all six correlations were in the expected direction, with greater cerebellar volume associated with higher FSIQ and lower SIPS-P and SRS-2 Total.

Deviation-score-by-group interaction models testing whether these associations differed between CNVs were also non-significant ($q > 0.05$) for all three measures (FSIQ: interaction p=0.18; SIPS-P: interaction p=0.45; SRS-2 Total: interaction p=0.70; Supplementary Figure S2).

The same correlation and interaction models were also examined at the regional level (28 regions × the same three measures) in an exploratory analysis. None survived FDR correction, and nominal associations are reported in Supplementary Figures S3–S4.

Supplementary Tables

Supplementary Table S1. Sample size by site, scanner, and group.

Site	Scanner	22qDel N	3q29Del N	TD scans (unique subjects)
UCLA	Trio (BMC)	30	—	44 (28)
UCLA	Trio (CCN)	45	—	46 (30)
UCLA	Prisma (CCN)	36	—	74 (58)
Emory	Magnetom Prisma	—	24	78 (78)

Note. 22qDel = 22q11.2 Deletion. 3q29Del = 3q29 Deletion. TD = typically developing. 22qDel and 3q29Del participants each contributed a single scan. TD scans reflects the number of scans used for scanner-specific calibration of the normative model. TD participants with scans on multiple scanners contributed a scan to calibration for each relevant scanner (unique subject counts shown in parentheses), so scan counts are not mutually exclusive across rows and do not sum to the total unique TD sample (N=187).

Supplementary Table S2a. One-sample t-tests vs. normative mean, all 28 regions (22qDel).

Region	β (Estimate)	t (Statistic)	95% CI Lower	95% CI Upper	p	p_fdr
CM	-1.739	-8.427	-2.148	-1.330	<0.001	<0.001
Left Crus I	-0.485	-4.654	-0.691	-0.278	<0.001	<0.001
Left Crus II	-0.605	-5.857	-0.809	-0.400	<0.001	<0.001
Left I–III	-0.483	-3.772	-0.736	-0.229	<0.001	<0.001
Left IV	-0.579	-4.459	-0.836	-0.322	<0.001	<0.001
Left IX	-0.330	-2.954	-0.551	-0.109	<0.001	<0.001
Left V	-0.911	-7.023	-1.168	-0.654	<0.001	<0.001
Left VI	-0.897	-9.706	-1.080	-0.714	<0.001	<0.001
Left VIIB	-1.124	-8.169	-1.396	-0.851	<0.001	<0.001
Left VIIIA	-0.931	-7.415	-1.180	-0.682	<0.001	<0.001
Left VIIIB	-0.917	-8.836	-1.122	-0.711	<0.001	<0.001
Left X	-1.117	-10.895	-1.320	-0.914	<0.001	<0.001
Right Crus I	-0.858	-7.779	-1.077	-0.640	<0.001	<0.001
Right Crus II	-1.308	-10.466	-1.556	-1.061	<0.001	<0.001
Right I–III	-0.959	-8.899	-1.173	-0.745	<0.001	<0.001
Right IX	-0.925	-8.355	-1.144	-0.705	<0.001	<0.001
Right V	-0.929	-8.538	-1.144	-0.713	<0.001	<0.001
Right VI	-0.772	-7.006	-0.991	-0.554	<0.001	<0.001
Right VIIB	-1.064	-9.934	-1.277	-0.852	<0.001	<0.001
Right VIIIA	-0.763	-7.279	-0.971	-0.556	<0.001	<0.001
Right VIIIB	-1.318	-8.807	-1.614	-1.021	<0.001	<0.001
Right X	-1.064	-8.308	-1.318	-0.810	<0.001	<0.001
Right IV	-1.285	-11.124	-1.514	-1.056	<0.001	<0.001
Vermis IX	-0.912	-6.003	-1.213	-0.611	<0.001	<0.001
Vermis VI	-0.648	-5.658	-0.875	-0.421	<0.001	<0.001
Vermis VII	-0.548	-3.868	-0.829	-0.267	<0.001	<0.001
Vermis VIII	-0.365	-4.056	-0.543	-0.187	<0.001	<0.001
Vermis X	-0.484	-3.880	-0.731	-0.237	<0.001	<0.001

Note. Estimates represent mean deviation scores relative to the normative mean. p_fdr = FDR-corrected p-value (Benjamini-Hochberg); CM = Corpus Medullare.

Supplementary Table S2b. One-sample t-tests vs. normative mean, all 28 regions (3q29Del).

Region	β (Estimate)	t (Statistic)	95% CI Lower	95% CI Upper	p	p_fdr
CM	-1.098	-4.764	-1.575	-0.621	<0.001	<0.001
Left Crus I	-1.269	-6.271	-1.687	-0.850	<0.001	<0.001
Left Crus II	-1.195	-5.434	-1.650	-0.740	<0.001	<0.001
Left I–III	-1.225	-3.568	-1.935	-0.515	0.002	0.002
Left IV	-1.758	-4.409	-2.583	-0.933	<0.001	<0.001
Left IX	-1.739	-5.162	-2.436	-1.042	<0.001	<0.001
Left V	-1.613	-6.226	-2.149	-1.077	<0.001	<0.001
Left VI	-0.078	-0.319	-0.585	0.429	0.753	0.753
Left VIIB	-1.726	-7.677	-2.192	-1.261	<0.001	<0.001
Left VIIIA	-1.043	-5.028	-1.472	-0.614	<0.001	<0.001
Left VIIIB	-1.046	-3.701	-1.631	-0.461	0.001	0.002
Left X	-0.775	-2.929	-1.322	-0.228	0.008	0.009
Right Crus I	-0.961	-3.619	-1.510	-0.412	0.001	0.002
Right Crus II	-1.326	-4.831	-1.894	-0.758	<0.001	<0.001
Right I–III	-1.206	-4.696	-1.737	-0.675	<0.001	<0.001
Right IX	-1.007	-4.121	-1.512	-0.501	<0.001	<0.001
Right V	-1.345	-4.163	-2.013	-0.677	<0.001	<0.001
Right VI	-0.550	-2.402	-1.024	-0.076	0.025	0.028
Right VIIB	-0.595	-2.486	-1.091	-0.100	0.021	0.024
Right VIIIA	-0.798	-4.034	-1.208	-0.389	0.001	<0.001
Right VIIIB	-0.366	-1.731	-0.805	0.072	0.097	0.102
Right X	-0.564	-2.289	-1.073	-0.054	0.032	0.035
Right IV	-1.039	-3.873	-1.595	-0.484	0.001	0.001
Vermis IX	-0.296	-1.716	-0.653	0.061	0.100	0.103
Vermis VI	-0.249	-1.287	-0.650	0.151	0.211	0.215
Vermis VII	-0.802	-3.582	-1.265	-0.339	0.002	0.002
Vermis VIII	-0.634	-3.333	-1.027	-0.240	0.003	0.004
Vermis X	-0.453	-2.255	-0.868	-0.037	0.034	0.037

Note. Estimates represent mean deviation scores relative to the normative mean. p_fdr = FDR-corrected p-value (Benjamini-Hochberg); CM = Corpus Medullare.

Supplementary Table S3. Between-group comparison of regional cerebellar volume deviation scores (22qDel vs. 3q29Del) from linear regression models (deviation score ~ CNV group), with FDR correction applied across the 28 regional models.

Region	Estimate	Std. Error	Statistic	95% CI Lower	95% CI Upper	p	p_fdr
CM	0.641	0.457	1.401	-0.264	1.546	0.163	0.305
Left Crus I	-0.784	0.243	-3.224	-1.265	-0.303	0.002	0.011
Left Crus II	-0.590	0.244	-2.415	-1.074	-0.107	0.017	0.079
Left I–III	-0.742	0.318	-2.336	-1.371	-0.114	0.021	0.079
Left IV	-1.179	0.335	-3.524	-1.840	-0.517	0.001	0.005
Left IX	-1.409	0.286	-4.923	-1.975	-0.843	<0.001	<0.001
Left V	-0.702	0.304	-2.310	-1.303	-0.101	0.022	0.079
Left VI	0.818	0.229	3.577	0.366	1.271	<0.001	0.005
Left VIIB	-0.603	0.314	-1.918	-1.224	0.019	0.057	0.178
Left VIIIA	-0.112	0.287	-0.390	-0.680	0.456	0.697	0.818
Left VIIIB	-0.130	0.259	-0.501	-0.641	0.382	0.617	0.785
Left X	0.343	0.252	1.358	-0.156	0.841	0.177	0.310
Right Crus I	-0.103	0.267	-0.384	-0.631	0.426	0.701	0.818
Right Crus II	-0.018	0.298	-0.059	-0.606	0.571	0.953	0.953
Right I–III	-0.247	0.261	-0.948	-0.763	0.268	0.345	0.536
Right IX	-0.082	0.264	-0.311	-0.603	0.440	0.756	0.847
Right V	-0.416	0.277	-1.501	-0.965	0.132	0.136	0.272
Right VI	0.222	0.260	0.856	-0.292	0.737	0.394	0.551
Right VIIB	0.469	0.256	1.833	-0.037	0.975	0.069	0.178
Right VIIIA	-0.035	0.244	-0.143	-0.517	0.447	0.886	0.948
Right VIIIB	0.951	0.337	2.823	0.285	1.618	0.005	0.031
Right X	0.500	0.298	1.677	-0.090	1.091	0.096	0.224
Right IV	0.246	0.278	0.884	-0.304	0.795	0.378	0.551
Vermis IX	0.616	0.337	1.827	-0.051	1.282	0.070	0.178
Vermis VI	0.399	0.263	1.518	-0.121	0.918	0.131	0.272
Vermis VII	-0.254	0.322	-0.788	-0.892	0.384	0.432	0.576
Vermis VIII	-0.269	0.213	-1.263	-0.690	0.152	0.209	0.344
Vermis X	0.031	0.284	0.108	-0.531	0.593	0.914	0.948

Note. Estimate reflects the difference in deviation score for 3q29Del relative to 22qDel (reference group). p_fdr = FDR-corrected p-value (Benjamini-Hochberg); CM = Corpus Medullare.

Supplementary Figures

Supplementary Figure S1. Spearman correlations (ρ) between total cerebellar volume deviation scores and three primary clinical measures (Full Scale IQ, SIPS Positive, SRS Total), by group. Color reflects the direction and magnitude of ρ. Correlations were weak and non-significant in both groups, but the direction of association was consistently as expected.

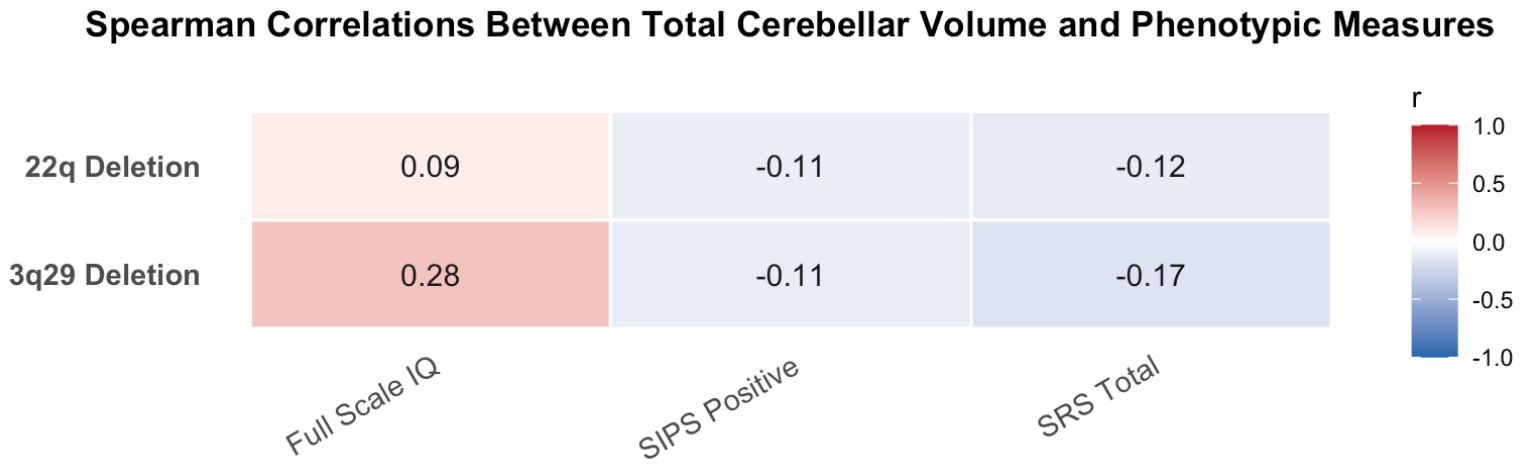

Supplementary Figure S2. Associations between total cerebellar volume deviation scores and three primary clinical measures (Full Scale IQ, SIPS Positive, SRS Total), by group, with linear regression fit lines and 95% confidence bands. r reflects Pearson correlation underlying each regression fit line and may differ from the Spearman ρ reported in the main text and Supplementary Figure S1, which is rank-based. Interaction p-values reflect the deviation-score-by-group interaction term (clinical score ~ CNV group × deviation score). Deviation-score-by-group interaction terms were non-significant for all three measures (FSIQ: p=0.18, FDR=0.53; SIPS-P: p=0.45, FDR=0.67; SRS-2 Total: p=0.70, FDR=0.70).

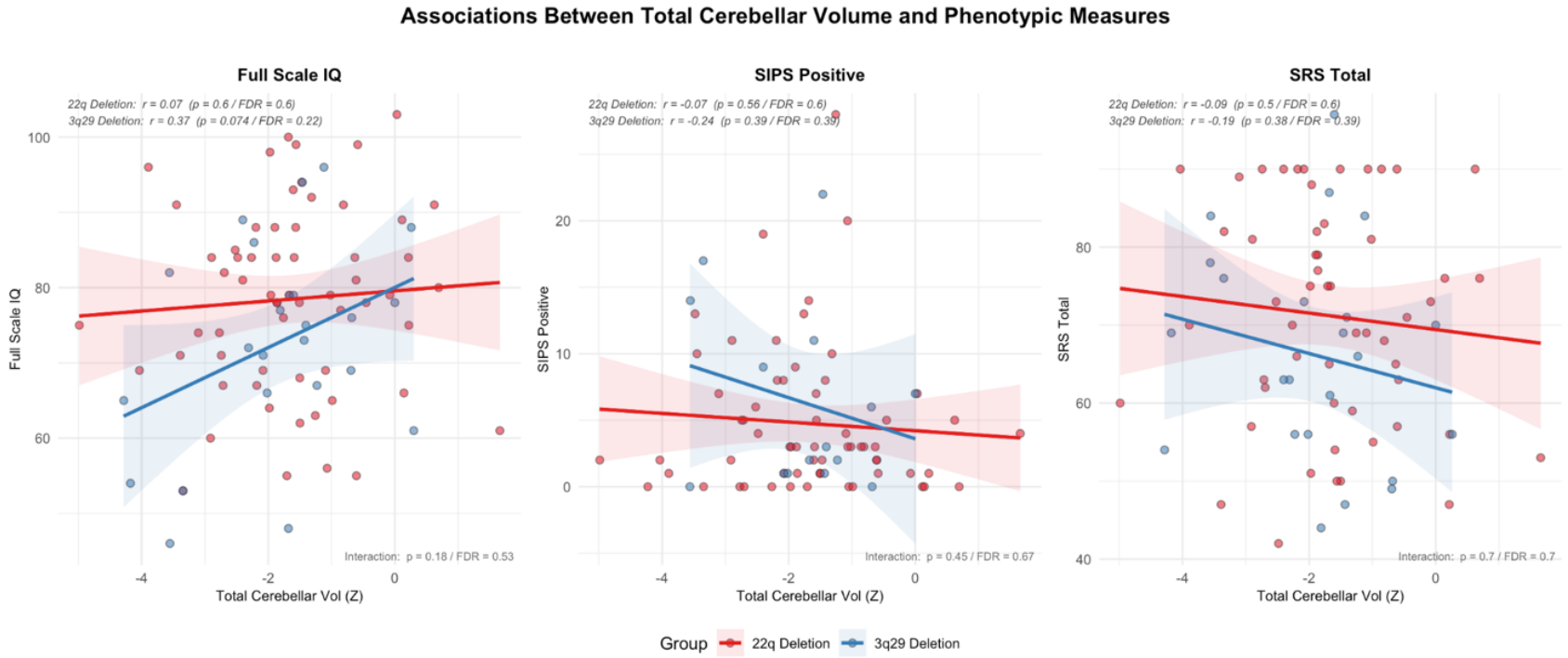

Supplementary Figure S3. Regional within-group Spearman correlations between cerebellar subregion volume deviation scores and three primary clinical measures, by group. Asterisks denote uncorrected significance (*p<.05, **p<.01, ***p<.001); none survived FDR correction across the 28 regional tests.

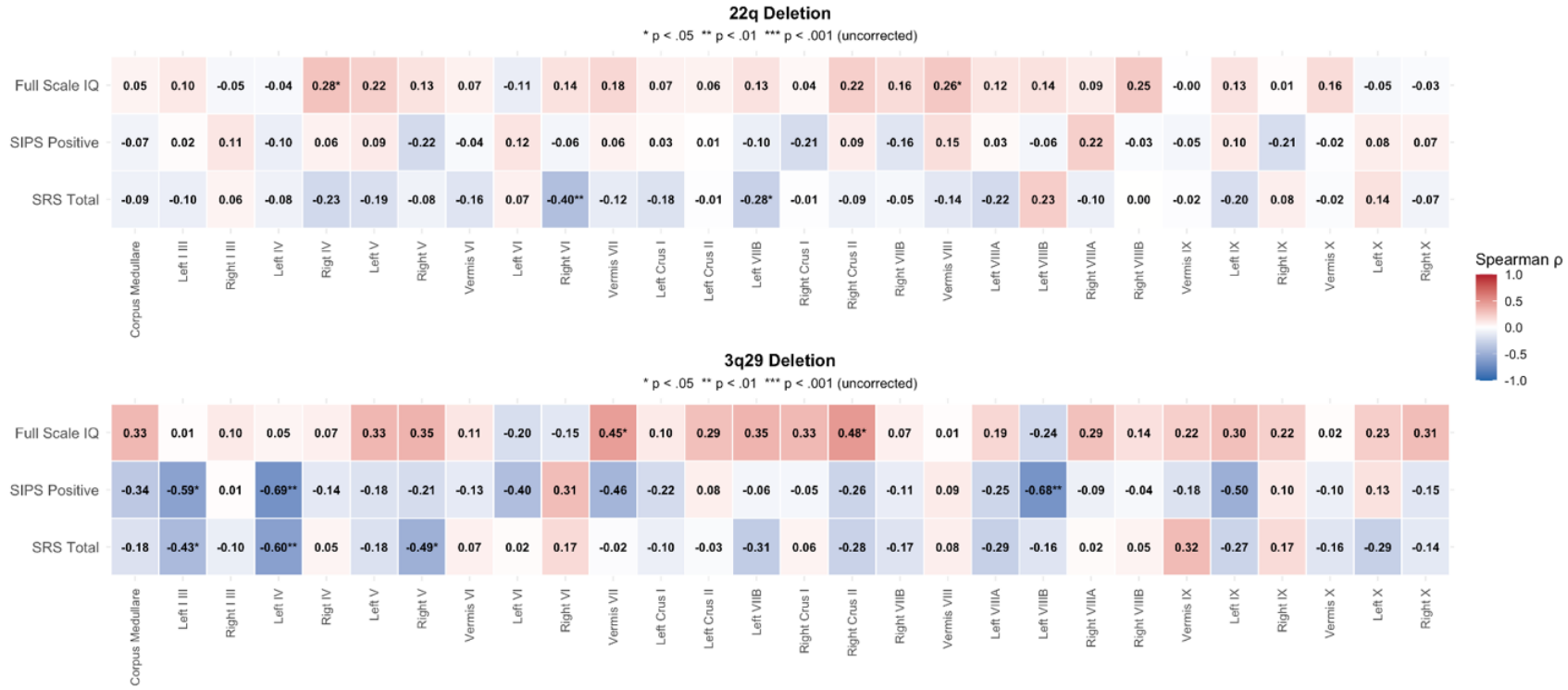

Supplementary Figure S4. Regional deviation-score-by-group interaction effects (clinical score ~ CNV group × deviation score) across all 28 cerebellar subregions and three clinical measures. Interaction estimate reflects the difference in the deviation-score–outcome relationship between groups; positive values indicate a stronger relationship in 3q29Del. Asterisks denote uncorrected significance (*p<.05, **p<.01, ***p<.001); none survived FDR correction across the 28 regional interaction tests.

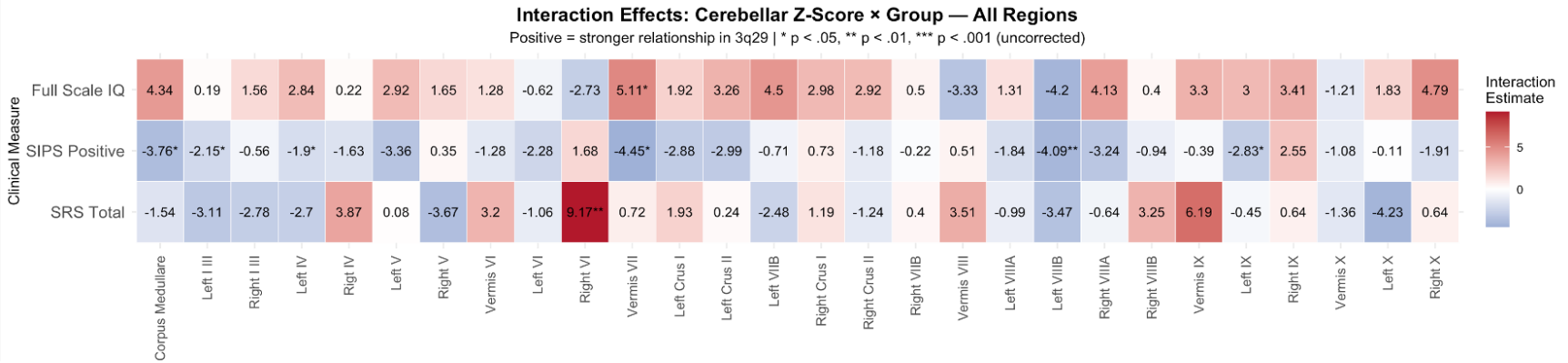

CONCLUSION

This dissertation used a genetics-first approach to investigate how high-risk copy number variants (CNVs) associated with schizophrenia and autism spectrum disorder (ASD) affect the cerebellum, and whether cerebellar alterations converge or diverge across these CNVs. Across the three manuscripts comprising this dissertation, cerebellar alterations were consistently observed in all CNVs examined, but their expression varied by genomic locus, gene dosage, region, and cerebellar phenotype. Contrary to our hypothesis, reciprocal 22q11.2 deletion (22qDel) and duplication (22qDup) did not uniformly follow a symmetric, opposing pattern of cerebellar alteration. Instead, the two CNVs showed markedly different patterns of involvement across cerebellar phenotypes, indicating that reciprocal gene dosage can affect distinct dimensions of cerebellar organization rather than producing a simple mirror effect. At the same time, specific regional alterations were shared between 22qDel and 22qDup, suggesting points of anatomical convergence despite broader differences in their cerebellar phenotypes. Comparing 22qDel and 3q29 deletion further revealed convergence in global cerebellar vulnerability alongside locus-specific regional effects.

The first manuscript provided the foundation for this work by establishing the regional cerebellar volumetric phenotype of reciprocal 22q11.2 CNVs. Using fine-grained lobule-level parcellation, we found widespread cerebellar volume reductions in 22qDel, affecting nearly all cerebellar subregions, whereas 22qDup showed a much subtler and more regionally selective pattern, with no significant reduction in total cerebellar volume. These findings indicate that reciprocal changes in 22q11.2 gene dosage do not produce a simple symmetric or linear effect on cerebellar anatomy.

Despite this broader divergence, Vermis VII was reduced in both CNVs, identifying a shared site of regional vulnerability and demonstrating that convergent and copy-number-specific effects can coexist within the same genetic locus.

The second manuscript showed that copy-number-specific effects becomes even more apparent when cerebellar organization is examined beyond volume. Incorporating diffusion MRI and resting-state fMRI revealed markedly different patterns of alteration in 22qDel and 22qDup. The volumetric pattern, characterized by pronounced and widespread alterations in 22qDel but comparatively limited effects in 22qDup, was reversed for white matter microstructure: 22qDup showed widespread alterations across all three cerebellar peduncles, whereas effects in 22qDel were comparatively circumscribed. Functional connectivity showed yet another pattern, with relatively selective reductions in cerebellar-cortical and cerebellar-subcortical connectivity in 22qDel and comparatively limited alterations in 22qDup. Integrating these modalities demonstrated that volume, white matter microstructure, and functional connectivity provide complementary rather than redundant information for CNV classification and for multivariate associations with cognitive and social functioning. These findings therefore extend the results of the first manuscript by showing that the neurobiological consequences of reciprocal gene dosage vary across distinct aspects of cerebellar structure and function rather than following a single uniform pattern.

The third manuscript asked whether the cerebellar vulnerability observed in 22qDel was specific to the 22q11.2 locus or reflected a broader feature of genetic risk for schizophrenia and ASD. Using normative modeling to directly compare independently ascertained 22qDel and 3q29Del cohorts, we found that both CNVs

showed substantial and statistically indistinguishable reductions in total cerebellar volume despite arising from distinct genomic loci and affecting largely non-overlapping sets of genes. This convergence suggests that reduced cerebellar volume may represent a shared downstream feature of genetically distinct forms of high neuropsychiatric risk rather than an effect unique to 22q11.2 deletion. At the same time, the regional distribution of these alterations differed between CNVs, indicating that shared global vulnerability can coexist with locus-specific anatomical patterning. Beyond these biological findings, this study also demonstrated the utility of normative modeling for comparing neuroimaging phenotypes across independently collected rare-variant cohorts, where conventional case-control comparisons are complicated by confounding between genetic group and acquisition site.

Taken together, these studies advance our understanding of cerebellar dysfunction in schizophrenia- and autism spectrum disorder-associated CNVs in several ways. First, they establish cerebellar involvement across multiple high-risk CNVs and across structural, microstructural, and functional phenotypes, extending its relevance beyond any single genetic variant or neuroimaging measure. Second, they demonstrate that this involvement is not characterized by a uniform signature of genetic risk: reciprocal changes in gene dosage can have markedly different consequences across cerebellar phenotypes, while genetically distinct deletions can converge in global cerebellar vulnerability yet retain locus-specific regional signatures. Third, the observed associations with cognitive and ASD-related social functioning, together with more tentative associations with psychosis-risk symptoms, highlight the potential relevance of cerebellar variation to dimensional neurobehavioral outcomes that cut across genetic

and diagnostic categories. Fourth, these findings demonstrate how fine-grained regional and multimodal characterization can reveal neurobiological effects that may be obscured when analyses are limited to global measures or a single imaging phenotype. More broadly, they position the cerebellum alongside cortical and subcortical systems as an informative target for psychiatric research and support its more routine inclusion in studies of neurodevelopmental and psychiatric disorders.

Future work integrating neuroimaging with complementary experimental approaches, including stem cell models, animal studies, and emerging cerebellum-specific transcriptomic resources, will be essential for clarifying the molecular and developmental mechanisms through which genetic risk alters cerebellar development. As tools for cerebellar imaging and analysis continue to mature, larger longitudinal and multimodal studies will be increasingly well positioned to characterize cerebellar alterations with greater anatomical and functional precision and to determine whether these structural and functional signatures can ultimately inform clinically meaningful markers of psychiatric risk and resilience.